Politecnico di Milano

School of Industrial and Information Engineering
Master of Science in Mathematical Engineering

MASTER THESIS

The DRPM Strikes Back: More Flexibility for a Bayesian Spatio-Temporal Clustering Model

Advisor
Prof. Alessandra Guglielmi

Coadvisor
Prof. Alessandro Carminati

Candidate
Federico Angelo Mor
Matr. 221429

Academic Year 2023–2024

to my cats Otto
and La Micia

Abstract

Clustering is a key technique for identifying patterns and structures in complex datasets, whose relevance is intensified in spatio-temporal contexts where observations are simultaneously influenced by multiple factors such as space, time, and covariates. This complexity can be effectively tamed by model-based clustering methods, which often provide more accurate and interpretable results with respect to traditional frequentist approaches thanks to the possibility of encoding data information directly inside the model. To this end, the Dependent Random Partition Model (Garrit L. Page et al., 2022) is one of the most relevant Bayesian models due to its explicit consideration of temporal dependence in the partitions. However, the current formulation of the model and the implementation of the associated MCMC algorithm lacks the inclusion of covariates, the handling of missing data, and the efficiency in execution times. Therefore, in this work we improve the original DRPM by addressing those issues through updates on the model formulation and a brand new implementation in Julia. These advancements are then tested on synthetic and real-world datasets, including air quality data from the AgrImOnIA project (Fassò et al., 2023) in Lombardy, Italy.

KEYWORDS: Bayesian modelling, clustering, spatio-temporal data, MCMC, Julia

Sommario

Il clustering è una tecnica fondamentale per identificare strutture e pattern in dataset complessi, la cui importanza è intensificata nei contesti spazio-temporali in cui le osservazioni sono influenzate simultaneamente da molteplici fattori come spazio, tempo e covariate. Questa complessità può essere efficacemente gestita da metodi di clustering basati su modelli, che spesso forniscono risultati più precisi e interpretabili rispetto agli approcci frequentisti tradizionali grazie alla possibilità di inserire informazioni riguardo ai dati direttamente all'interno del modello. In tal senso, il Dependent Random Partition Model (Garrit L. Page et al., 2022) è uno dei modelli bayesiani più rilevanti in quanto tiene conto in modo esplicito della dipendenza temporale delle partizioni. Tuttavia, l'attuale formulazione del modello e la sua corrispondente implementazione dell'algoritmo di campionamento mancano dell'inclusione di covariate, della gestione dei dati mancanti, e di efficienza nei tempi di esecuzione. In questo lavoro abbiamo quindi migliorato l'originale DRPM affrontando tali problemi tramite aggiornamenti sulla formulazione del modello e una fiammante implementazione in Julia. Questi sviluppi sono stati poi testati su dataset sintetici e reali, compresi i dati sulla qualità dell'aria in Lombardia del progetto AgrImOnIA (Fassò et al., 2023).

Parole chiave: modellistica bayesiana, clustering, dati spazio-temporali, MCMC, Julia

Contents

List of Figures

List of Tables

Introduction

Clustering is a fundamental technique of unsupervised learning where a set of data points has to be divided into homogenous groups of units which exhibit a similar behaviour relative to a target variable. It has long been a powerful tool for identifying structures and patterns in data, especially in contexts where relationships between observations are complex such as when the target variable is affected by multiple factors simultaneously. For this reason, clustering methods have become increasingly popular across a variety of scientific fields, including social sciences, climate and environmental analysis, economics, and healthcare.

Clustering approaches are generally divided into two main categories: algorithmic and model-based methods.

Algorithmic methods such as hierarchical, partition-based, or density-based methods, address the clustering problem as an optimization problem where a certain metric has to be minimised (or maximised). For instance, partition-based methods as k-means (Hartigan et al., 1979) generate clusters around a set of centroids which are iteratively updated to minimize the within-cluster variance, i.e. the mean squared distance of the units from their assigned cluster centroid. However, these methods require specifying the desired number k of clusters in advance and are limited to numerical data. Hierarchical clustering methods, on the other hand, build a tree-like structure of clustering solutions, represented as a dendrogram, which captures the relationships among potential clusters (Jain et al., 1988) (Kaufman et al., 1990). This is done through either an agglomerative (bottom-up) strategy, where each unit starts in her own cluster that gets iteratively combined with other units or clusters, or in a divisive (top-down) strategy, where units start in a single cluster that is iteratively subdivided. These methods do not require a predefined number of clusters, but are highly sensitive to the choice of the distance metric which drives all merging and splitting decisions. Consequently, changing the distance metric can lead to significantly different clustering configurations. Lastly, density-based methods such as DBSCAN (Ester et al., 1996) define clusters through a density metric, which can produce more flexible structures with clusters of varying shapes unlike the ones generated by means of a distance metric. However, these methods remain sensitive to the choice of the density parameters and may yield clusters that are less interpretable and irregular.

In summary, these algorithmic approaches are largely heuristic (Gormley et al., 2022), performing well only with well-separated clusters or standard geometric forms but often failing in more complex scenarios. Furthermore, lacking a solid

statistical foundation, these methods can lead to unsatisfactory results and provide no assessment about clustering uncertainty.

An alternative and more flexible approach is therefore provided by model-based methods, which assume a probabilistic modelling of the data. This is generally achieved through a mixture model (Bouveyron et al., 2019) (Grün, 2018) (Böhning, 2007), where each mixture component corresponds to a cluster with its specific cluster parameters. In this way, each observation is assumed to have arisen from one of J possible groups which are mixed together in various proportions. More formally, for each unit $i = 1, \dots, n$ we have that

$$f(y_i|\boldsymbol{\pi}, \boldsymbol{\vartheta}_1^\star, \dots, \boldsymbol{\vartheta}_J^\star) = \sum_{j=1}^{J} \pi_j f_j(y_i|\boldsymbol{\vartheta}_j^\star)$$

where y_i is the data point of the i-th observation, $\boldsymbol{\pi}$ is the set of weights satisfying $\pi_j \in [0, 1]$ for $j = 1, \dots, J$ and $\sum_{j=1}^{J} \pi_j = 1$, $\boldsymbol{\vartheta}_j^\star$ are the cluster-specific parameters, and $f_j(\cdot|\boldsymbol{\vartheta}_j^\star)$ is the density of the j-th cluster (Grazian, 2023). A common modelling choice is a gaussian mixture model (GMM), where each cluster follows a normal distribution and thus making $\boldsymbol{\vartheta_j^\star} = (\mu_j^\star, \sigma_j^{2\star})$, or $\boldsymbol{\vartheta_j^\star} = (\boldsymbol{\mu}_j^\star, \Sigma_j^\star)$ in the multivariate case. This choice is flexible and effective since, especially in the multivariate case, gaussian distribution are able to capture very different clustering structures (Franzén, 2008).

In this model-based approach, the goal is to estimate the cluster-specific parameters $\boldsymbol{\vartheta}_1, \dots, \boldsymbol{\vartheta}_J$ and the mixing proportions $\pi_1, \dots, \pi_J$. The estimation step is often performed through the Expectation-Maximization (EM) algorithm (McLachlan et al., 2008) (Ng et al., 2004), which iteratively refines the estimates of the parameters via maximum likelihood estimation (MLE). Once the cluster-specific parameters are estimated, each observation can be assigned to a component, i.e. to a cluster, based on the highest posterior probability of belonging to that component, which can be computed through the Bayes rule.

This approach through a mixture model can be naturally reframed into a Bayesian context. As opposed to MLE, Bayesian mixture models incorporate prior information on the parameters, allowing to assess uncertainty in the clustering structure (Wade, 2023) since each parameter is treated as a random variable with a corresponding prior distribution. The Bayesian framework is considerably much powerful and accommodates more complex formulations. For instance, by adopting a Bayesian non-parametric approach, an infinite mixture model (Grazian, 2023), which does not require a predetermined number J of components, can be introduced.

However, implementing Bayesian models requires the design of Markov Chain Monte Carlo (MCMC) algorithms, which can often be challenging and computationally intensive. In MCMC algorithms, complicated or impossible analytical calculations are replaced by simulated approximations (Franzén, 2008) derived from a Markov chain that ultimately generates samples from the posterior distribution of the model parameters, allowing inference on the generated clusters (A. Gelman et al., 2003) (Robert et al., 2000). The iterative nature of MCMC, along with the need for a burn-in period to allow convergence of the chain to its stationary distribution, implies that considerable computational resources may be

needed, particularly for models with high-dimensional parameter spaces or when working with large-scale datasets. As a result, while Bayesian methods provide a robust framework for modelling uncertainty and incorporating prior knowledge, they also demand significant computational effort and expertise in algorithm design to effectively realize their full potential.

Nonetheless, the effectiveness of Bayesian model-based approaches, along with their computational demands, becomes particularly pronounced when applied to spatio-temporal datasets. This type of data, in which observations are collected over time and across various spatial locations, is inherently complex due to the interplay between spatial and temporal dimensions; a complexity that is further compounded when covariates are also available. Consequently, compared to traditional algorithmic methods, model-based methods are fairly more suited to tackle this task as they are able to integrate all these different levels of information. A model-based analysis of spatio-temporal data should also account for the temporal dependencies among the partitions to more effectively identify trends occurring over time and thus producing clusters that evolve in a more gentle and interpretable way. Additionally, these methods should also provide efficient implementations suitable for large scale datasets, which are commonly accessible in this spatio-temporal context.

Recently, the use of Bayesian models to perform clustering has become more popular, particularly in this field of spatio-temporal datasets. Bayesian clustering, in fact, allows to incorporate prior information into the model thereby enhancing the quality of the results. Throughout the years, several models have been proposed in the Bayesian literature. Among these, the Dependent Random Partition Model (DRPM) (Garrit L. Page et al., 2022) is particularly relevant for explicitly addressing the temporal dependence of partitions into the model formulation. However, the current implementation of DRPM's MCMC algorithm, written in C and accessible via an R interface, lacks some significant features. These comprise the inclusion of covariates, that could further improve the generation and informativeness of the clusters, the handling of missing data, and an efficient implementation that would accelerate the fitting process.

In this work, we aim to tackle these three issues by increasing the flexibility of the original model. We will demonstrate how our updates can lead to improved results and faster execution times.

Chapter 1 provides a brief overview of the literature on Bayesian clustering models for spatio-temporal data, followed by an in-depth analysis and description of the Dependent Random Partition Model and our proposed generalization.

Chapter 2 explores the computational aspects of implementing the MCMC algorithm, motivating our choice of the Julia programming language and discussing various optimization opportunities that emerged during the development process.

In Chapter 3 we evaluate the performance of both the original DRPM formulation and our generalization. We start by comparing their results under identical testing conditions, specifically using the same dataset, hyperparameters values, and MCMC iteration settings. Next, we examine the effectiveness of our updates by considering

fits that involve missing data and fits that incorporate covariates. These experiments will be conducted using both a synthetic and a real-world dataset. Finally, we present a comparative analysis of the computational performances of the two models, detailing execution times with respect to the size of the dataset and the information levels included in the fit.

Finally, in Chapter 4, we briefly review the strengths and drawbacks this work revealed and suggest possible further improvements.

Chapter 1

Description of the model

> *"Come on, gentlemen, why shouldn't we get rid of all this calm reasonableness with one good kick, just so as to send all these logarithms to the devil and be able to live our own lives at our own sweet will?"*
> — Fëdor Dostoevskij, *Notes from the Underground*

Bayesian models for clustering can be grouped into two main classes, each characterized by distinct methodologies and assumptions regarding the underlying data distribution.

The first class of models assumes data points (or random effects) to be independent and identically distributed (i.i.d.) from a mixture density (Bouveyron et al., 2019) (Grün, 2018) (Böhning, 2007), where each mixture component corresponds to a cluster with its cluster-specific parameters. In this way, each observation is assumed to arise from one of the J possible groups which are mixed together in various proportions. For each unit $i = 1, \dots, n$, this relationship can be expressed as

$$f(y_i|\boldsymbol{\pi}, \boldsymbol{\vartheta}_1^\star, \dots, \boldsymbol{\vartheta}_J^\star) = \sum_{j=1}^{J} \pi_j f_j(y_i|\boldsymbol{\vartheta}_j^\star) \tag{1.1}$$

where y_i is the data point corresponding to the i-th observation, $\boldsymbol{\pi}$ represents the set of weights satisfying $\pi_j \in [0, 1]$ for $j = 1, \dots, J$ and $\sum_{j=1}^{J} \pi_j = 1$, $\boldsymbol{\vartheta}_j^\star$ are the cluster-specific parameters, and $f_j(\cdot|\boldsymbol{\vartheta}_j^\star)$ denotes the density function of the j-th cluster (Grazian, 2023).

In this model-based approach, the objective is to estimate the cluster-specific parameters $\boldsymbol{\vartheta}_1^\star, \dots, \boldsymbol{\vartheta}_J^\star$ and the mixing proportions $\pi_1, \dots, \pi_J$. While these estimates can be obtained through algorithmic optimization techniques such as the Expectation-Maximization (EM) algorithm (McLachlan et al., 2008) (Ng et al., 2004) which iteratively refines the estimates of the parameters via maximum likelihood estimation (MLE), a more natural modelling is provided by the Bayesian framework. Bayesian mixture models incorporate prior information about the parameters, facilitating an assessment of uncertainty in the clustering structure (Wade, 2023). In this context, each parameter is treated as a random variable with

an associated prior distribution. This leads (1.1) to be reformulated into

$$\begin{aligned} y_i|c_i, \boldsymbol{\pi}, \boldsymbol{\vartheta}_1^\star, \ldots, \boldsymbol{\vartheta}_J^\star &\overset{\text{iid}}{\sim} f_{c_i}(y_i|\boldsymbol{\vartheta}_{c_i}^\star) \\ c_1, \ldots, c_n &\sim \text{Cat}(\pi_1, \ldots, \pi_J) \\ \boldsymbol{\vartheta}_1^\star, \ldots, \boldsymbol{\vartheta}_J^\star &\overset{\text{iid}}{\sim} F_0 \\ \pi_1, \ldots, \pi_J &\sim \text{Dir}(\gamma_1, \ldots, \gamma_J) \end{aligned} \tag{1.2}$$

where the cluster labels $c_1, \ldots, c_n$ are assigned a multinomial distribution with probabilities defined by the vector of weights $\boldsymbol{\pi}$, the cluster-specific parameters $\boldsymbol{\vartheta}_j^\star$ are assigned a prior distribution F_0, and the weights are assigned a Dirichlet distribution characterized by parameters γ_j which regulate the information incorporated into the model about prior cluster assignments (Grazian, 2023). The clustering labels c_i, which identify the component of the mixture each unit is associated to, define the clustering of the units.

However, the Bayesian framework is notably powerful and accommodates more complex formulations. In fact, for the second class of models, we transition to a Bayesian non-parametric context wherein an infinite mixture model can be introduced. This model does not necessitate a predetermined number J of components, leading to a formulation in which the likelihood of each unit is assigned conditioned to a random parameter, namely

$$\begin{aligned} y_i|\boldsymbol{\vartheta}_i &\overset{\text{ind}}{\sim} f(y_i|\boldsymbol{\vartheta}_i) \\ \boldsymbol{\vartheta}_1, \ldots, \boldsymbol{\vartheta}_n|P &\overset{\text{iid}}{\sim} P \\ P &\sim \text{discrete RPM} \end{aligned} \tag{1.3}$$

where RPM denotes a random probability measure (Grazian, 2023). The discreteness of P implies the existence of ties among the parameters $\boldsymbol{\vartheta}_1, \ldots, \boldsymbol{\vartheta}_n$ which induce a partition ρ_n identifiable by units that exhibit identical values of the parameter $\boldsymbol{\vartheta}_i$. More precisely, letting $\boldsymbol{\vartheta}_1^\star, \ldots, \boldsymbol{\vartheta}_K^\star$ represent the unique values of $\boldsymbol{\vartheta}_1, \ldots, \boldsymbol{\vartheta}_n$, the generic h-cluster can be defined as $S_h = \{i \in \{1, \ldots, n\} : \boldsymbol{\vartheta}_i = \boldsymbol{\vartheta}_h^\star\}$. Therefore, is second class of models specifies the conditional distribution of data points given a realization of the partition of the units, and a prior is assigned to this partition by means of the discreteness of the RPM.

One of the principal tools employed in infinite mixture models is the Dirichlet process (DP) (Ferguson, 1973). This allows for modelling the discrete RPM in (1.3) as $P|\alpha, P_0 \sim DP(\alpha, P_0)$, where P_0 is the base distribution and α is the concentration parameter. The Dirichlet process plays a significant role in Bayesian nonparametrics in general, but particularly in clustering. Its effectiveness is also secured by the various implementation possibilities given by the stick-breaking representation (Teh, 2010), the Pólya urn representation (Blackwell et al., 1973), and the Chinese restaurant process (CRP) (Aldous, 1985).

Implementing Bayesian models requires the design of Markov Chain Monte Carlo (MCMC) algorithms, which can often be complex and computationally intensive. In MCMC algorithms, complicated or impossible analytical calculations are replaced by simulated approximations (Franzén, 2008) derived from a Markov

chain that ultimately generates samples from the posterior distribution of the model parameters, allowing inference on the generated clusters (A. Gelman et al., 2003) (Robert et al., 2000). The iterative nature of MCMC, along with the need for a burn-in period to allow convergence of the chain to its stationary distribution, implies that considerable computational resources may be needed, particularly for models with high-dimensional parameter spaces or when working with large datasets.

In summary, while Bayesian methods offer a robust framework for modelling uncertainty and incorporating prior knowledge, they also demand substantial computational effort and expertise in algorithm design to fully realize their potential.

The effectiveness of Bayesian model-based approaches, along with their computational demands, becomes particularly pronounced when applied to spatio-temporal datasets. Such data, characterized by observations collected over time and across various spatial locations, is inherently complex due to the interplay between spatial and temporal dimensions; a complexity that is further compounded when covariates are also available.

Recently, the use of Bayesian models for clustering has gained popularity, especially in the context of spatio-temporal datasets. Bayesian clustering models facilitate the incorporation of prior information into the model, thereby enhancing both flexibility of the formulation and interpretability of the results. Over the years, several models have been proposed in the Bayesian literature; among these, the Dependent Random Partition Model (DRPM) (Garrit L. Page et al., 2022) is particularly relevant for explicitly addressing in its formulation the temporal dependencies among the partitions. This characteristic allows for a more effective identification of trends over time, resulting in clusters that evolve in a more gentle and interpretable way.

Several Bayesian models that establish temporal correlations among sequences of random probability measures have been developed (Nieto-Barajas et al., 2012) (Antoniano Villalobos et al., 2015) (Gutiérrez et al., 2016) (Jo et al., 2017) (Kalli et al., 2018) (De Iorio and Kottas, 2018) (De Iorio, Favaro, et al., 2019) (Caron et al., 2017). However, these models implement temporal dependence through the atoms or weights associated with the representation of the discrete RPM. Consequently, the induced random partitions typically exhibit only weak dependence; even when the sequence of random probability measures is highly correlated, as there is no guarantee that correlated parameters will yield strong correlations among the partitions themselves (Garrit L. Page et al., 2022). Therefore, when the sequence of partitions is the primary inferential object of interest, it is essential to model these partitions directly rather than relying on induced random partition models as seen in equation (1.3).

We now examine how (Garrit L. Page et al., 2022) modelled the temporal dependence within the sequence of partitions, which will lead to the formulation of the Dependent Random Partition Model presented in (1.8). First, we define the notation employed throughout this work. We consider a spatio-temporal context where there are n units to be clustered at all time points $t = 1, \ldots, T$. Each unit is represented as $i = 1, \ldots, n$. We denote by $\rho_t = \{S_{1t}, \ldots, S_{k_t t}\}$ the partition

at time t of the n experimental units, composed by k_t clusters. An alternative representation of this partition is possible through cluster labels $\boldsymbol{c}_t = \{c_{1t}, \dots, c_{nt}\}$, with $c_{it} = j$ indicating that unit i belongs to cluster S_{jt}. Finally, we will denote with a $\star$ superscript all the variables or quantities which are cluster-specific.

Introducing temporal dependence in a collection of partitions requires the formulation of a joint probability model for $(\rho_1, \dots, \rho_T)$, denoted as $P(\rho_1, \dots, \rho_T)$. Temporal dependence among the ρ_t's implies that the cluster configuration in ρ_t may be influenced by the cluster configurations found in $\rho_{t-1}, \rho_{t-2}, \dots, \rho_1$. However, this principle is too complex and general to be modelled efficiently; therefore (Garrit L. Page et al., 2022) restricted this temporal connection to a first-order Markovian structure. Specifically, the conditional distribution of ρ_t given all the predecessors $\rho_{t-1}, \rho_{t-2}, \dots, \rho_1$ actually depends only on ρ_{t-1}. This leads to the construction of the joint probability model for $(\rho_1, \dots, \rho_T)$ as

$$P(\rho_1, \dots, \rho_T) = P(\rho_T|\rho_{T-1}) \cdots P(\rho_2|\rho_1)P(\rho_1) \tag{1.4}$$

Here, $P(\rho_1)$ is an exchangeable partition probability function (EPPF), which describes how the n experimental units at time period 1 are grouped into k_1 distinct clusters. A commonly encountered EPPF is that induced by a Dirichlet process, implemented by (Garrit L. Page et al., 2022) through a Chinese restaurant process (CRP) (De Blasi et al., 2015). The EPPF used is given by the following product partition model (PPM) structure

$$P(\rho_1|M) \propto \prod_{j=1}^{k_1} M \cdot (|S_j| - 1)! \tag{1.5}$$

where k_1 denotes the number of clusters in ρ_1 and M is a concentration parameter that controls the number of clusters. Sections 1.2 and 1.3 will detail how this EPPF can be adapted to incorporate spatial and covariates information.

To characterize the other terms $P(\rho_t|\rho_{t-1})$ in (1.4) (whose derivation will be detailed in Section 1.1), the following auxiliary variables need to be introduced to explicitly model how ρ_{t-1} influences ρ_t. For all units $i = 1, \dots, n$ we define

$$\gamma_{it} = \begin{cases} 1 & \text{if unit } i \text{ is } \textit{not} \text{ reallocated when moving from time } t-1 \text{ to } t \\ 0 & \text{otherwise (namely, unit } \textit{is} \text{ reallocated)} \end{cases} \tag{1.6}$$

These parameters model the similarity between ρ_{t-1} and ρ_t. If the partitions ρ_{t-1} and ρ_t are highly dependent, their cluster configurations will change minimally, resulting in only a few of the n experimental units changing their cluster assignments. Conversely, partitions exhibiting low dependence will likely manifest significantly different cluster configurations, leading to a majority of the units being reallocated.

By construction, we set $\gamma_{i1} = 0$ for all i, meaning that at the first time instant all units will get reallocated since there is no partition at time $t = 0$. (Garrit L. Page et al., 2022) assume $\gamma_{it} \overset{\text{ind}}{\sim} \text{Ber}(\alpha_t)$ where $\alpha_t \in [0, 1]$ serves as a temporal dependence parameter. At one extreme, $\alpha_t = 1$ denotes perfect temporal dependence, with $\rho_t = \rho_{t-1}$; conversely, $\alpha_t = 0$ implies full independence of ρ_t from ρ_{t-1}. The

parameter α_t can be either global (denoted as α), or specific to time and/or unit (represented as α_t, α_i, or α_{it}). For clarity, the vector $\boldsymbol{\gamma}_t = (\gamma_{1t}, \ldots, \gamma_{nt})$ is introduced, so that the T pairs of parameters $(\boldsymbol{\gamma}_j, \rho_j)$ get explicitly reported in the augmented formulation of the joint model (1.4), which becomes

$$P(\boldsymbol{\gamma}_1, \rho_1, \ldots, \boldsymbol{\gamma}_T, \rho_T) = P(\rho_T|\boldsymbol{\gamma}_T, \rho_{T-1})P(\boldsymbol{\gamma}_T) \cdots P(\rho_2|\boldsymbol{\gamma}_2, \rho_1)P(\boldsymbol{\gamma}_2)P(\rho_1) \quad (1.7)$$

Once the partition model is specified, there is considerable flexibility in how to define the remainder of the Bayesian model. To facilitate the propagation of temporal dependence throughout the model, an autoregressive AR(1) component is incorporated at both the data level and the cluster-specific parameter level. This approach led (Garrit L. Page et al., 2022) to the model formulation presented in (1.8),

$$\begin{aligned}
Y_{it}|Y_{it-1}, \boldsymbol{\mu}^\star_t, \boldsymbol{\sigma}^{2\star}_t, \boldsymbol{\eta}, \boldsymbol{c}_t &\overset{\text{ind}}{\sim} \mathcal{N}(\mu^\star_{c_{it}t} + \eta_{1i}Y_{it-1}, \sigma^{2\star}_{c_{it}t}(1-\eta^2_{1i})) \\
Y_{i1} &\overset{\text{ind}}{\sim} \mathcal{N}(\mu^\star_{c_{i1}1}, \sigma^{2\star}_{c_{i1}1}) \\
\xi_i = \text{Logit}(\tfrac{1}{2}(\eta_{1i}+1)) &\overset{\text{ind}}{\sim} \text{Laplace}(a, b) \\
(\mu^\star_{jt}, \sigma^\star_{jt}) &\overset{\text{ind}}{\sim} \mathcal{N}(\vartheta_t, \tau^2_t) \times \mathcal{U}(0, A_\sigma) \\
\vartheta_t|\vartheta_{t-1} &\overset{\text{ind}}{\sim} \mathcal{N}((1-\varphi_1)\varphi_0 + \varphi_1\vartheta_{t-1}, \lambda^2(1-\varphi^2_1)) \\
(\vartheta_1, \tau_t) &\overset{\text{iid}}{\sim} \mathcal{N}(\varphi_0, \lambda^2) \times \mathcal{U}(0, A_\tau) \\
(\varphi_0, \varphi_1, \lambda) &\sim \mathcal{N}(m_0, s^2_0) \times \mathcal{U}(-1, 1) \times \mathcal{U}(0, A_\lambda) \\
\{\boldsymbol{c}_t, \ldots, \boldsymbol{c}_T\} &\sim \text{tRPM}(\boldsymbol{\alpha}, M) \text{ with } \alpha_t \overset{\text{iid}}{\sim} \text{Beta}(a_\alpha, b_\alpha)
\end{aligned} \quad (1.8)$$

where Y_{it} denotes the response variable measured at the i-th unit at time t, $\mathcal{N}$ denotes the gaussian distribution, $\mathcal{U}$ denotes the uniform distribution, and $\text{tRPM}(\boldsymbol{\alpha}, M)$ represents the temporal random partition model (1.7) parametrised by $\alpha_1, \ldots, \alpha_T$ and the EPPF in (1.5).

Our generalization of the original DRPM is presented in (1.9), with a visual representation provided in Figure 1.1. Changes and additions that differ from the original model (1.8) are highlighted in dark red.

$$\begin{aligned}
Y_{it}|Y_{it-1}, \boldsymbol{\mu}^\star_t, \boldsymbol{\sigma}^{2\star}_t, \boldsymbol{\eta}, \boldsymbol{c}_t &\overset{\text{ind}}{\sim} \mathcal{N}(\mu^\star_{c_{it}t} + \eta_{1i}Y_{it-1} + \boldsymbol{x}^T_{it}\boldsymbol{\beta}_t, \sigma^{2\star}_{c_{it}t}(1-\eta^2_{1i})) \\
Y_{i1} &\overset{\text{ind}}{\sim} \mathcal{N}(\mu^\star_{c_{i1}1} + \boldsymbol{x}^T_{i1}\boldsymbol{\beta}_1, \sigma^{2\star}_{c_{i1}1}) \\
\boldsymbol{\beta}_t &\overset{\text{ind}}{\sim} \mathcal{N}_p(\boldsymbol{b}, s^2 I) \\
\xi_i = \text{Logit}(\tfrac{1}{2}(\eta_{1i}+1)) &\overset{\text{ind}}{\sim} \text{Laplace}(a, b) \\
(\mu^\star_{jt}, \sigma^{2\star}_{jt}) &\overset{\text{ind}}{\sim} \mathcal{N}(\vartheta_t, \tau^2_t) \times \text{invGamma}(a_\sigma, b_\sigma) \\
\vartheta_t|\vartheta_{t-1} &\overset{\text{ind}}{\sim} \mathcal{N}((1-\varphi_1)\varphi_0 + \varphi_1\vartheta_{t-1}, \lambda^2(1-\varphi^2_1)) \\
(\vartheta_1, \tau^2_t) &\overset{\text{iid}}{\sim} \mathcal{N}(\varphi_0, \lambda^2) \times \text{invGamma}(a_\tau, b_\tau) \\
(\varphi_0, \varphi_1, \lambda^2) &\sim \mathcal{N}(m_0, s^2_0) \times \mathcal{U}(-1, 1) \times \text{invGamma}(a_\lambda, b_\lambda) \\
\{\boldsymbol{c}_t, \ldots, \boldsymbol{c}_T\} &\sim \text{tRPM}(\boldsymbol{\alpha}, M) \text{ with } \alpha_t \overset{\text{iid}}{\sim} \text{Beta}(a_\alpha, b_\alpha)
\end{aligned} \quad (1.9)$$

In our updated formulation, we opted to model the variances $\sigma^{2\star}_{jt}$, τ^2_t, and λ^2 using an inverse gamma distribution instead of the uniform distribution employed originally by (Garrit L. Page et al., 2022). This choice is more sophisticated, as tuning the parameters of an invGamma(a, b) distribution is more complex than simply setting bounds of a $\mathcal{U}(l, u)$. However, our choice should ensure better mixing within the Markov chain. In fact, as will be derived in Section 1.1, the inverse gamma distributions recover conjugacy in the model, allowing for variance updates to be performed using the analytically exact Gibbs sampler rather than relying on the acceptance-rejection method of Metropolis algorithm.

Moreover, we introduced a regression parameter $\boldsymbol{\beta}_t$ in the likelihood, to improve accuracy in the fitted estimates of the target variable. We chose to make this parameter only time-dependent, rather than also unit-dependent, to simplify what is already a quite complex formulation.

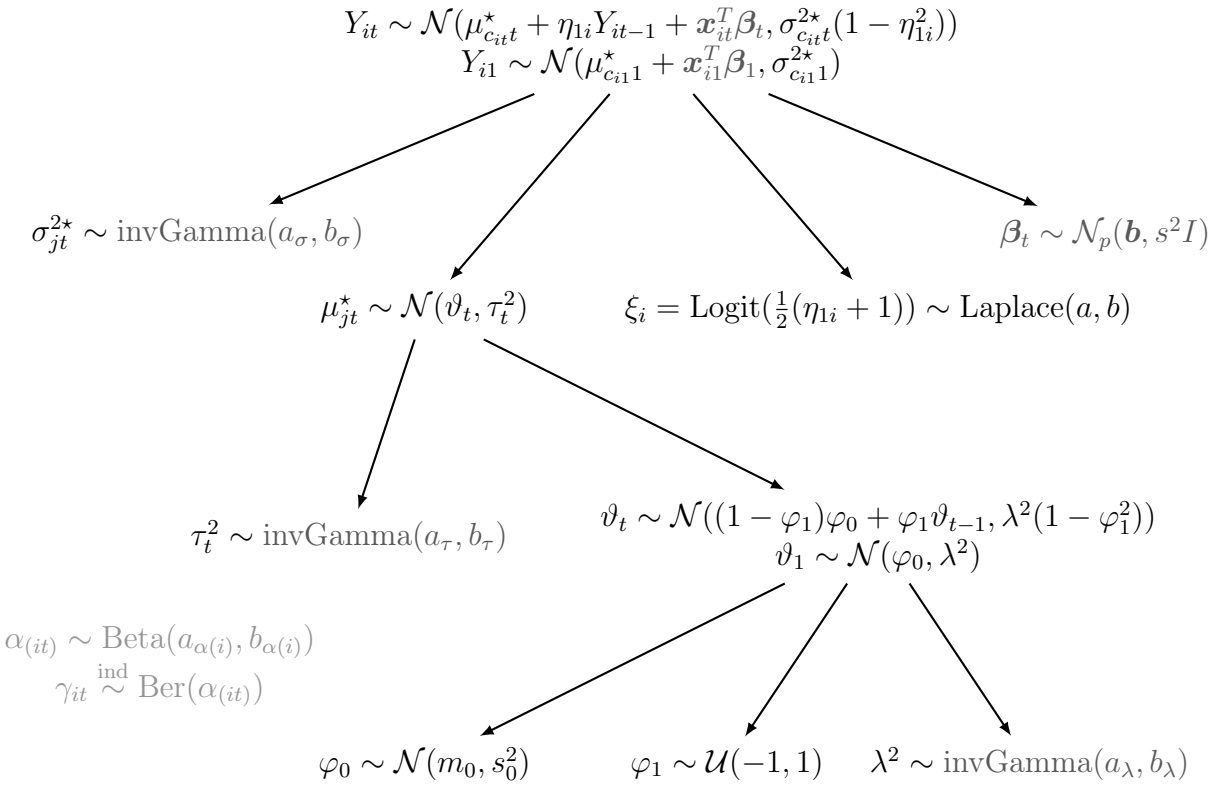

Figure 1.1: Graph visualization of the DRPM model, with highlighted in dark red the changes that we made to the original formulation and in gray the internal variables of the model.

We will now dive deeper into the characteristics of the original DRPM formulation by outlining its associated MCMC algorithm. Subsequently, we will describe how the prior distribution for the partitions $\rho_1, \ldots, \rho_T$ can be augmented with spatial information and, in our generalized model, with covariates, through dedicated cohesions functions and similarities functions respectively. Additionally, we will examine the behaviour of the cohesion and similarity functions proposed in the literature and implemented in our generalized model by conducting experiments using a test case partition.

For the sake of clarity, throughout this work we will refer to CDRPM for the original model formulation by (Garrit L. Page et al., 2022), and to JDRPM for our updated version. The letters C and J denote the programming languages used to implement their corresponding MCMC algorithms: C for the former, Julia for the latter.

1.1 MCMC algorithm

We now detail the MCMC algorithm developed by (Garrit L. Page et al., 2022), which is necessary for sampling from the posterior distributions implied by model (1.8). The MCMC algorithm associated to our generalized model (1.9) required only minor adjustments to the original structure.

To develop the MCMC algorithm, the iterative structure of (1.7) suggests the use of a Gibbs sampler, where $\boldsymbol{\gamma}_t$ and ρ_t are updated sequentially. The Markovian assumption reduces computational costs as we only need to consider ρ_{t-1} and ρ_{t+1} when updating ρ_t. To perform this update, the terms $P(\rho_1)$ and $P(\rho_t|\rho_{t-1})$ of (1.7) need to be clarified. While $P(\rho_1)$ is defined by (1.5), the derivation of $P(\rho_t|\rho_{t-1})$ necessitates the concept of compatibility.

Definition 1.1 (compatibility)**.** Two partitions ρ_t and ρ_{t-1} are said to be *compatible* with respect to $\boldsymbol{\gamma}_t$ if ρ_t can be obtained from ρ_{t-1} by reallocating items as indicated by γ_t; that is, by moving the units i for which $\gamma_{it} = 0$.

To perform this compatibility check, it suffices to ensure that the reduced partitions from ρ_t and ρ_{t-1} are identical. Here, "reduced" refers to the restriction of partitions ρ_t and ρ_{t-1} to the units that cannot move. Indeed, if these fixed units are clustered in the same way, then the free movers from ρ_t can be assigned labels to match the ones assigned in ρ_{t-1}. Denoting the set of fixed units at time t as $\mathfrak{R}_t = \{i : \gamma_{it} = 1\}$, this check translates into verifying that $\rho_t^{\mathfrak{R}_t} = \rho_{t-1}^{\mathfrak{R}_t}$.

This compatibility must be verified during the update steps of parameters γ_{it} and cluster labels c_{it} to ensure that the new sampled draws remain valid and coherent across all partitions and parameters involved. For instance, when updating γ_{it} during each iteration d of the algorithm, potential issues arise when transitioning from $\gamma_{it}^{(d-1)} = 0$ to $\gamma_{it}^{(d)} = 1$. This transition indicates that a unit i previously free to be reassigned (according to the parameters from the previous iteration) is now deemed to stay fixed in her cluster. However, this change may conflict with the current sampled values of partitions $\rho_{t-1}^{(d)}$ and $\rho_t^{(d-1)}$. Therefore, compatibility between their reductions to the units in the set $\mathfrak{R}_t \cup \{i\}$ needs to be checked. If this check fails, the tentative update $\gamma_{it}^{(d-1)} = 0 \to \gamma_{it}^{(d)} = 1$ is disallowed, and we enforce $\gamma_{it}^{(d)} = 0$ in the sampling algorithm.

Similar checks are conducted when updating ρ_t. In this step, only units that can actually move, i.e. units with $\gamma_{it} = 0$, are updated, and therefore there are no compatibility issues between ρ_{t-1} and ρ_t. However, since the update of γ_{it} occurs prior to the update of the partition, compatibility must be verified between ρ_t and

ρ_{t+1}. Further details on this updating constraints can be found in the supplementary material of (Garrit L. Page et al., 2022).

Once this compatibility concept is introduced, we can finally derive $P(\rho_t|\rho_{t-1})$. Let $\mathcal{P}$ denote the set of all partitions of the n units and $\mathcal{P}_{C_t} = \{\rho_t \in \mathcal{P} : \rho_{t-1}^{\Re_t} = \rho_t^{\Re_t}\}$ the collection of partitions at time t that are compatible with ρ_{t-1} based on $\boldsymbol{\gamma}_t$. Then, by construction, we find that $P(\rho_t|\rho_{t-1})$ is a random partition distribution with support $\mathcal{P}_{C_t}$ and density

$$P(\rho_t = \lambda|\boldsymbol{\gamma}_t, \rho_{t-1}) = \frac{P(\rho_t = \lambda)\mathbb{1}_{[\lambda\in\mathcal{P}_{C_t}]}}{\sum_{\lambda'} P(\rho_t = \lambda')\mathbb{1}_{[\lambda'\in\mathcal{P}_{C_t}]}}$$

While this formulation is not statistically appealing, (Garrit L. Page et al., 2022) proved that, under the construction outlined thus far, marginally $\rho_1, \ldots, \rho_T$ are identically distributed with law derived from the EPPF used to model ρ_1. This result, along with the previously outlined compatibility analysis, enables the derivation of the complete update rules rules for γ_{it} and c_{it}.

Once the sampling scheme for γ_{it} and ρ_t is established, updating the other parameters becomes straightforward. Each parameter will either require a Gibbs step (Geman et al., 1984) (Tanner et al., 1987) or a Metropolis step (Metropolis et al., 1953), depending on the conjugacy of the prior associated with that parameter.

We now report the update rules for all parameters involved in our generalized model JDRPM, presented in (1.9), detailing the differences compared to the original CDRPM formulation (1.8). The derivation of the following full conditionals, with the extended calculations provided in Appendix A, was theoretically straightforward, relying on the principle that *posterior* $\propto$ *likelihood* $\cdot$ *prior*. However, we followed useful suggestions and tricks from (Duncan, 2016).

- update $\sigma_{jt}^{2\star}$. This full conditional derivation is characteristic of JDRPM only, since in CDRPM the variance had a uniform law and was therefore updated through a Metropolis step.

  for $t = 1$: $f(\sigma_{jt}^{2\star}|-) \propto$ kernel of a invGamma$(a_{\sigma(\text{post})}, b_{\sigma(\text{post})})$ with

  $$a_{\tau(\text{post})} = a_\sigma + \frac{|S_{jt}|}{2} \quad b_{\tau(\text{post})} = b_\sigma + \frac{1}{2}\sum_{i\in S_{jt}}(Y_{it} - \mu_{jt}^\star - \boldsymbol{x}_{it}^T\boldsymbol{\beta}_t)^2$$

  for $t > 1$: $f(\sigma_{jt}^{2\star}|-) \propto$ kernel of a invGamma$(a_{\sigma(\text{post})}, b_{\sigma(\text{post})})$ with

  $$a_{\tau(\text{post})} = a_\sigma + \frac{|S_{jt}|}{2} \quad b_{\tau(\text{post})} = b_\sigma + \frac{1}{2}\sum_{i\in S_{jt}}(Y_{it} - \mu_{jt}^\star - \eta_{1i}Y_{it-1} - \boldsymbol{x}_{it}^T\boldsymbol{\beta}_t)^2 \tag{1.10}$$

- update $\mu_{jt}^\star$. The update rule is the same for both JDRPM and CDRPM, and requires a Gibbs step defined by the following full conditional.

  for $t = 1$: $f(\mu_{jt}^\star|-) \propto$ kernel of a $\mathcal{N}(\mu_{\mu_{jt}^\star(\text{post})}, \sigma^2_{\mu_{jt}^\star(\text{post})})$ with

  $$\sigma^2_{\mu_{jt}^\star(\text{post})} = \frac{1}{\frac{1}{\tau_t^2} + \frac{|S_{jt}|}{\sigma_{jt}^{2\star}}} \quad \mu_{\mu_{jt}^\star(\text{post})} = \sigma^2_{\mu_{jt}^\star(\text{post})}\left(\frac{\vartheta_t}{\tau_t^2} + \frac{\sum_{i\in S_{jt}}(Y_{i1} - \boldsymbol{x}_{it}^T\boldsymbol{\beta}_t)}{\sigma_{jt}^{2\star}}\right)$$

for $t > 1$: $f(\mu^\star_{jt}|-) \propto$ kernel of a $\mathcal{N}(\mu_{\mu^\star_{jt}(\text{post})}, \sigma^2_{\mu^\star_{jt}(\text{post})})$ with

$$\sigma^2_{\mu^\star_{jt}(\text{post})} = \frac{1}{\frac{1}{\tau_t^2} + \frac{\sum_{i\in S_{jt}} \frac{1}{1-\eta_{1i}^2}}{\sigma^{2\star}_{jt}}} \quad \mu_{\mu^\star_{jt}(\text{post})} = \sigma^2_{\mu^\star_{jt}(\text{post})} \left(\frac{\vartheta_t}{\tau_t^2} + \frac{\sum_{i\in S_{jt}} \frac{Y_{it} - \eta_{1i} Y_{i,t-1} - \boldsymbol{x}_{it}^T \boldsymbol{\beta}_t}{1-\eta_{1i}^2}}{\sigma^{2\star}_{jt}} \right) \tag{1.11}$$

- update $\boldsymbol{\beta}_t$. This full conditional derivation is characteristic of JDRPM only, since the insertion of a regression term in the likelihood is a feature introduced by our generalized model.

  for $t = 1$: $f(\boldsymbol{\beta}_t|-) \propto$ kernel of a $\mathcal{N}(\boldsymbol{b}_{(\text{post})}, A_{(\text{post})})$ with

  $$A_{(\text{post})} = \left(\frac{1}{s^2} I + \sum_{i=1}^n \frac{\boldsymbol{x}_{it} \boldsymbol{x}_{it}^T}{\sigma^{2\star}_{c_{it}t}} \right)^{-1} \quad \boldsymbol{b}_{(\text{post})} = A_{(\text{post})} \left(\frac{\boldsymbol{b}}{s^2} + \sum_{i=1}^n \frac{(Y_{it} - \mu^\star_{c_{it}t}) \boldsymbol{x}_{it}}{\sigma^{2\star}_{c_{it}t}} \right)$$

  i.e. $f(\boldsymbol{\beta}_t|-) \propto$ kernel of a $\mathcal{N}\text{Canon}(\boldsymbol{h}_{(\text{post})}, J_{(\text{post})})$ with

  $$\boldsymbol{h}_{(\text{post})} = \left(\frac{\boldsymbol{b}}{s^2} + \sum_{i=1}^n \frac{(Y_{it} - \mu^\star_{c_{it}t}) \boldsymbol{x}_{it}}{\sigma^{2\star}_{c_{it}t}} \right) \quad J_{(\text{post})} = \left(\frac{1}{s^2} I + \sum_{i=1}^n \frac{\boldsymbol{x}_{it} \boldsymbol{x}_{it}^T}{\sigma^{2\star}_{c_{it}t}} \right)$$

  for $t > 1$: $f(\boldsymbol{\beta}_t|-) \propto$ kernel of a $\mathcal{N}(\boldsymbol{b}_{(\text{post})}, A_{(\text{post})})$ with

  $$A_{(\text{post})} = \left(\frac{1}{s^2} I + \sum_{i=1}^n \frac{\boldsymbol{x}_{it} \boldsymbol{x}_{it}^T}{\sigma^{2\star}_{c_{it}t}} \right)^{-1} \quad \boldsymbol{b}_{(\text{post})} = A_{(\text{post})} \left(\frac{\boldsymbol{b}}{s^2} + \sum_{i=1}^n \frac{(Y_{it} - \mu^\star_{c_{it}t} - \eta_{1i} Y_{it-1}) \boldsymbol{x}_{it}}{\sigma^{2\star}_{c_{it}t}} \right)$$

  i.e. $f(\boldsymbol{\beta}_t|-) \propto$ kernel of a $\mathcal{N}\text{Canon}(\boldsymbol{h}_{(\text{post})}, J_{(\text{post})})$ with

  $$\boldsymbol{h}_{(\text{post})} = \left(\frac{\boldsymbol{b}}{s^2} + \sum_{i=1}^n \frac{(Y_{it} - \mu^\star_{c_{it}t} - \eta_{1i} Y_{it-1}) \boldsymbol{x}_{it}}{\sigma^{2\star}_{c_{it}t}} \right) \quad J_{(\text{post})} = \left(\frac{1}{s^2} I + \sum_{i=1}^n \frac{\boldsymbol{x}_{it} \boldsymbol{x}_{it}^T}{\sigma^{2\star}_{c_{it}t}} \right) \tag{1.12}$$

  Here $\mathcal{N}\text{Canon}(\boldsymbol{h}, J)$ is the canonical formulation of the $\mathcal{N}(\boldsymbol{\mu}, \Sigma)$, with $\boldsymbol{h} = \Sigma^{-1}\boldsymbol{\mu}$ and $J = \Sigma^{-1}$. This other distribution facilitates the sampling, since these full conditional computations allow to derive directly the parameters of the canonical one, e.g. the inverse of the variance matrix rather than the variance matrix itself; and therefore sampling through it does not require any inversion of matrices which would produce more computational load, numerical instabilities, and loss of accuracy. As a consequence, in Julia we can write `rand(MvNormalCanon(h_star, J_star))` rather than the riskier one `rand(MvNormal(inv(J_star)*h_star, inv(J_star)))`; which apart from the previously mentioned disadvantages would be a statistically equivalent form.

- update η_{1i}. The update rule is the same for both JDRPM and CDRPM, and requires a Metropolis step.

- update τ_t^2. This full conditional derivation is characteristic of JDRPM only, since in CDRPM the variance had a uniform law and was therefore updated through a Metropolis step.

  $$f(\tau_t^2|-) \propto \text{kernel of a invGamma}(a_{\tau(\text{post})}, b_{\tau(\text{post})}) \text{ with}$$

$$a_{\tau(\text{post})} = \frac{k_t}{2} + a_\tau \quad b_{\tau(\text{post})} = \frac{\sum_{j=1}^{k_t}(\mu^\star_{jt} - \vartheta_t)^2}{2} + b_\tau \tag{1.13}$$

- update ϑ_t. The update rule is the same for both JDRPM and CDRPM, and requires a Gibbs step defined by the following full conditional.

$$\begin{aligned}
&\text{for } t = T\text{: } f(\vartheta_t|-) \propto \text{kernel of a } \mathcal{N}(\mu_{\vartheta_t(\text{post})}, \sigma^2_{\vartheta_t(\text{post})}) \text{ with}\\
&\sigma^2_{\vartheta_t(\text{post})} = \frac{1}{\frac{1}{\lambda^2(1-\varphi_1^2)} + \frac{k_t}{\tau_t^2}}\\
&\mu_{\vartheta_t(\text{post})} = \sigma^2_{\vartheta_t(\text{post})}\left(\frac{\sum_{j=1}^{k_t}\mu^\star_{jt}}{\tau_t^2} + \frac{(1-\varphi_1)\varphi_0 + \varphi_1\vartheta_{t-1}}{\lambda^2(1-\varphi_1^2)}\right)\\
&\text{for } 1 < t < T\text{: } f(\vartheta_t|-) \propto \text{kernel of a } \mathcal{N}(\mu_{\vartheta_t(\text{post})}, \sigma^2_{\vartheta_t(\text{post})}) \text{ with}\\
&\sigma^2_{\vartheta_t(\text{post})} = \frac{1}{\frac{1+\varphi_1^2}{\lambda^2(1-\varphi_1^2)} + \frac{k_t}{\tau_t^2}}\\
&\mu_{\vartheta_t(\text{post})} = \sigma^2_{\vartheta_t(\text{post})}\left(\frac{\sum_{j=1}^{k_t}\mu^\star_{jt}}{\tau_t^2} + \frac{\varphi_1(\vartheta_{t-1}+\vartheta_{t+1}) + \varphi_0(1-\varphi_1)^2}{\lambda^2(1-\varphi_1^2)}\right)\\
&\text{for } t = 1\text{: } f(\vartheta_t|-) \propto \text{kernel of a } \mathcal{N}(\mu_{\vartheta_t(\text{post})}, \sigma^2_{\vartheta_t(\text{post})}) \text{ with}\\
&\sigma^2_{\vartheta_t(\text{post})} = \frac{1}{\frac{1}{\lambda^2} + \frac{\varphi_1^2}{\lambda^2(1-\varphi_1^2)} + \frac{k_t}{\tau_t^2}}\\
&\mu_{\vartheta_t(\text{post})} = \sigma^2_{\vartheta_t(\text{post})}\left(\frac{\varphi_0}{\lambda^2} + \frac{\varphi_1(\vartheta_{t+1} - (1-\varphi_1)\varphi_0)}{\lambda^2(1-\varphi_1^2)} + \frac{\sum_{j=1}^{k_t}\mu^\star_{jt}}{\tau_t^2}\right)
\end{aligned} \tag{1.14}$$

- update φ_0. The update rule is also the same for both JDRPM and CDRPM, and requires a Gibbs step defined by the following full conditional.

$$\begin{aligned}
&f(\varphi_0|-) \propto \text{kernel of a } \mathcal{N}(\mu_{\varphi_0(\text{post})}, \sigma^2_{\varphi_0(\text{post})}) \text{ with}\\
&\sigma^2_{\varphi_0(\text{post})} = \frac{1}{\frac{1}{s_0^2} + \frac{1}{\lambda^2} + \frac{(T-1)(1-\varphi_1)^2}{\lambda^2(1-\varphi_1^2)}}\\
&\mu_{\varphi_0(\text{post})} = \sigma^2_{\varphi_0(\text{post})}\left(\frac{m_0}{s_0^2} + \frac{\vartheta_1}{\lambda^2} + \frac{1-\varphi_1}{\lambda^2(1-\varphi_1^2)}\sum_{t=2}^{T}(\vartheta_t - \varphi_1\vartheta_{t-1})\right)
\end{aligned} \tag{1.15}$$

- update λ^2. This full conditional derivation is characteristic of JDRPM only, since in CDRPM the variance had a uniform law and was therefore updated through a Metropolis step.

$$\begin{aligned}
&f(\lambda^2|-) \propto \text{kernel of a invGamma}(a_{\lambda(\text{post})}, b_{\lambda(\text{post})}) \text{ with}\\
&a_{\lambda(\text{post})} = \frac{T}{2} + a_\lambda\\
&b_{\lambda(\text{post})} = \frac{(\vartheta_1 - \varphi_0)^2}{2} + \sum_{t=2}^{T}\frac{(\vartheta_t - (1-\varphi_1)\varphi_0 - \varphi_1\vartheta_{t-1})^2}{2} + b_\lambda
\end{aligned} \tag{1.16}$$

- update α. The update rule is the same for both JDRPM and CDRPM, and requires a Gibbs step defined by the following full conditional.

$$\text{if global } \alpha\text{: } f(\alpha|-) \propto \text{kernel of a Beta}(a_{\alpha(\text{post})}, b_{\alpha(\text{post})}) \text{ with}$$
$$a_{\alpha(\text{post})} = a_\alpha + \sum_{i=1}^{n}\sum_{t=1}^{T}\gamma_{it} \quad b_{\alpha(\text{post})} = b_\alpha + nT - \sum_{i=1}^{n}\sum_{t=1}^{T}\gamma_{it}$$
$$\text{if time specific } \alpha\text{: } f(\alpha_t|-) \propto \text{kernel of a Beta}(a_{\alpha(\text{post})}, b_{\alpha(\text{post})}) \text{ with}$$
$$a_{\alpha(\text{post})} = a_\alpha + \sum_{i=1}^{n}\gamma_{it} \quad b_{\alpha(\text{post})} = b_\alpha + n - \sum_{i=1}^{n}\gamma_{it}$$
$$\text{if unit specific } \alpha\text{: } f(\alpha_i|-) \propto \text{kernel of a Beta}(a_{\alpha(\text{post})}, b_{\alpha(\text{post})}) \text{ with}$$
$$a_{\alpha(\text{post})} = a_{\alpha i} + \sum_{t=1}^{T}\gamma_{it} \quad b_{\alpha(\text{post})} = b_{\alpha i} + T - \sum_{t=1}^{T}\gamma_{it}$$
$$\text{if time and unit specific } \alpha\text{: } f(\alpha_{it}|-) \propto \text{kernel of a Beta}(a_{\alpha(\text{post})}, b_{\alpha(\text{post})}) \text{ with}$$
$$a_{\alpha(\text{post})} = a_{\alpha i} + \gamma_{it} \quad b_{\alpha(\text{post})} = b_{\alpha i} + 1 - \gamma_{it} \tag{1.17}$$

- update a missing observation Y_{it}. This full conditional derivation is characteristic of JDRPM only, since the handling of missing data feature introduced by our generalized model. Experiments conducted in Sections 3.2.2 and 3.3.1 will confirm the correctness of this derivation.

$$\text{for } t = 1\text{: } f(Y_{it}|-) \propto \mathcal{N}(\mu_{Y_{it}(\text{post})}, \sigma^2_{Y_{it}(\text{post})}) \text{ with}$$
$$\sigma^2_{Y_{it}(\text{post})} = \frac{1}{\frac{1}{\sigma^{2\star}_{c_{it}t}} + \frac{\eta^2_{1i}}{2\sigma^{2\star}_{c_{it+1}t+1}(1-\eta^2_{1i})}}$$
$$\mu_{Y_{it}(\text{post})} = \sigma^2_{Y_{it}(\text{post})}\left(\frac{\mu^\star_{c_{it}t} + \boldsymbol{x}^T_{it}\boldsymbol{\beta}_t}{\sigma^{2\star}_{c_{it}t}} + \frac{\eta_{1i}(Y_{it+1} - \mu^\star_{c_{it+1}t+1} - \boldsymbol{x}^T_{it+1}\boldsymbol{\beta}_{t+1})}{\sigma^{2\star}_{c_{it+1}t+1}(1-\eta^2_{1i})}\right)$$
$$\text{for } 1 < t < T\text{: } f(Y_{it}|-) \propto \mathcal{N}(\mu_{Y_{it}(\text{post})}, \sigma^2_{Y_{it}(\text{post})}) \text{ with}$$
$$\sigma^2_{Y_{it}(\text{post})} = \frac{1-\eta^2_{1i}}{\frac{1}{\sigma^{2\star}_{c_{it}t}} + \frac{\eta^2_{1i}}{\sigma^{2\star}_{c_{it+1}t+1}}}$$
$$\mu_{Y_{it}(\text{post})} = \sigma^2_{Y_{it}(\text{post})}\left(\frac{\mu^\star_{c_{it}t} + \eta_{1i}Y_{it-1} + \boldsymbol{x}^T_{it}\boldsymbol{\beta}_t}{\sigma^{2\star}_{c_{it}t}(1-\eta^2_{1i})} + \frac{\eta_{1i}(Y_{it+1} - \mu^\star_{c_{it+1}t+1} - \boldsymbol{x}^T_{it+1}\boldsymbol{\beta}_{t+1})}{\sigma^{2\star}_{c_{it+1}t+1}(1-\eta^2_{1i})}\right)$$
$$\text{for } t = T\text{: } f(Y_{it}|-) \text{ is just the likelihood of } Y_{it} \tag{1.18}$$

- update φ_1. The update rule is the same for both JDRPM and CDRPM, and requires a Metropolis step.

Finally, in Algorithm 1 we provide a brief outline of the steps involved in the MCMC sampling algorithm for our generalized model. The computation of the LPML and WAIC metrics follows established methodologies from (Christensen et al., 2010) and (Andrew Gelman et al., 2013)

Algorithm 1: Pseudocode for the MCMC fitting algorithm of our generalized model (1.9).

```
for d = 1, ..., draws do
    if target variable has missing values then
        update the missing Y_it's using (1.18)
    end
    for t = 1, ..., T do
        for i = 1, ..., n do
            if t = 1 then
                γ_it = 0
            else
                update γ_it
            end
        end
        for i ∈ {ξ : γ_ξt = 0} do
            update c_it (i.e. update ρ_t)
        end
        update μ*_jt using (1.11)
        update σ²*_jt using (1.10)
        if are there covariates in the likelihood then
            update β_t using (1.12)
        end
        update ϑ_t using (1.14)
        update τ²_t using (1.13)
    end
    if update_eta = true then
        update η_1i using Metropolis sampling
    end
    if update_alpha = true then
        update α using (1.17)
    end
    update φ_0 using (1.15)
    if update_phi1 = true then
        update φ_1 using Metropolis sampling
    end
    update λ² using (1.16)
    if d > burnin and d % thin = 0 then
        save MCMC current iterate
    end
end
compute LPML and WAIC metrics
```

The core of the clustering process, as we described, involves updating γ_{it} and ρ_t. Their update step is inherently complex, as it necessitates checking for compatibility issues. The approach entails simulating the assignment of each unit i, currently belonging to cluster j, to either one of the existing clusters or to a new singleton cluster. For each scenario, we compute the probability of this assignment to occur, from which we derive weights to inform the sampling decision for the next iteration. Key elements influencing the definition of these weights include spatial cohesions and, in our JDRPM updated formulation, covariate similarities. We will now explore both these functions.

1.2 Spatial cohesions

Based on our generic joint probability model of (1.7), it is straightforward to incorporate additional information into the partition model such as space or covariates. The incorporation of spatial information can be effectively accommodated through the EPPF in our framework, resulting in spatially informed clusters that evolve over time (Garrit L. Page et al., 2022).

To introduce this extension, let $\boldsymbol{s}_i$ denote the spatial coordinates of the i-th (noting that these coordinates do not change over time), and let $\boldsymbol{s}^\star_{jt}$ denote the subset of spatial coordinates of the units belonging to cluster S_{jt}. Then, we can express the EPPF for the t-th partition in the following product form

$$P(\rho_t|M,\mathcal{S}) \propto \prod_{j=1}^{k_t} C(S_{jt}, \boldsymbol{s}^\star_{jt}|M,\mathcal{S}) \tag{1.19}$$

Compared to the original formulation of (1.5), where $P(\rho_t|M) \propto \prod_{j=1}^{k_t} c(S_{jt}|M)$, (1.19) incorporates a spatial component into the partition weights through the spatial cohesion function $C(S_{jt}, \boldsymbol{s}^\star_{jt}|M,\mathcal{S})$. The original term $c(S_{jt}|M)$ describes how units inside cluster S_{jt} are likely to be clustered together a priori, while the cohesion function $C(S_{jt}, \boldsymbol{s}^\star_{jt}|M,\mathcal{S})$, parametrised by a set of parameters $\mathcal{S}$, measures the compactness of the spatial coordinates $\boldsymbol{s}^\star_{jt}$.

With these two functions established, we transition to a spatially informed dependent random partition model, so that in models (1.8) and (1.9) we can replace tRPM($\boldsymbol{\alpha}, M$) with stRPM($\boldsymbol{\alpha}, M, \mathcal{S}$) to denote our spatio-temporal random partition model (1.7) parametrised by $\alpha_1, \ldots, \alpha_T$ and the EPPF in (1.19).

In this section, we will present the different cohesions functions available in both CDRPM and JDRPM implementations. We will discuss their definition and conduct experiments on each cohesion function, to observe how their tuning parameters influence the computed values. For these experiments, we will consider the clusters configuration illustrated in Figure 1.2, which represents the spatial coordinates of the units of the spatio-temporal dataset that will be used in Chapter 3. For visualization purposes, these values will be presented in a log-transformed form to better highlight differences among the weights assigned to each cluster. Moreover, for clarity, we will use the notation S_h to refer to a generic h-th cluster, rather

than the more precise notation S_{jt}, as we now focus on analysing the behaviour of spatial cohesions.

The underlying idea of the following formulas is to favour few spatially connected clusters rather than numerous singleton clusters, thereby yielding more interpretable and meaningful results. In fact, all formulations employ the term $M \cdot \Gamma(|S_h|)$ which is used to encourage a small number of large clusters (Garritt L. Page et al., 2016) and was employed in the original EPPF formulation of (1.5). The he parameter M regulates the number of clusters, as from literature it is known that the expected number of clusters a priori under the DP induced probability distribution on partitions is approximately $M \log\left(\frac{M+n}{M}\right)$ (Garritt L. Page et al., 2016). However, when this term is coupled with other distance penalties, as in the following cases, it becomes unclear how the number of expected clusters a priori grows as a function of M. In our analysis, we considered $M = 1$.

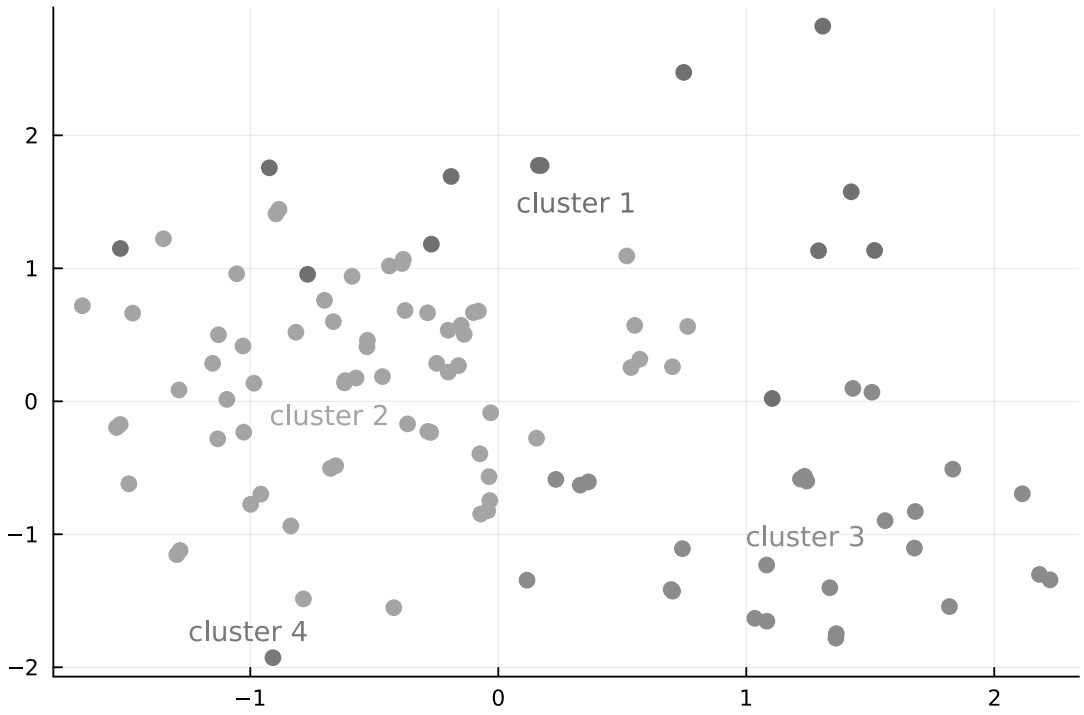

Figure 1.2: Partition considered for the spatial cohesion analysis.

$$C_1(S_h, \boldsymbol{s}_h^\star) = \begin{cases} \dfrac{M \cdot \Gamma(|S_h|)}{\Gamma(\alpha \mathcal{D}_h)\mathbb{1}_{[\mathcal{D}_h \geq 1]} + \mathcal{D}_h \mathbb{1}_{[\mathcal{D}_h < 1]}} & \text{if } |S_h| > 1 \\ M & \text{if } |S_h| = 1 \end{cases} \tag{1.20}$$

The first cohesion function (Denison et al., 2001) considers $\mathcal{D}_h = \sum_{i \in S_h} \|\boldsymbol{s}_i - \bar{\boldsymbol{s}}_h\|$ as the total distance from the units to the cluster centroid $\bar{\boldsymbol{s}}_h$. The definition of this cohesion is an adjustment of a decreasing function in terms of $\mathcal{D}_h$ to assign higher weights to denser clusters, i.e., those with lower values of $\mathcal{D}_h$. The additional parameter α provides control on the level of penalization.

$$C_2(S_h, \boldsymbol{s}_h^\star) = M \cdot \Gamma(|S_h|) \cdot \prod_{i,j \in S_h} \mathbb{1}_{[\|\boldsymbol{s}_i - \boldsymbol{s}_j\| \leq a]} \tag{1.21}$$

The second cohesion function (Garritt L. Page et al., 2016) establishes a hard cluster boundary, assigning a weight of 1 only if all distances between every possible pair of points within the cluster are below the threshold parameter a, i.e. if all units are "close enough" to each other. If even a single pair of points does not meet this criterion, the returned value is 0, reflecting the maximum penalization. The strictness of this requirement can be adjusted through the parameter a.

However, C_1 and C_2 do not preserve the exchangeability property. This means that marginalizing the random partition model over the last of m units does not yield the same model as if only $m-1$ units were considered. This coherence property, known as sample size consistency or addition rule (De Blasi et al., 2015), is often desirable for theoretical or computational purposes. In contrast, the following two cohesion functions are able to provide such property.

$$C_3(S_h, \boldsymbol{s}_h^\star) = M \cdot \Gamma(|S_h|) \cdot \int \prod_{i \in S_h} q(\boldsymbol{s}_i|\boldsymbol{\xi}_h) q(\boldsymbol{\xi}_h)\, d\boldsymbol{\xi}_h \tag{1.22}$$

Cohesion 3 (Müller et al., 2011), referred to as auxiliary similarity function, treats spatial the spatial coordinates $\boldsymbol{s}_i$ as if they were random variables, applying on them a model such as the Normal/Normal-Inverse-Wishart, where $\boldsymbol{\xi} = (\boldsymbol{m}, V)$, $\boldsymbol{s}|\boldsymbol{\xi} \sim \mathcal{N}(\boldsymbol{m}, V)$ and $\boldsymbol{\xi} \sim \mathcal{NIW}(\boldsymbol{\mu}_0, \kappa_0, \nu_0, \Lambda_0)$. This cohesion function assigns a larger weight to clusters that yield larger marginal likelihood values, i.e. clusters which the random model considers more likely to occur.

$$C_4(S_h, \boldsymbol{s}_h^\star) = M \cdot \Gamma(|S_h|) \cdot \int \prod_{i \in S_h} q(\boldsymbol{s}_i|\boldsymbol{\xi}_h) q(\boldsymbol{\xi}_h|\boldsymbol{s}_h^\star)\, d\boldsymbol{\xi}_h \tag{1.23}$$

Cohesion 4 (Quintana et al., 2015), referred to as double dipper cohesion, employs the posterior predictive distribution rather than the prior predictive distribution used in cohesion 3.

$$C_5(S_h, \boldsymbol{s}_h^\star) = M \cdot \Gamma(|S_h|) \cdot \exp\left\{ -\varphi \sum_{i \in S_h} \|\boldsymbol{s}_i - \bar{\boldsymbol{s}}_h\| \right\} \tag{1.24}$$

$$C_6(S_h, \boldsymbol{s}_h^\star) = M \cdot \Gamma(|S_h|) \cdot \exp\left\{ -\varphi \log\left(\sum_{i \in S_h} \|\boldsymbol{s}_i - \bar{\boldsymbol{s}}_h\| \right) \right\} \tag{1.25}$$

The final two cohesions derive from the cluster variance/entropy similarity function (Garritt L. Page et al., 2018), a very general methodology to measure the closeness of a set of values which in fact will come back in the covariates similarities. Similar with cohesion 1, both C_5 and C_6 employ a summary metric that quantifies the the closeness of the spatial coordinates $\boldsymbol{s}_h^\star$ by summing the distances of the units from the cluster centroid. The parameter φ controls the degree to which dissimilar values are penalized.

All these cohesion functions appeared to agree on the ranking of the clusters shown in Figure 1.2. Cohesion 3 and 4, corresponding to Figures 1.5 and 1.6, clearly indicate the order of clusters as orange, green, purple, and blue, sorted from highest to lowest cohesion weight. This ranking is also reflected in the results of the other cohesions; however, different evaluations can emerge by adjusting their associated tuning parameters. For instance, Figures 1.3, 1.7, and 1.8, corresponding to C_1, C_5 and C_6, show how the singleton (purple) cluster tends to receive the highest weight as the penalization parameters increase. In contrast, cohesion 2, illustrated in Figure 1.4, ranks the singleton cluster at the top, followed by the green cluster, being the first among the non-singletons that activates C_2 when increasing its threshold parameter a, and lastly by clusters orange and blue.

1.3 Covariates similarities

The incorporation of covariates information, a characteristic feature of our generalized model, can be integrated into the EPPF (1.19) in a way similar to that used for the spatial information. To introduce this extension, let $X^\star_{jt}$ denote the $p \times |S_{jt}|$ matrix that contains the covariates of the units belonging to cluster S_{jt}, i.e. $X^\star_{jt} = \{\boldsymbol{x}^\star_{it} = (x_{it1}, \dots, x_{itp})^T : i \in S_{jt}\}$. In the current implementation of JDRPM we chose to treat each covariate individually. Therefore, the new term in the definition of the EPPF for $P(\rho_t)$ will be a function of the vector $\boldsymbol{x}^\star_{jtr}$ that collects the values of the r-th covariate for the units inside cluster S_{jt}, i.e. row r of matrix $X^\star_{jt}$. Then, each contribution of the covariates will be considered independently, leading to an EPPF in the form

$$P(\rho_t|M, \mathcal{S}, \mathcal{C}) \propto \prod_{j=1}^{k_t} C(S_{jt}, \boldsymbol{s}^\star_{jt}|M, \mathcal{S}) \left(\prod_{r=1}^{p} g(S_{jt}, \boldsymbol{x}^\star_{jtr}|\mathcal{C}) \right) \tag{1.26}$$

This approach is convenient as it can seamlessly accommodate numerical and categorical covariates. Nonetheless, a unified and multidimensional treatment of the covariates would be possible, with appropriate adjustments to the similarity functions, and would yield an EPPF in the form

$$P(\rho_t|M, \mathcal{S}, \mathcal{C}) \propto \prod_{h=1}^{k_t} C(S_{jt}, \boldsymbol{s}^\star_{jt}|M, \mathcal{S}) g(S_{jt}, X^\star_{jt}|\mathcal{C}) \tag{1.27}$$

We therefore transition to a spatially and covariates-informed dependent random partition model, so that in model (1.9) we can replace tRPM($\boldsymbol{\alpha}, M$) with stRPMx($\boldsymbol{\alpha}, M, \mathcal{S}, \mathcal{C}$) to denote our spatio-temporal covariates-informed random partition model (1.7) parametrised by $\alpha_1, \dots, \alpha_T$ and the EPPF defined in (1.26).

As in the previous section, we will now present the covariates similarity functions implemented in the JDRPM model, discussing their definition and conducting experiments on each function. These experiments refer to the test case partition illustrated in Figure 1.9, which considers the `Altitude` covariate from the spatio-temporal dataset that will be used in Chapter 3. For consistency, we will again employ a simplified notation by omitting spatio-temporal indicators.

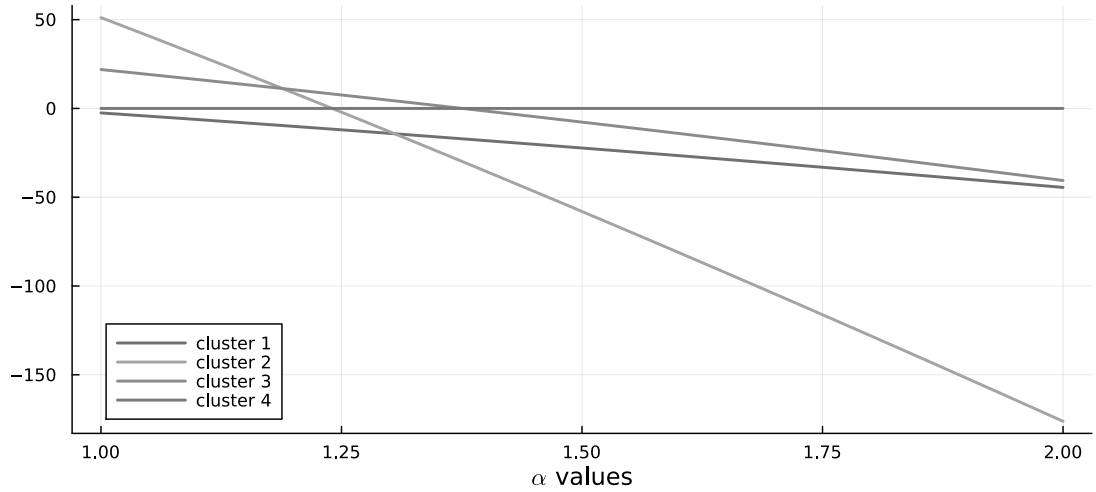

Figure 1.3: Cohesions 1 log-transformed values computed on the test case partition of Figure 1.2, with respect to different values of its tuning parameter α.

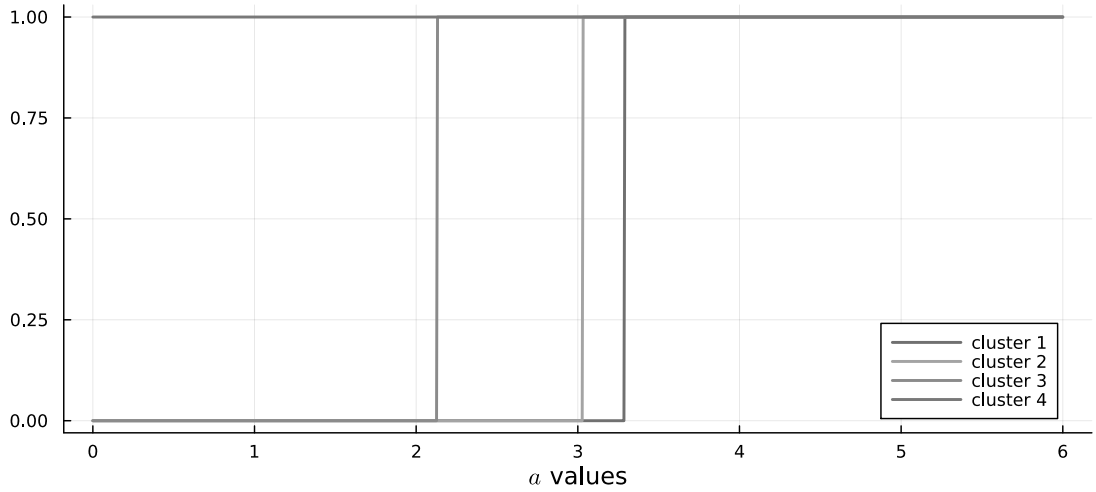

Figure 1.4: Cohesions 2 values computed on the test case partition of Figure 1.2, with respect to different values of its tuning parameter a. The term $M \cdot \Gamma(|S_h|)$ was ignored to highlight the boundary effect which this cohesion provides.

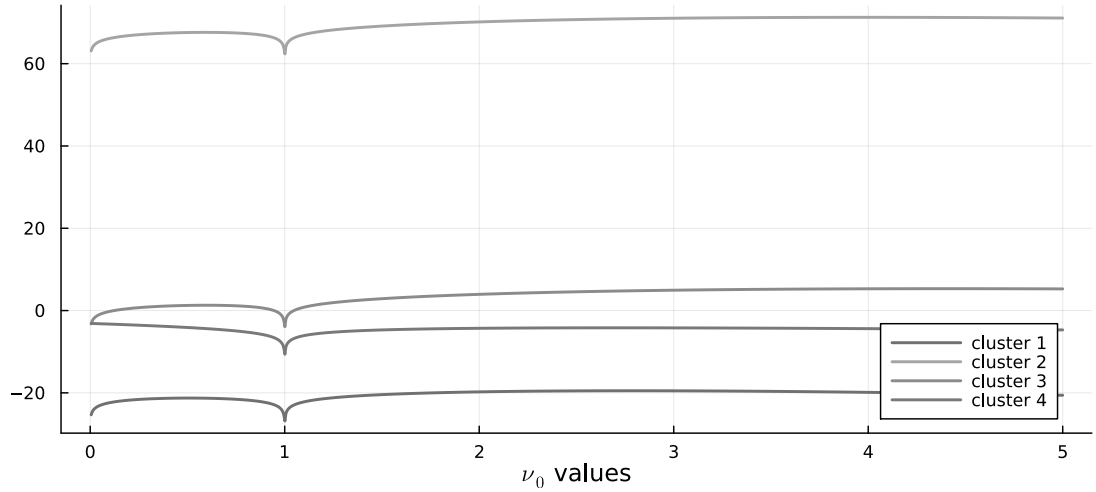

Figure 1.5: Cohesions 3 log-transformed values computed on the test case partition of Figure 1.2, with respect to different values of its tuning parameter ν_0.

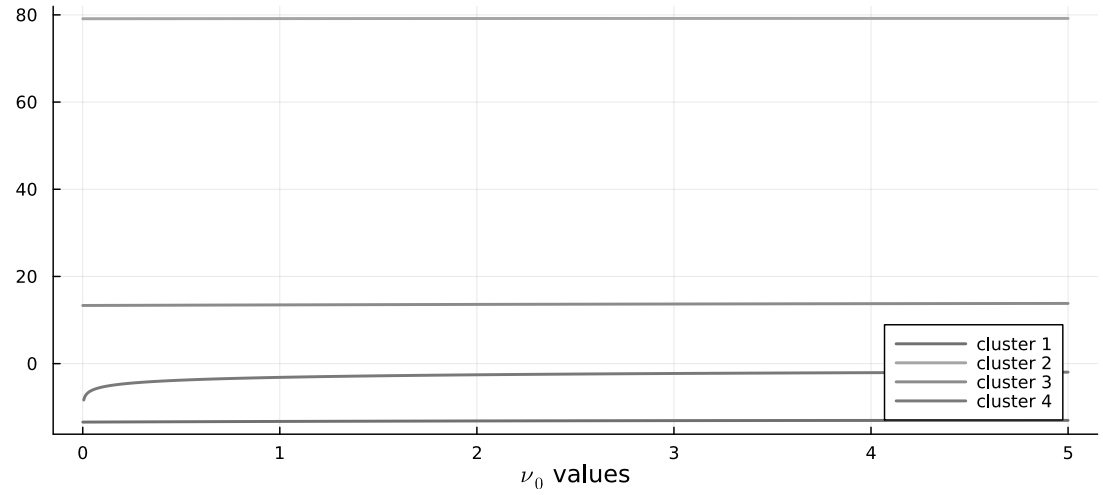

Figure 1.6: Cohesions 4 log-transformed values computed on the test case partition of Figure 1.2, with respect to different values of its tuning parameter ν_0.

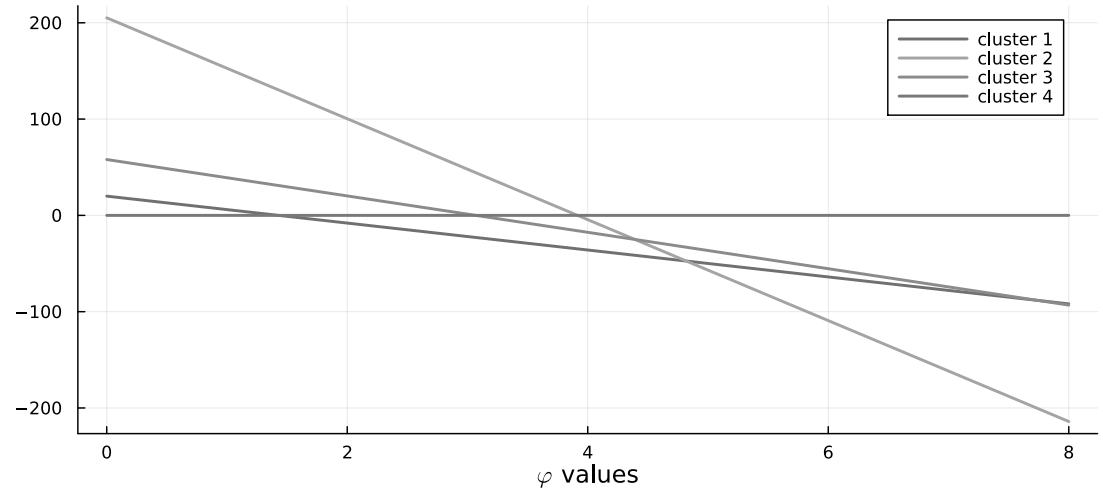

Figure 1.7: Cohesions 5 log-transformed values computed on the test case partition of Figure 1.2, with respect to different values of its tuning parameter φ.

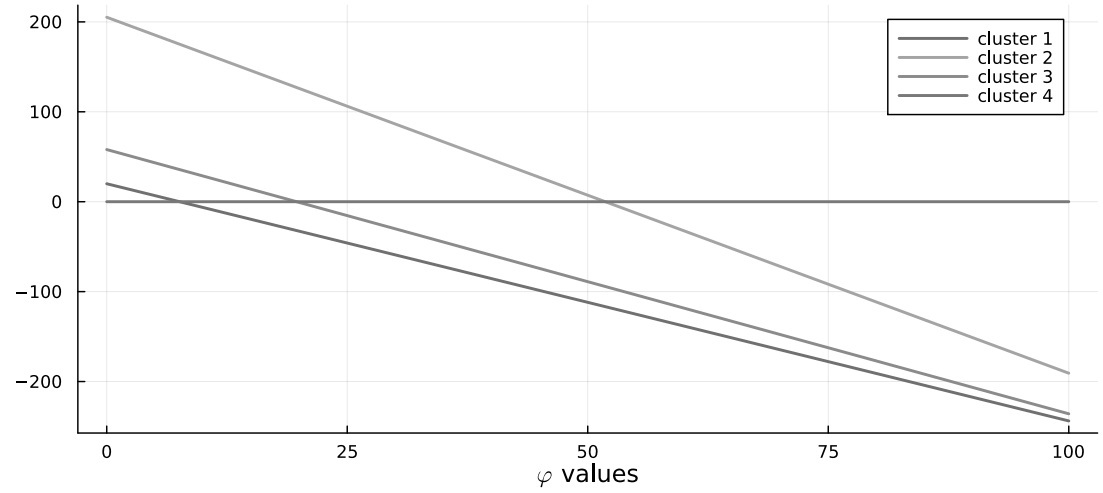

Figure 1.8: Cohesions 6 log-transformed values computed on the test case partition of Figure 1.2, with respect to different values of its tuning parameter φ.

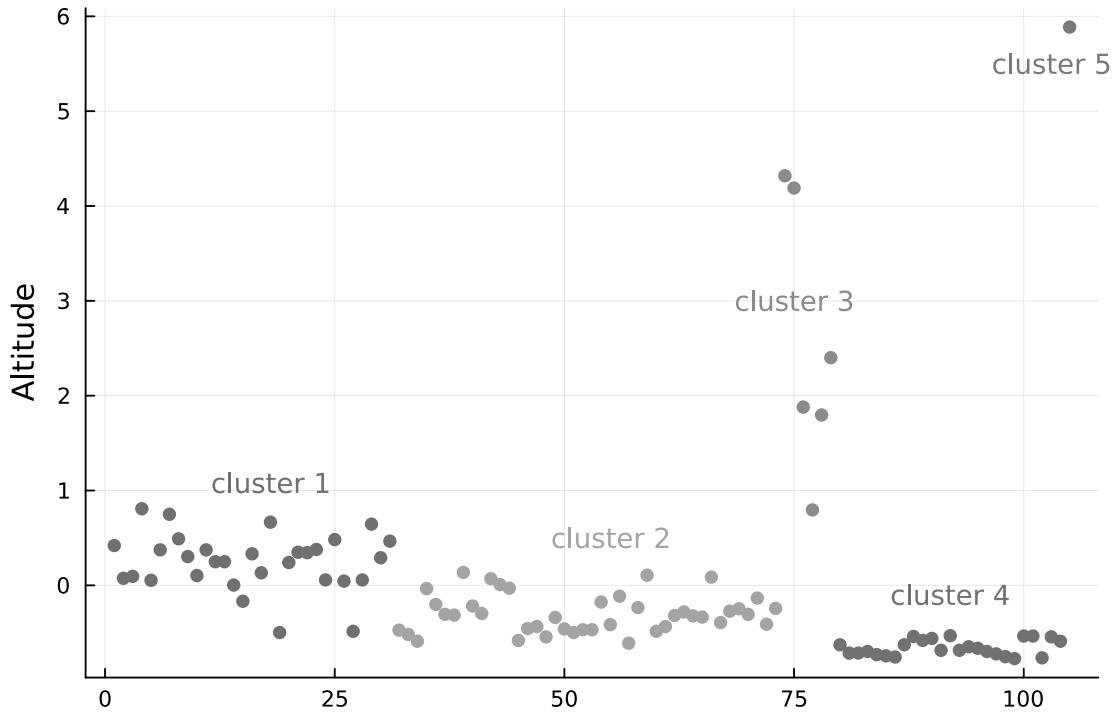

Figure 1.9: Partition considered for the covariate similarity analysis.

The first similarity is the cluster variance/entropy similarity function (Garritt L. Page et al., 2018) which is suitable for both numerical and categorical covariates.

$$g_1(S_h, \boldsymbol{x}_h^\star) = \exp\left\{-\varphi H(S_h, \boldsymbol{x}_h^\star)\right\} \tag{1.28}$$

Here, $H(S_h, \boldsymbol{x}_h^\star) = \sum_{i \in S_h} (x_i - \bar{x}_h)^2$ for numerical covariates, where $\bar{x}_h$ is the mean value of the vector $\boldsymbol{x}_h^\star$, while $H(S_h, \boldsymbol{x}_h^\star) = -\sum_{c=1}^{C} \hat{p}_c \log(\hat{p}_c)$ for categorical covariates, with $\hat{p}_c$ denoting the relative frequency at which each category appears. The parameter φ controls the degree of penalization applied to dissimilar values. This similarity function can be easily extended to the multidimensional case, for numerical covariates, with the H function becoming $H(S_h, X_h^\star) = \sum_{r=1}^{p} \|\boldsymbol{x}_r - \bar{\boldsymbol{x}}_h\|^2$.

Another commonly used similarity function is the Gower similarity (Gower, 1971). The core idea behind this function is to compare all cluster-specific pair-wise similarities, leading to the total Gower similarity function.

$$g_2(S_h, \boldsymbol{x}_h^\star) = \exp\left\{-\alpha \sum_{i,j \in S_h, i \neq j} d(x_i, x_j)\right\} \tag{1.29}$$

However, this function g_2 is strictly increasing with respect to cluster size, which tends to promote a large number of small clusters (Garritt L. Page et al., 2018). To address this issue, a correction can be applied that accounts for the size of the cluster S_h, leading to the average Gower similarity function.

$$g_3(S_h, \boldsymbol{x}_h^\star) = \exp\left\{-\frac{2\alpha}{|S_h|(|S_h|-1)} \sum_{i,j \in S_h, i \neq j} d(x_i, x_j)\right\} \tag{1.30}$$

In both functions, $d(x_i, x_j)$ represents the Gower dissimilarity between x_i and x_j. For numerical covariates, it is defined as $d(x_i, x_j) = |x_i - x_j|/R$, where $R = \max(\boldsymbol{x}) - \min(\boldsymbol{x})$ denotes the range of the covariate values across all units; for categorical covariates, it is defined as $d(x_i, x_j) = \mathbb{1}_{[x_i \neq x_j]}$. As a dissimilarity metric, values closer to 0 indicate similar data points, while values closer to 1 indicate similar data; therefore the negative sign in the exponents of g_2 and g_3 converts these functions into measures of similarity. These similarity functions can be naturally extended to the multivariate context, resulting in $g_2(S_h, X_h^\star)$ and $g_2(S_h, X_h^\star)$. In this case, the comparison is performed on vectors of covariates, rather than individual values, through the function d becoming $d(\boldsymbol{x}_i, \boldsymbol{x}_j) = \frac{1}{p}\sum_{r=1}^{p} d(x_{ir}, x_{jr})$.

$$g_4(S_h, \boldsymbol{x}_h^\star) = \int \prod_{i \in S_h} q(x_i|\boldsymbol{\xi}_h) q(\boldsymbol{\xi}_h)\, d\boldsymbol{\xi}_h \tag{1.31}$$

The final similarity function (Garritt L. Page et al., 2016), referred to as auxiliary similarity function, employs a similar approach to that used in spatial cohesion 3 by treating covariates as if they were random variables. However, in this unidimensional setting, we choose a Normal/Normal-Inverse-Gamma model with parameters $\boldsymbol{\xi} = (\mu, \sigma^2)$, $x|\boldsymbol{\xi} \sim \mathcal{N}(\mu_0, \sigma^2)$, and $\mu \sim \mathcal{N}(\mu_0, \sigma^2/\lambda_0)$, $\sigma^2 \sim \text{invGamma}(a_0, b_0)$, i.e. $\boldsymbol{\xi} \sim \mathcal{N}\text{invGamma}(\mu_0, \lambda_0, a_0, b_0)$. Nonetheless, a multivariate extension is possible through the same Normal/Normal-Inverse-Wishart model employed for the spatial coordinates.

All these similarity functions appeared to agree on the ranking of the clusters shown in Figure 1.9. The purple cluster, the singleton, consistently ranked at the top across all similarity functions, with the exception of certain parameter combinations in g_4. All the similarities, except for g_2, agreed on the classification of non-singleton clusters, with red exhibiting the highest similarity, followed by orange, blue, and green. This is illustrated in Figures 1.10, 1.12, which corresponds to functions g_1 and g_3, as well as in Figures 1.13 through 1.15, corresponding to g_4. In contrast, Figure 1.11 shows that similarity 2 ranks the green and red clusters at the top, followed by blue and orange. This classification is intriguing because the green cluster appeared relatively sparse according to Figure 1.9, yet it captured all "outlier" values, thereby justifying an high similarity score. Notably, similarities 2 and 4 seem to be the only functions able to assign substantial weight to the green partition.

Other experiments were also conducted on different covariates and clusters configurations. Similarity 4 exhibited significant flexibility in computing the similarity weights by adjusting the parameters that govern the invGamma distribution for σ^2. This was also evident by Figures 1.13 through 1.15, from the experiments on the `Altitude` covariate, where different parameters a_0 and b_0 led g_4 to various possible rankings in the clusters. This flexibility suggests that covariates should be standardized prior to their use, to simplify the analysis and ensure a uniform selection of the most appropriate set of parameters. In any case, the JDRPM implementation is not rigid in this regard as it allows for separate assignments of parameters a_0 and b_0 for each covariate included in the prior.

In contrast, similarity 1 proved to be the most predictable function, consistently

yielding reasonable cluster rankings across all experiments. For instance, Figure 1.10 shows how g_1 proposed the ranking red, orange, blue and green, which are intuitively valid by looking at the configuration of Figure 1.9. However, g_1 tends to penalize a lot sparse clusters, suggesting that alternative distance metrics, rather than the L^2 norm, could be employed in the computation of $H(S_h, \boldsymbol{x}_h^\star)$.

Lastly, in Table 1.1 we present a brief exemplification of the behaviour of these similarity functions with categorical covariates. Similarity 4 is not included because it is applicable only to numerical covariates.

Table 1.1: Values of the three similarity functions applicable to categorical covariates, computed on a string of 20 characters (A and B), with the numbers next to each letter indicating their frequency.

$\boldsymbol{x}_h^\star$	Similarity 1	Similarity 2	Similarity 3
10 A, 10 B	0.5	3.7201e-44	0.5908
11 A, 9 B	0.5025	1.0112e-43	0.5939
12 A, 8 B	0.5102	2.0311e-42	0.6033
13 A, 7 B	0.5234	3.0144e-40	0.6194
14 A, 6 B	0.5429	3.3057e-37	0.6427
15 A, 5 B	0.5699	2.6786e-33	0.6739
16 A, 4 B	0.6063	1.6038e-28	0.7140
17 A, 3 B	0.6553	7.0955e-23	0.7646
18 A, 2 B	0.7225	2.3195e-16	0.8274
19 A, 1 B	0.8199	5.6028e-09	0.9048
20 A, 0 B	1.0	1.0	1.0

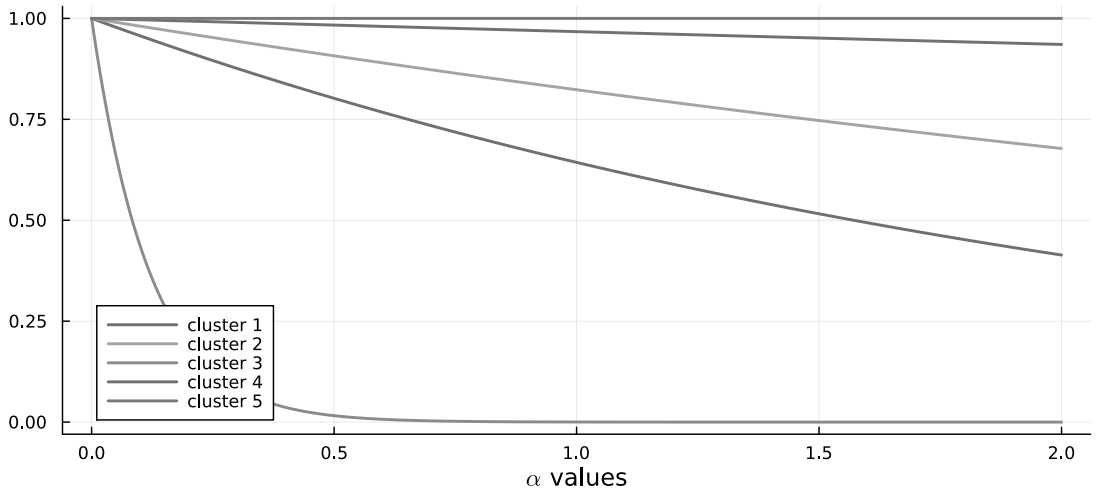

Figure 1.10: Similarity 1 values computed on the test case partition of Figure 1.9, with respect to different values of its tuning parameter α.

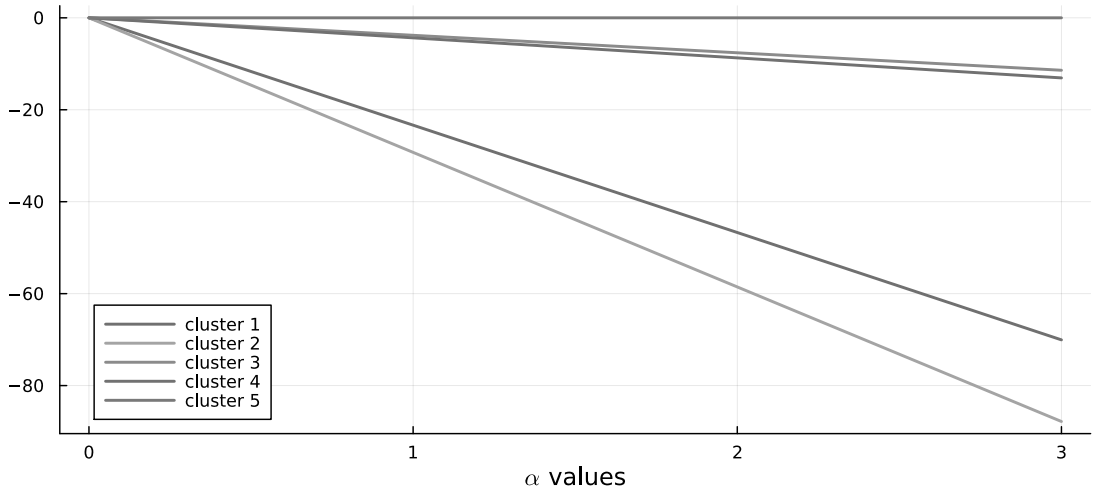

Figure 1.11: Similarity 2 log-transformed values computed on the test case partition of Figure 1.9, with respect to different values of its tuning parameter α.

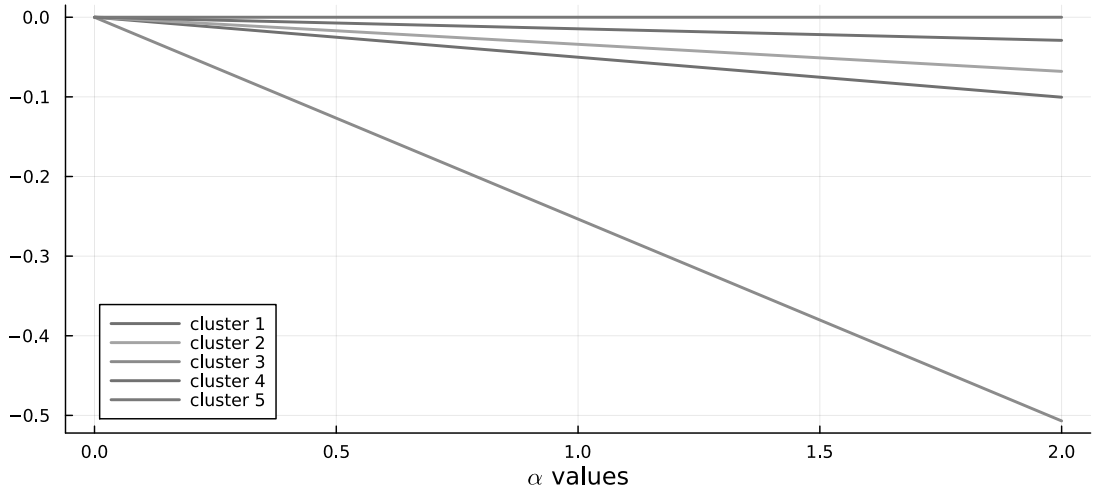

Figure 1.12: Similarity 3 log-transformed values computed on the test case partition of Figure 1.9, with respect to different values of its tuning parameter α.

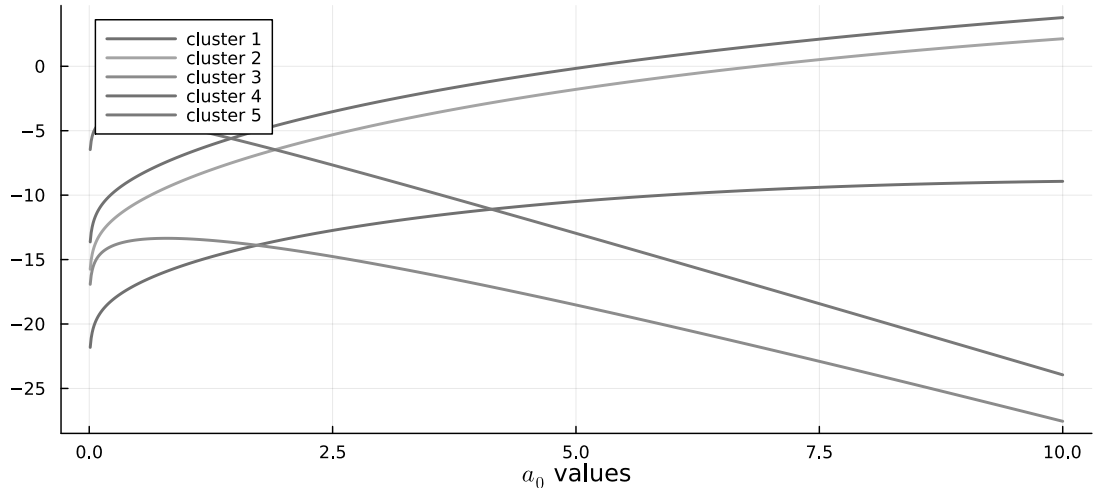

Figure 1.13: Similarity 4 log-transformed values values computed on the test case partition of Figure 1.9, with respect to different values of its tuning parameter a_0. The other parameters has been set to $\mu_0 = 0$, $\lambda_0 = 1$, $b_0 = 1$.

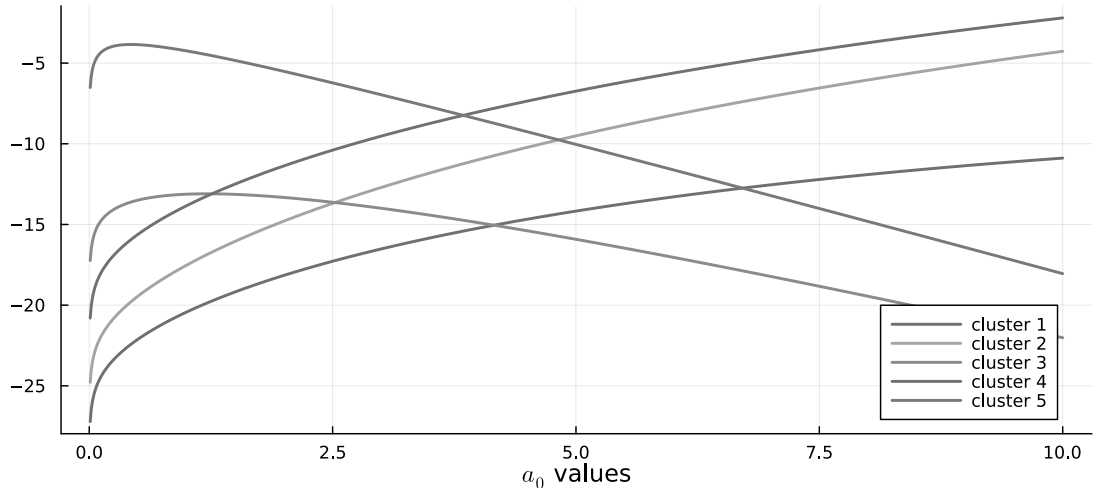

Figure 1.14: Similarity 4 log-transformed values computed on the test case partition of Figure 1.9, with respect to different values of its tuning parameter a_0. The other parameters has been set to $\mu_0 = 0$, $\lambda_0 = 1$, $b_0 = 2$.

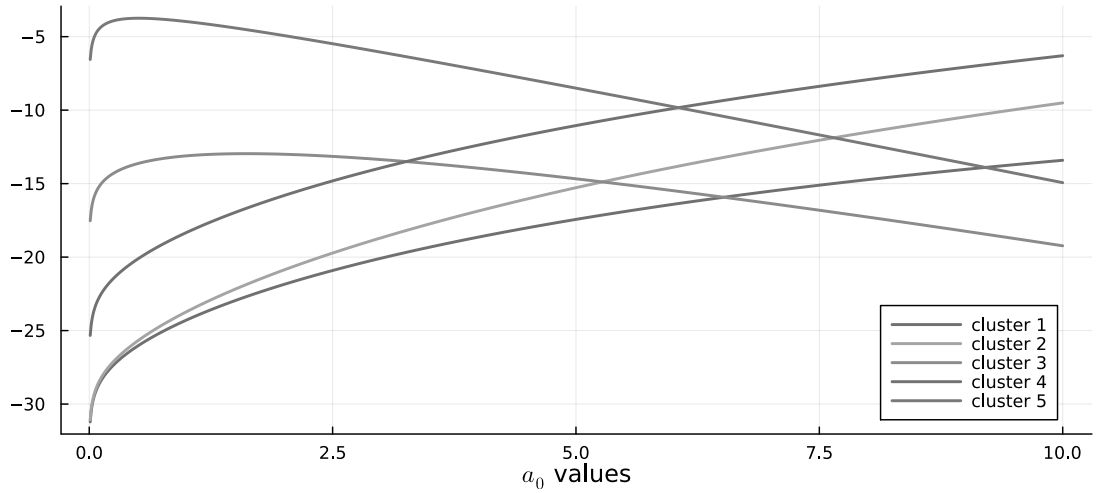

Figure 1.15: Similarity 4 log-transformed values computed on the test case partition of Figure 1.9, with respect to different values of its tuning parameter a_0. The other parameters has been set to $\mu_0 = 0$, $\lambda_0 = 1$, $b_0 = 3$.

Chapter 2

Implementation and optimizations

"You see, I've brought you my Nellie," I said, going in.
— Fëdor Dostoevskij, *Humiliated and Insulted*

The MCMC algorithm to compute the posterior samples of our updated model, described in Section 1.1, has been implemented in Julia (Bezanson et al., 2017).

Julia is a relatively new programming language that combines the ease and expressiveness of high-level languages with the efficiency and performance characteristic of low-level languages. This balance is primarily achieved through just-in-time (JIT) compilation, using the LLVM framework, along with features such as dynamic multiple dispatch and extensive code specialization against multiple run-time types. Such design enables Julia to be used interactively, in the same fashion to the R, MATLAB, or Python consoles, while also supporting the traditional execution style of statically compiled languages like C, C++, and Fortran. This flexibility facilitates faster development phases, since code sections can be easily evaluated and tested, even line by line, while still guaranteeing efficient implementations through the compilation process. Performance is further enhanced by the native integration of optimized BLAS (Lawson et al., 1979) and LAPACK libraries for linear algebra operations, which are essential for many scientific applications. Moreover, Julia features an extensive ecosystem currently comprising over ten thousand packages that span nearly all branches of science and engineering. Most of these packages are well-tested and highly optimized, thus significantly reducing the implementation time required to users. For instance, in this work, we employed the `Distributions` (Besançon et al., 2021) (Lin et al., 2019) and `Statistics` packages, whereas the original C implementation required developing all statistical functionalities from scratch. Given these benefits, choosing Julia was a natural decision.

As we will discuss in Chapter 3, we obtained improved performance in Julia, with respect to the original C implementation, despite the increased complexity of the model and the associated MCMC algorithm. This enhancement came at the reasonable cost of a modest increase in memory requirements, which nowadays is generally manageable given the current available technologies. Such improvement

was made possible through various refinements and optimizations, which we now briefly outline.

2.1 Optimizations

One of the primary challenges encountered during the implementation of the MCMC algorithm in Julia was managing the amount of memory and allocations that some functions, structures, or algorithms would require. Initially, during the development and testing phases, where the correctness of the algorithm was the only priority, we observed that a significant portion of execution time was actually consumed by Julia's garbage collector, which had the burden of tracking all the allocated memory and reclaim the unused one in order to make it available again for new computations. Therefore, an obvious optimization strategy has been to minimize unnecessary allocations and manage memory more efficiently. Additionally, ensuring type stability in the code is another crucial factor for enhancing performance; and Julia provides several tools to inspect and address both aspects.

Regarding type stability, there are various tools available, such as the `Cthulhu` package or the simple `@code_warntype` macro, which help to verify that a function is type-stable, which means that the types of all variables can be correctly predicted by the compiler and remain consistent throughout execution. Type stability is essential for performance as it allows the compiler to generate optimized machine code, eliminating the overhead associated with run-time type checks. In fact, Julia is dynamically-typed, meaning that variables do not need to be explicitly declared with their types, unlike fully statically-typed languages such as C. In Julia, for instance, a variable initialized as an integer could later become a float or even a string, during execution. However, for performance reasons, such dynamisms should be avoided. Using the tools mentioned earlier we successfully reduced unnecessary type instabilities; however, however, we retained some degree of instability to maintain a certain level of flexibility, e.g. to allow the selection of cohesion and similarity functions at runtime.

Regarding memory issues, we deeply inspected the code performance using the `ProfileCanvas` package. This profiler generates a flame graph, illustrated in Figure 2.1, which represents different sections of code with regions whose size is proportional to specific metrics such as execution time or, in this analysis, the amount of memory allocations required for each section. The flame graph is read from left to right regarding the order of execution of the different sections, and from top to bottom according to the stack trace, meaning the order of subsequent function calls originating from the initial top one. This visualization enables to detect whether execution time is spent on productive operations or rather on less efficient activities such as garbage collection and runtime evaluations, thereby highlighting the portions of code that could possibly be optimized.

The key solution derived from this analysis has been to refactor the code to operate more in-place. This involved passing as arguments the variables that would be modified by a function, and applying those changes directly within the

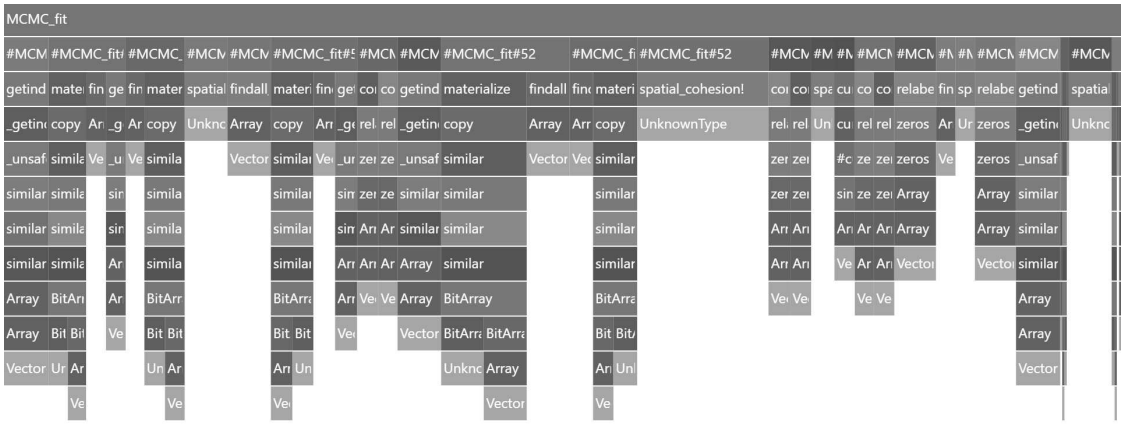

Figure 2.1: Flame graph derived from an example JDRPM fit with $n = 20$ and $T = 50$, ran for 10000 iterates.

function, rather than returning values and subsequently using them to update the original variables. Additionally, we preallocated all the modelling and working variables and implemented other straightforward improvements, thanks to the Julia language functionalities, such as the `@view` macro. This macro allows to eliminate unnecessary copies of vectors and matrices by passing references to the specific slices needed for a certain computation, rather than passing the entire structures. For example, when only the first row of a matrix `M` needs to be passed to a function, using `@view M[1,:]` instead of `M[1,:]` prevents a memory allocation.

Another valuable package to conduct performance analyses was `BenchmarkTools` (Chen et al., 2016), which allowed to compare entire functions as well as specific portions of code. Regarding the latter, this package facilitates straightforward testing of different versions of equivalent instructions to determine which is the most efficient, as in this case, where we are computing the current number of clusters by counting the non-zero entries of the `nh_tmp` variable

```
using BenchmarkTools
nh_tmp = rand(100)
@btime nclus_temp = sum($nh_tmp .> 0)
# 168.956 ns (2 allocations: 112 bytes)
@btime nclus_temp = count(x->(x>0), $nh_tmp)
# 11.612 ns (0 allocations: 0 bytes)
```

or this other, where we are retrieving the indexes of the units assigned to cluster k

```
n = 100; rho_tmp = rand((1:5),n); k = 1
@btime findall(j -> ($rho_tmp)[j]==$k, 1:n) # with anonymous function
# 272.302 ns (5 allocations: 384 bytes)
@btime findall_faster(j -> ($rho_tmp)[j]==$k, 1:n) # custom implementation
# 214.259 ns (3 allocations: 960 bytes)
@btime findall($rho_tmp .== $k) # with element-wise comparison
# 184.112 ns (3 allocations: 320 bytes)
```

The `$` symbol is employed for interpolating a variable, ensuring to treat the variable as a local variable within the scope of benchmark, thereby eliminating any performance bias that might arise from accessing a global variable.

During the final stages of code refinement, we also exploited low-level tools such as the `--track-allocation` option, which requests Julia to execute the code while also annotating the source file, line by line, to indicate where allocations occurred and of which amount.

These tools collectively contributed to achieving an optimal level of performance. Table 2.1 provides a final reference of the effectiveness of these optimizations.

Table 2.1: Performance analysis of JDRPM's MCMC algorithm implementations, comparing an early stage code to the final version. The metrics are derived from an example fit ran for 1000 iterations, using a dataset with $n = 50$ and $T = 20$. The "% gc time" metric represents the percentage of execution time spent in garbage collection operations.

	execution time	memory allocated	% gc time
early stage version	17.314s	18.233 GiB	9.22%
final version	**4.515s**	**2.236 GiB**	**4.64%**

2.1.1 Optimizing spatial cohesions

The issue of memory allocation was particularly pronounced in the computation of spatial cohesions. This computation occurs in both the update steps of γ_{it} and ρ_t, which are nested within outer loops on draws, time, and units, and involve additional loops over clusters. Consequently, these cohesion computations would potentially be executed millions of times during each fit: simple inspection of the MCMC algorithm suggests a number of calls between dTn and dTn^2, where d represents the number of iterations, T the time horizon, and n the number of units. A more precise estimate is not possible due to the variability and randomness inherent in the inner loops which depend on the distribution of the clusters. Given this context, optimizing the performance of the cohesion functions was crucial to provide fast execution times.

The optimization efforts focused on carefully designing the implementations of the cohesion functions. Cohesions 1, 2, 5, and 6 did not present any complications or need for further optimization: the natural conversion into code from their mathematical models proved to be already optimally performing.

The main challenges emerged with cohesions 3 and 4, the auxiliary and double dippery, which involve linear algebra operations with vectors and matrices that would increase the computational demands. The initial implementation of these cohesions was notably slow due to the overhead associated with allocating and freeing the memory of vectors and matrices at each call. As a result, a significant portion of execution time was devoted to garbage collection rather than to actual computations. A preliminary solution involved resorting to a scalar implementation, which processed each component individually rather than operating on entire vectors and matrices. This approach effectively eliminated the overhead associated with the more complex memory structures. Ultimately, we succeeded in combining the readability of the first method with the efficiency of the second method into a final, refined solution. Listing 1 showcases the logic behind the three different solutions.

Listing 1: Snippets of Julia code for the three implementation solutions of the spatial cohesions 3 and 4. The first is the naive vector implementation, the second is its scalar conversion, and the third is the static vector solution.

```
# original vector version
sbar = [mean(s1), mean(s2)] # this is a standard vector
# all the following matrices and vector will be standard structures
vtmp = sbar - mu_0
Mtmp = vtmp * vtmp'
Psi_n = Psi + S + (k0*sdim) / (k0+sdim) * Mtmp

# scalar-only version
sbar1 = mean(s1); sbar2 = mean(s2)
vtmp_1 = sbar1 - mu_0[1]
vtmp_2 = sbar2 - mu_0[2]
Mtmp_1 = vtmp_1^2
Mtmp_2 = vtmp_1 * vtmp_2
Mtmp_3 = copy(Mtmp_2)
Mtmp_4 = vtmp_2^2
aux1 = k0 * sdim; aux2 = k0 + sdim
Psi_n_1 = Psi[1] + S1 + aux1 / (aux2) * Mtmp_1
Psi_n_2 = Psi[2] + S2 + aux1 / (aux2) * Mtmp_2
Psi_n_3 = Psi[3] + S3 + aux1 / (aux2) * Mtmp_3
Psi_n_4 = Psi[4] + S4 + aux1 / (aux2) * Mtmp_4

# static improved version
sbar1 = mean(s1); sbar2 = mean(s2)
sbar = SVector((sbar1, sbar2)) # this is a statically-sized vector
# all the following matrices and vector will be statically-sized
vtmp = sbar .- mu_0
Mtmp = vtmp * vtmp'
aux1 = k0 * sdim; aux2 = k0 + sdim
Psi_n = Psi .+ S .+ aux1 / (aux2) .* Mtmp
```

This final version employs the `StaticArrays` package of Julia, which enables more efficient use of vectors and matrices when their sizes are known at compile time. This is suited for the spatial cohesion computations as we consistently work with 2×1 vectors and 2×2 matrices, due to the context of planar spatial coordinates. The benefits of this final implementation include preserving the natural mathematical form of the first solution, thus enhancing code clarity, while also capitalizing on the performance improvements seen in the second solution. In fact, with static structures, the compiler is able to optimize all memory allocations related to vectors and matrices just as it does with simple scalar variables.

Figure 2.2 provides a performance comparison of the three solutions. Panel 2.2c proves that the scalar and static versions exhibited similar performance, and both significantly outpaced the initial vector implementation, and both are significantly faster than the initial vector implementation. Additionally, panels 2.2a and 2.2b highlight the substantial reduction in memory requirements compared to the first solution. This comparison was conducted by running the three implementations against multiple sets of spatial coordinates with a varying number of units n.

Notably, the CDRPM implementation of the corresponding MCMC algorithm was not required to consider these optimizations, since C does not natively support

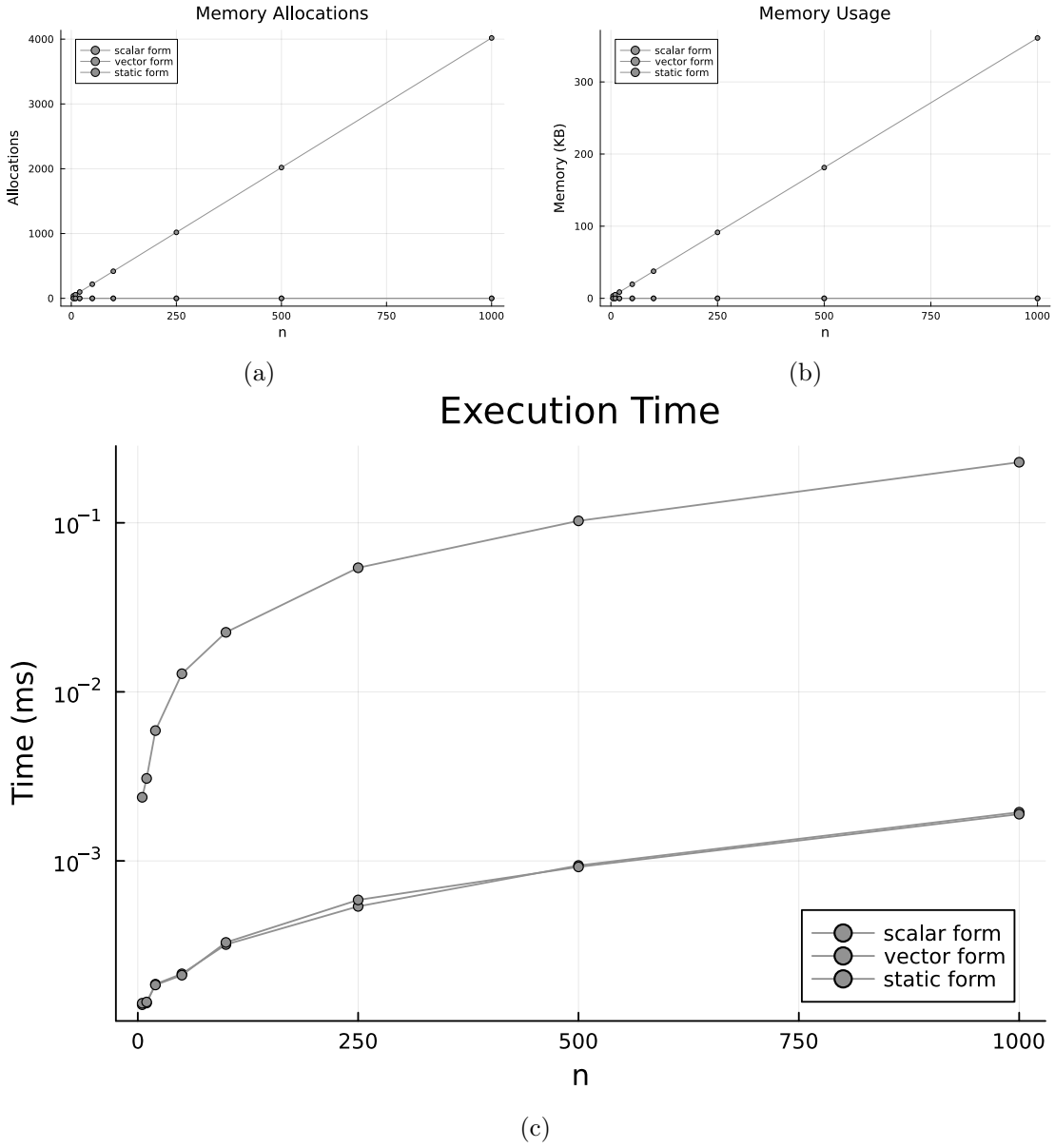

Figure 2.2: Performance comparison among the three versions of the cohesion 4 function. Similar results stand for cohesion 3. Panels (a) and (b) are constant at zero for both the scalar and static cases.

vectors and matrices and was therefore forced to the scalar implementation without much deliberation.

2.1.2 Optimizing covariates similarities

Another significant challenge that we faced consisted in optimizing the computation of the similarity functions. As the cohesion functions, the similarities would potentially be called millions of times, if not more, considering that multiple covariates can be incorporated in the prior and thus introducing an additional loop based on p, the number of included covariates. As in the case of the previous

analysis, many of the similarity functions did not exhibit a significant need for optimization. However, the fourth function, the auxiliary similarity function, required optimization due to the computational load associated with calculating the sum of the squares of the covariate values, as illustrated in Listing 2.

Listing 2: Similarity 4 function implementation, with all optimizing annotations. The performance analysis will just focus on that inside loop.

```
function similarity4(X_jt::AbstractVector{<:Real}, mu_c::Real, lambda_c::Real,
↪  a_c::Real, b_c::Real, lg::Bool)
    n = length(X_jt)
    nm = n/2
    xbar = mean(X_jt)
    aux2 = 0.
    @inbounds @fastmath @simd for i in eachindex(X_jt)
        aux2 += X_jt[i]^2
    end
    aux1 = b_c + 0.5 * (aux2 - (n*xbar + lambda_c*mu_c)^2/(n+lambda_c) +
    ↪  lambda_c*mu_c^2 )
    out = -nm*log2pi + 0.5*log(lambda_c/(lambda_c+n)) + lgamma(a_c+nm) -
    ↪  lgamma(a_c) + a_c*log(b_c) + (-a_c-nm)*log(aux1)
    return lg ? out : exp(out)
end
```

The optimization strategy involved annotating the loop with several macros provided by Julia. They were the following:

- `@inbounds` eliminates array bounds checking within expressions. This allows the compiler to bypass these checks, thus saving execution time. This annotation is safe to use as long as we can guarantee that the code will not access elements outside the array bounds; otherwise undefined behavior may occur. In our case, the loop structure is simple and safe, so this assumption holds true.

- `@fastmath` executes a modified version of the expression that may invoke functions violating strict IEEE semantics[1]. For instance, using this macro could result in $(a + b) + c \neq a + (b + c)$, but only in highly pathological cases. Again, this is not an issue for our loop, which computes $\sum X_i^2$, as there is no intrinsic "correct order" for performing this operation.

- `@simd` (Single Instruction Multiple Data) allows the compiler to apply further optimizations to the loop. This technique is akin to parallelism; however, rather than distributing the computational load across multiple processors, `@simd` vectorizes the loop. This means that the CPU can execute the same instruction (summing the square of the i-th component into a reduction variable) on multiple data chunks simultaneously using vector registers. As a result, this approach accelerates computation by eliminating the need to process each element of the vector individually.

[1]Institute of Electrical and Electronics Engineers. The IEEE-754 standard specifies floating-point formats, which dictate how real numbers are represented in hardware, along with the expected behavior of arithmetic operations on them, including precision, rounding, and the handling of special values (e.g., NaN (Not a Number) and infinity).

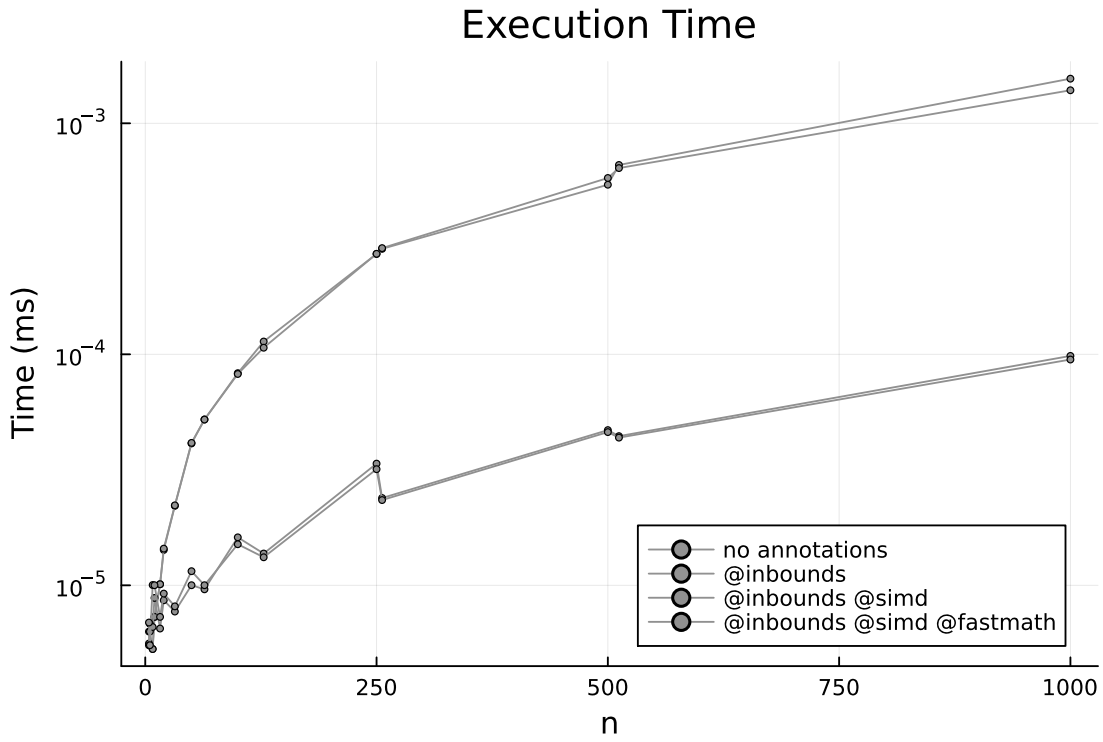

Figure 2.3: Performance comparison of the different loop annotations in the similarity 4 implementation.

As illustrated in Figure 2.3, the observed performance difference primarily arises from the use of `@simd`, while the other two annotations have minimal impact. Consequently, to address concerns from pure mathematicians, we opted to remove the `@fastmath` annotation, retaining only `@inbounds` and `@simd`. Memory allocation and usage panels are not reported since the analysis focused solely on evaluating the performance of the inner loop, which does not present any memory-related issues.

Moreover, we observe that experiments employing the `@simd` annotation tend to run faster when n is a power of two compared to n being its nearest rounded integers (for instance, 256 versus 250 or 512 versus 500), even though this configuration involves processing a relatively larger dataset. This pattern underscores the effectiveness of the SIMD approach: nding on the architectures, CPUs can support various register sizes (e.g. 64, 128, 256, or 512 bits). When the total memory occupied by the data points aligns perfectly with these register sizes, i.e. when the number of elements is a power of two, the data can be efficiently loaded into registers without any waste. Conversely, if the data size does not match, there will be "leftover chunks" that still need to be processed, which can introduce some overhead due to the inefficiencies associated with this imperfect fit.

Chapter 3

Analysis of the models

In the following analyses, we will make use of the Adjusted Rand Index (ARI) (Hubert et al., 1985) to compare the partitions generated by the models. The ARI index serves as a correlation metric that quantifies the similarity between two clusterings. Specifically, for two partitions ρ_1 and ρ_2, the function $\text{ARI}(\rho_1, \rho_2)$ produces a value within the range $[-1, 1]$ where higher values indicating greater agreement between the partitions. A perfect match $\rho_1 = \rho_2$ is represented with the limit case $\text{ARI}(\rho_1, \rho_2) = 1$.

We will employ this index to analyse the temporal evolution of the partitions, examining whether ρ_{t+k} correlates with ρ_t, and to evaluate the level of agreement between the two models, by comparing clusters estimates generated by CDRPM and JDRPM. These cluster estimates will be computed using the `salso` function, with the binder loss, using the associated `salso` library (David B. Dahl et al., 2022) on R.

All analyses of this Chapter were conducted on a laptop equipped with 8 GB of RAM and a 1.80 GHz CPU base clock speed. The software used was R (R Core Team, 2024), interfaced with Julia through the `JuliaConnectoR` library (Lenz et al., 2022). This library handled all the communication between R and Julia, where the JDRPM's MCMC algorithm is implemented. The CDRPM implementation is also accessible from R via a dedicated package, `drpm`, developed by (Garrit L. Page et al., 2022), which similarly employs a wrapper to invoke the C code where the MCMC algorithm is implemented.

3.1 Comparing the two algorithms

Our model, along with its corresponding Julia implementation, represents an enhancement over the original DRPM and its associated C implementation. The improvements, as outlined in previous chapters, include the ability to incorporate covariates into both the prior and likelihood levels of the Bayesian model, the possibility of allowing for missing data in the response variable, and the guarantee of greater computational efficiency. In this regard, our updates serve as extensions to the original model. Therefore, when tested under equivalent hyperparameters

and MCMC configurations, both models are expected to perform similarly and produce comparable clusters estimates for a given dataset.

To evaluate the numerical performance of both algorithms, we will analyse posterior samples and cluster estimates in two scenarios: first using a synthetic dataset that includes only the response variable, and secondly employing a real-world spatio-temporal dataset. The latter also provides covariates; however, their effects will be extensively examined in the dedicated Section 3.3.

3.1.1 On a synthetic dataset

For the initial comparison we generated a dataset of $n = 10$ units and $T = 12$ time instants. The data generating function was the same employed in (Garrit L. Page et al., 2022) for their analyses and it allows for the creation of data points with temporal dependence, which could be adjusted through specific parameters. Regarding the MCMC setup, both algorithms were executed deriving 2000 iterates from a total of 50000 iterations, by discarding the first 40000 as burnin and then thinning by 5. Both models were fitted using a time specific α and using their full formulations, i.e. including and updating also the optional autoregression parameters η_{1i} and φ_1.

Table 3.1: Comparison between CDRPM and JDRPM fits and their associated algorithms, in the simulated data scenario.

	MSE mean	MSE median	execution time
CDRPM	1.6221	1.5823	19s
JDRPM	**1.2634**	**1.2034**	**13s**

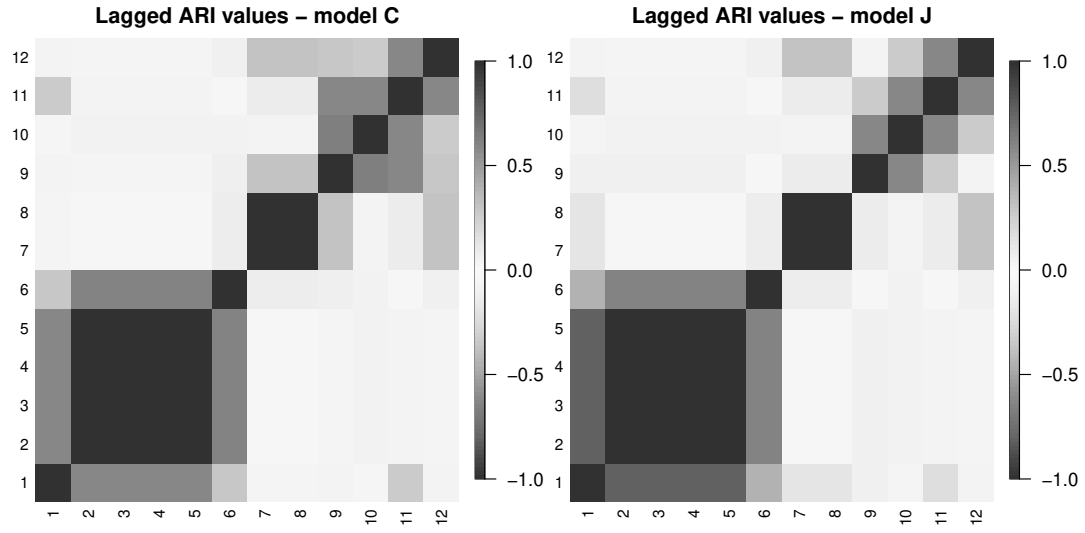

Figure 3.1: Lagged ARI values of CDRPM and JDRPM fits, in the simulated data scenario.

During this testing phase, the clusters were defined solely by the target values from Y_{it}, and both models achieved satisfactory results. Fitted values are presented

in Figure 3.4 alongside the original data. From Table 3.1 we can see how JDRPM exhibited greater accuracy, as proven by the lower mean squared error (MSE), and a faster execution time. In the table, the MSEs were computed by comparing the fitted values generated by the models, estimated by taking the the mean and median of the 2000 iterations, with the true values of the target variable. We do not report fitting metrics for WAIC and LPML since both models were conceptually equivalent and tested under identical hyperparameters and MCMC configurations. Consequently, any observed differences in these metrics would be likely attributable to chance.

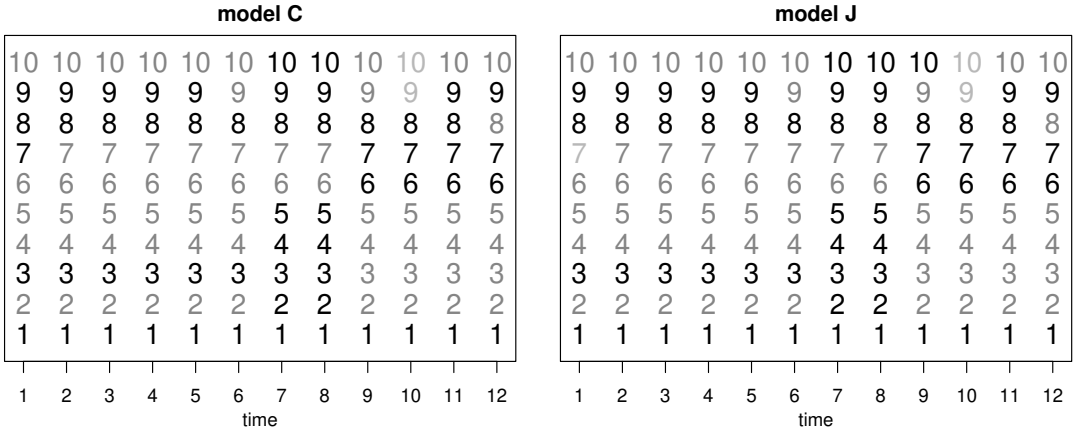

Figure 3.2: Clusters estimates produced by CDRPM and JDRPM fits, in the simulated data scenario. Time instants are annotated on the x axis, units are indicated vertically by their number, and colors represent the cluster label.

The resulting partitions were remarkably similar. As illustrated in Figure 3.1, both models effectively captured the temporal dynamics of the response variable. Moreover, Figure 3.2 confirms the agreement in the cluster estimates; however, it also reveals two minor differences which we will now discuss.

A closer examination of the clusters presented in Figure 3.3 reveals interesting distinctions at times $t = 1$ and $t = 9$. At $t = 1$, JDRPM classified unit 7 as a singleton within the green cluster, whereas CDRPM assigned unit 7 to the black cluster. Both classifications are reasonable: the data point is indeed closer to the black cluster, but it later aligns more distinctly to the red cluster; suggesting the classification given by JDRPM as a detection of its initial anomalous behaviour. At $t = 10$, both models successfully identified a small, temporary third cluster resulting from the transition of units 9 and 10. The JDRPM interprets this transition as a label swap: between times $t = 9$ and $t = 11$, unit 9 shifts from the red cluster to the black cluster, while unit 10 from the black cluster to red cluster. In contrast, at $t = 9$ CDRPM assigns both units to the red cluster, potentially reflecting a misclassification considering the temporal trend of unit 10 which, until $t = 10$, indicated a closer alignment with the black cluster.

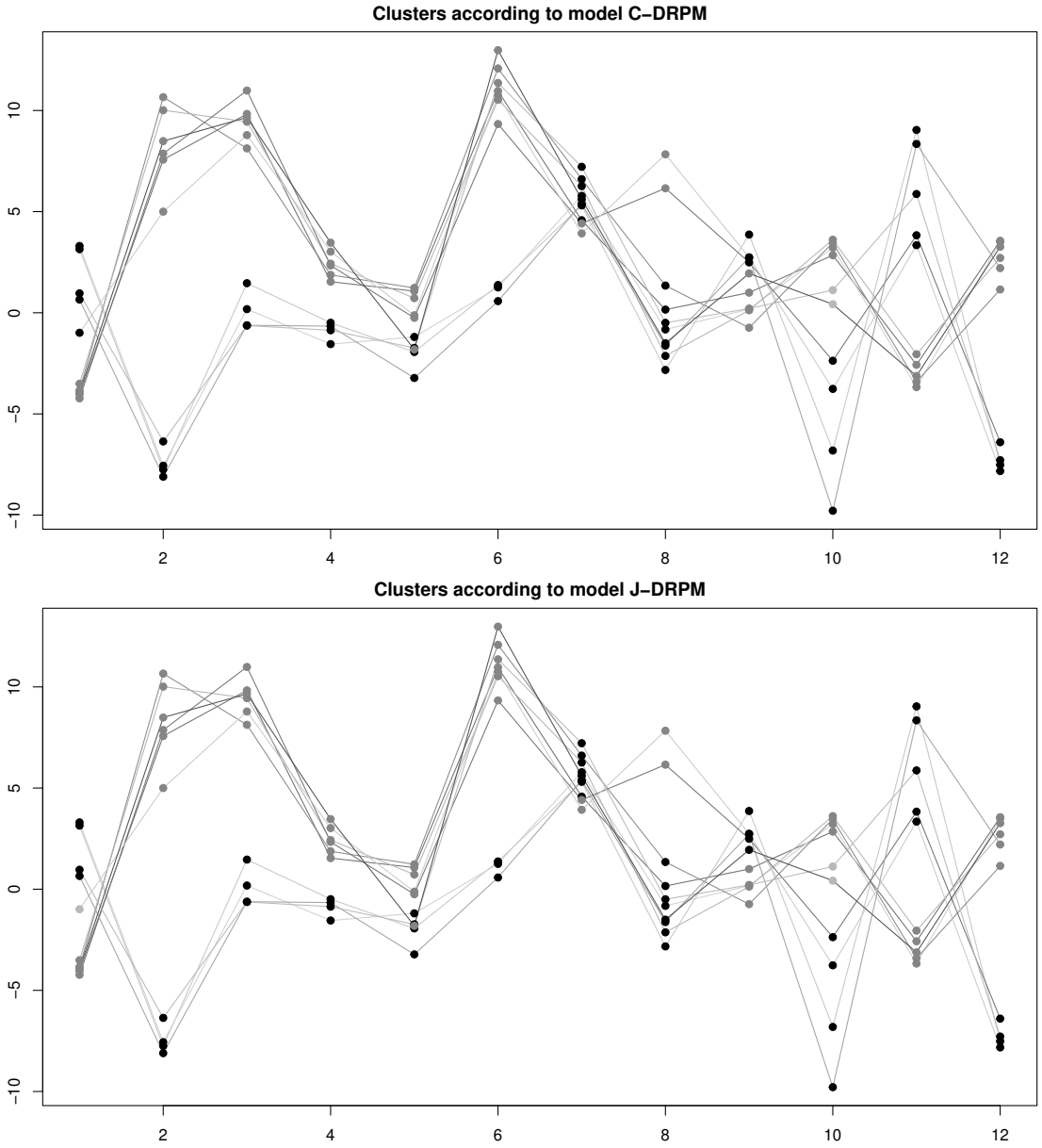

Figure 3.3: Visual representation of the clusters estimates produced by CDRPM and JDRPM fits, in the simulated data scenario. Cluster labels are represented as colored dots overlaid to the trend of the target variable.

3.1.2 On spatio-temporal data

In this section we examine a real-world application by fitting CDRPM and JDRPM on a spatio-temporal dataset. Specifically, we used the AgrImOnIA dataset (Fassò et al., 2023) which encompasses measurements of air pollutants, together with many other environmental variables, in the Lombardy region of Italy from 2016 to 2021.

For our subsequent analyses, we employed a dataset comprising weekly averages from the year 2018. The target variable chosen for these studies was PM_{10}, which represents the concentration of particulate matter with a diameter of less than

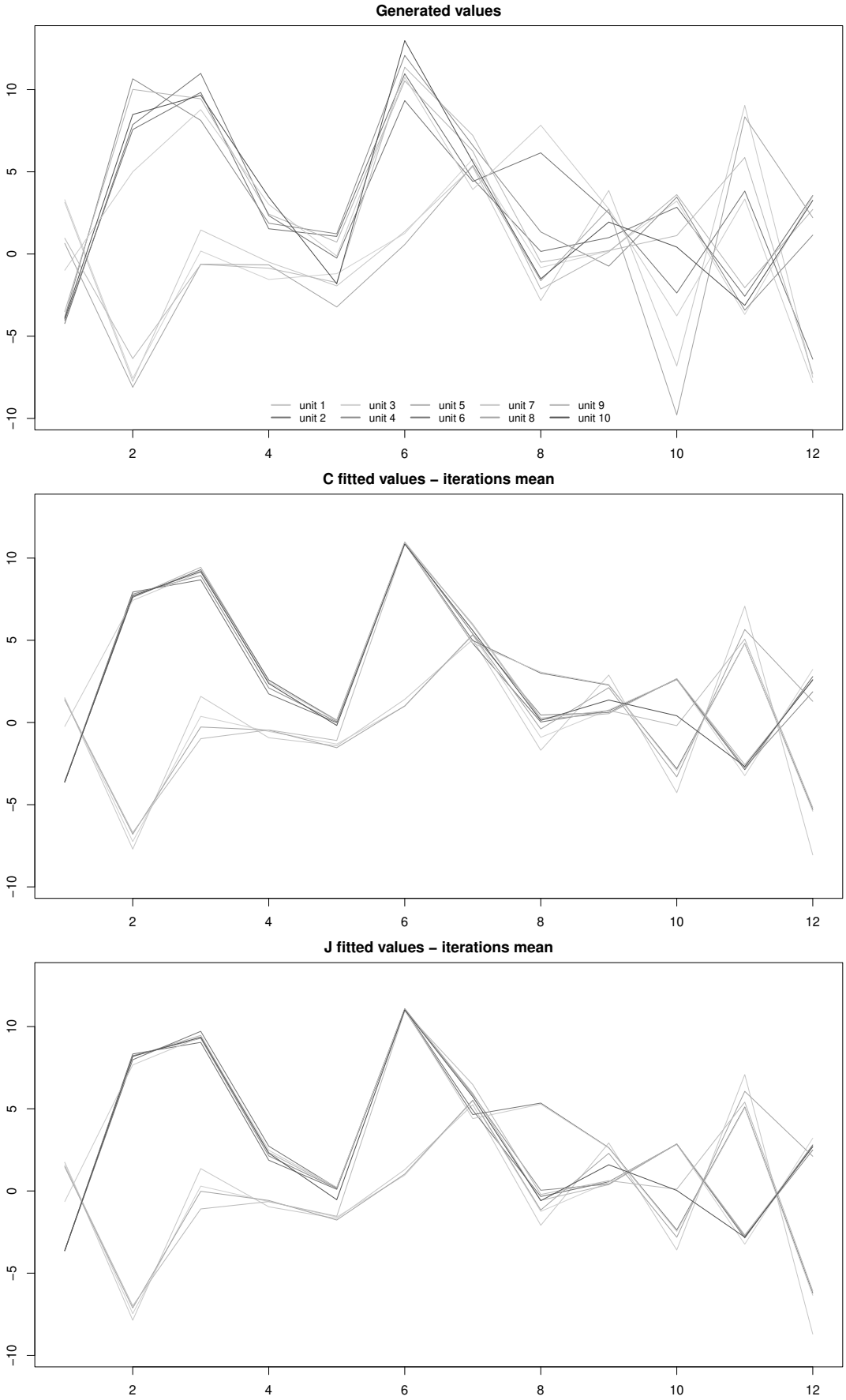

Figure 3.4: Fitted values of CDRPM (middle) and JDRPM (bottom) fits, in the simulated data scenario, alongside the generated target values (top).

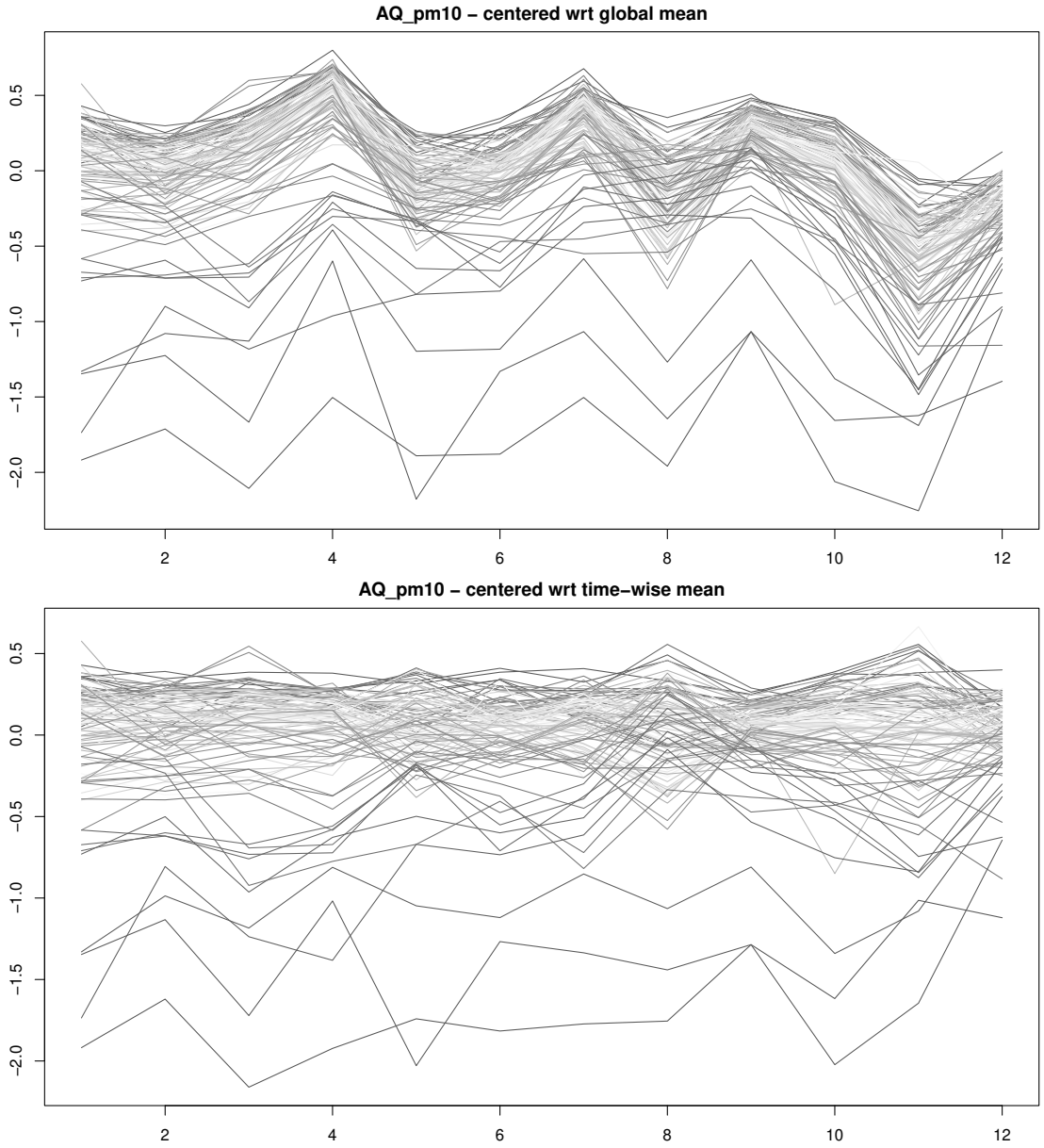

Figure 3.5: Values of the target variable `AQ_pm10` adjusted using the global mean (top) and the time-wise mean (bottom). Coloring is based on the ranking of PM_{10} values of the units according to their median, from highest (red) to lowest (blue).

10 µm. This variable underwent log-transformation, to recover a normal distribution, and was centered with respect to time-wise means. More precisely, each observation Y_{it} was adjusted by subtracting the mean $\bar{Y}_t$ of all observations at that time instant t. This approach, consistent with the methodology employed by (Garrit L. Page et al., 2022) during their analyses, helps to emphasize variations within each time point rather than across the entire dataset. This approach is particularly beneficial for understanding how individual units deviate from their typical behavior at specific times, thereby highlighting temporal trends and anomalies. Moreover, this method effectively mitigates any temporal bias that may arise from periods in which all target values are disproportionately high or low due to external anomalous factors.

In contrast, the traditional approach of centering the data around their global mean $\bar{Y}$ would primarily facilitate the detection of overall trends, without providing an elaborate examination of each time step. For instance, preliminary analyses using global centering revealed only three clusters across all time points. While this result is indeed valid in light of the trend illustrated in Figure 3.5, our alternative approach produced multiple clusters, thereby enhancing the specialization of the clusters and also their interpretability.

To perform the fit, we used all the available stations in the dataset, amounting to $n = 105$, but restricted the time horizon to $T = 12$, corresponding to a three-month monitoring period. This limitation was implemented solely to reduce the computational time required to conduct the analyses. As in the previous section, both CDRPM and JDRPM algorithms were fitted with a time-specific parameter α and using their complete model formulations including the optional parameters η_{1i} and φ_1. Regarding the spatial cohesion, we selected C_3, the auxiliary similarity function. To ensure convergence, we inspected the trace plots of both model and, in the case of JDRPM, we checked numerical diagnostics as the Effective Sample Size (ESS) and $\hat{R}$. In fact, JDRPM is able to provide such statistical assessments directly from the fitting function. Regarding the MCMC setup, we derived 4000 iterates from 110000 total iterations, by discarding the first 90000 as burnin and then thinning by 5.

Table 3.2: Comparison between CDRPM and JDRPM fits and their associated algorithms, in the real-world scenario.

	MSE mean	MSE median	execution time
CDRPM	0.0142	0.0149	1h38m
JDRPM	**0.0131**	**0.0138**	**48m**

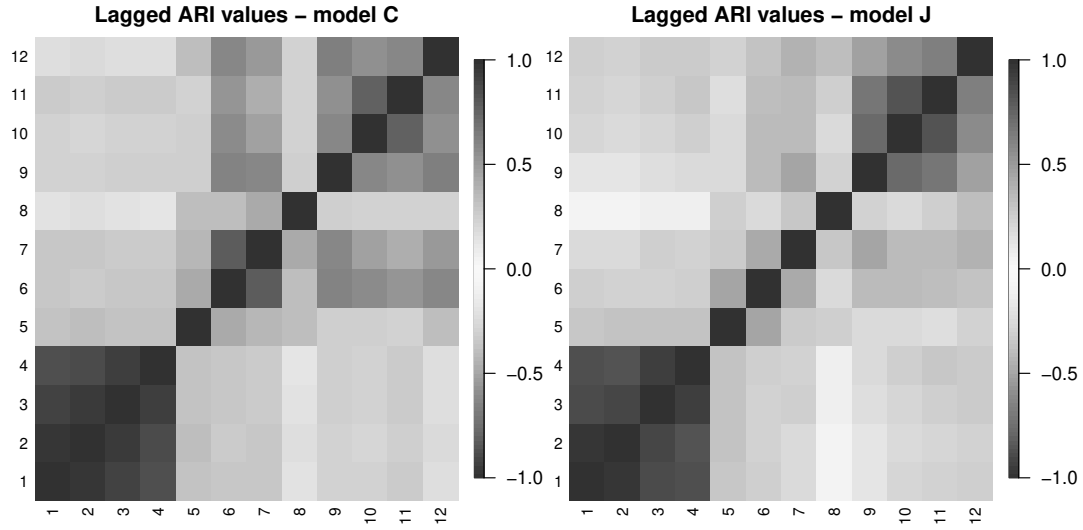

Figure 3.6: Lagged ARI values of CDRPM and JDRPM fits, in the real-world scenario.

Table 3.2 demonstrates that both models achieved remarkable accuracy in their fitted values, with JDRPM leading over CDRPM in terms of MSEs. As previously

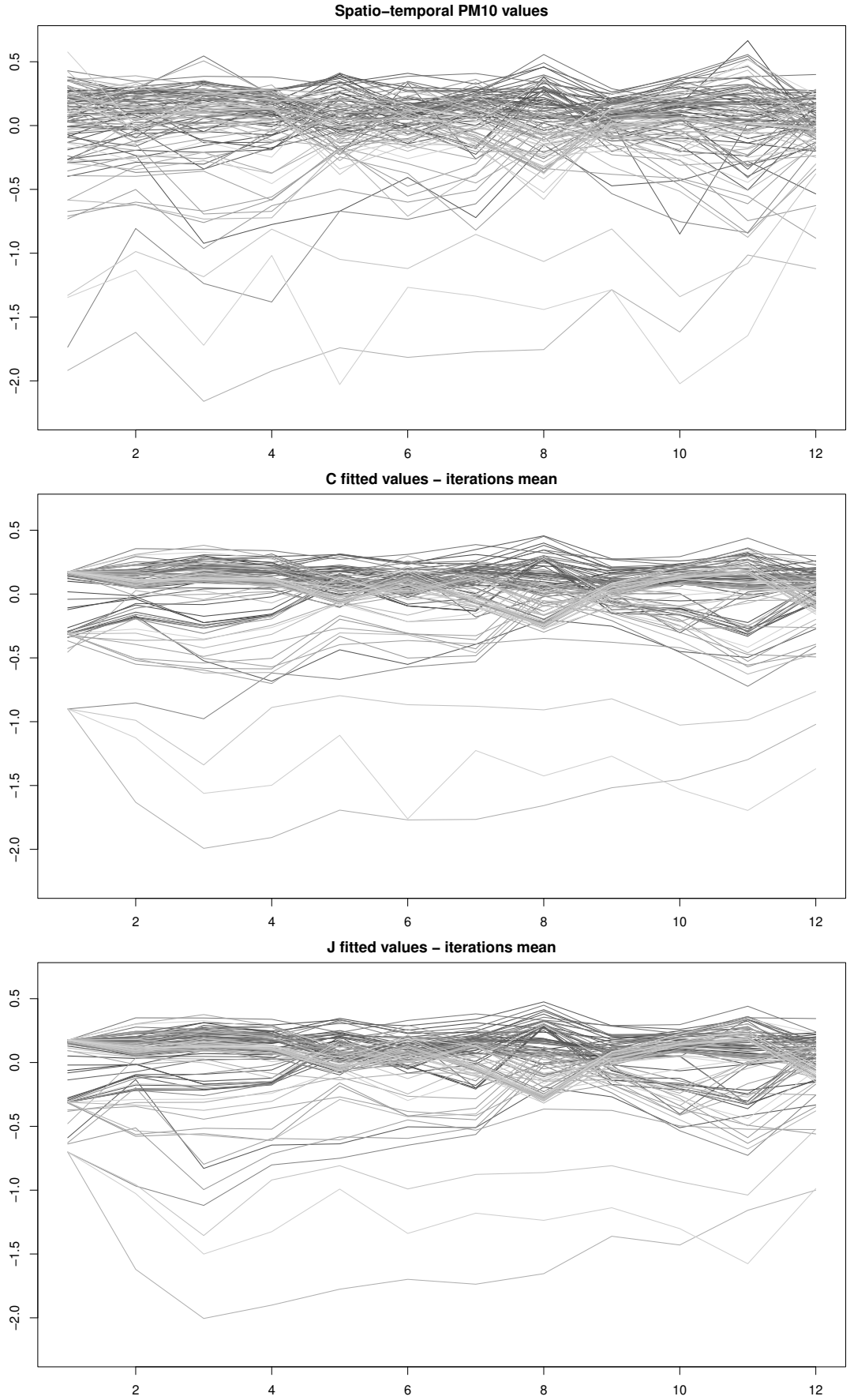

Figure 3.7: Fitted values of CDRPM (middle) and JDRPM (bottom) fits, in the real-world scenario, alongside the generated target values (top).

mentioned, we have chosen not to report the fitting metrics for WAIC and LPML due to the theoretical equivalence of the evaluated models and their corresponding MCMC algorithms. While execution times are included, they may not fully reflect the actual performance, as I was concurrently engaged in writing this thesis, which limited my laptop's computational resources during the fitting process. A more precise assessment of performance timings will be presented in Section 3.4.

Figure 3.6 reveals a similar temporal trend, further validating the correct implementation of JDRPM's MCMC algorithm. In terms of clusters similarity, a partition plot as in Figure 3.2 would appear more congested due to the increased number of units. To effectively convey this information, we computed the adjusted Rand index $\text{ARI}(\rho_{\text{JDRPM}}(t), \rho_{\text{CDRPM}}(t))$ for all time points $t = 1, \dots, 12$. The results yielded a mean of 0.80 and a median of 0.86, signifying a strong agreement between the clusters estimates generated by the two models.

A visual representation of the clusters estimates generated by the two models is provided in Figures C.1 and C.2. Nevertheless, a more comprehensive analysis and discussion will take place in Section 3.3.2, where we will also examine fits with the effects of covariates in the prior and likelihood levels.

3.2 Performance with missing values

In this section, we replicate the analyses and evaluations from Section 3.1, this time focusing on scenarios involving missing values. Our objective is to investigate how the JDRPM performs in the absence of complete datasets and to determine whether it maintains effective performance under such conditions.

Given the extent of missing values in the AgrImOnIA dataset (Fassò et al., 2023), which was used for the spatio-temporal analysis, we opted to set 10% of the values as missing (NAs). To implement this, we randomly selected $nT/10$ indexes from the sets $[1, \dots, n]$ and $[1, \dots, T]$ to identify all the pairs (i, t) that would be designated as missing in the target variable Y_{it}. The ability to handle missing data is an enhancement introduced by the JDRPM; therefore these studies cannot be repeated with the original CDRPM model, which does not accept incomplete datasets.

All the following fits were conducted under the same conditions of their full-dataset counterpart, i.e. using the same models formulation, parameters, and MCMC setup.

3.2.1 No spatial information

The JDRPM model demonstrates remarkable performance even in the presence of missing values. As shown in Table 3.3, the model's performance is understandably lower compared to the full dataset scenario; however, it clearly remains satisfactory. The MSE has naturally increased due to the partial absence of data points which led to less accurate fitted values for the corresponding missing entries. Nevertheless,

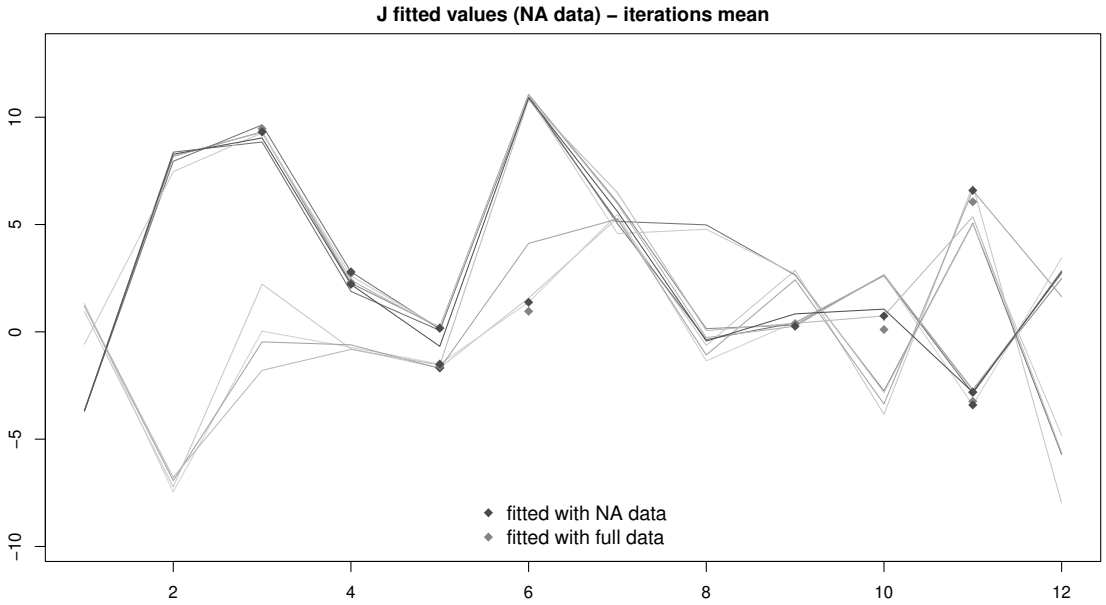

Figure 3.8: Fitted values of JDRPM fit, in the simulated data scenario, with missing values in the target variable. Special square markers are devoted to the data points which were missing, highlighting the gaps between the fitted values on the full dataset (green) and the fitted values on the dataset with missing values (red).

the fitted values, illustrated in Figure 3.8, remain closely aligned with the ones derived from the full dataset analysis.

Table 3.3: Comparison of JDRPM fits, in the simulated data scenario, on a complete dataset and on a dataset with missing values.

	MSE mean	MSE median	LPML	WAIC	exec. time
NA data	1.4721	1.2101	-236.93	401.44	13s
full data	1.2634	1.2034	-223.36	393.97	13s

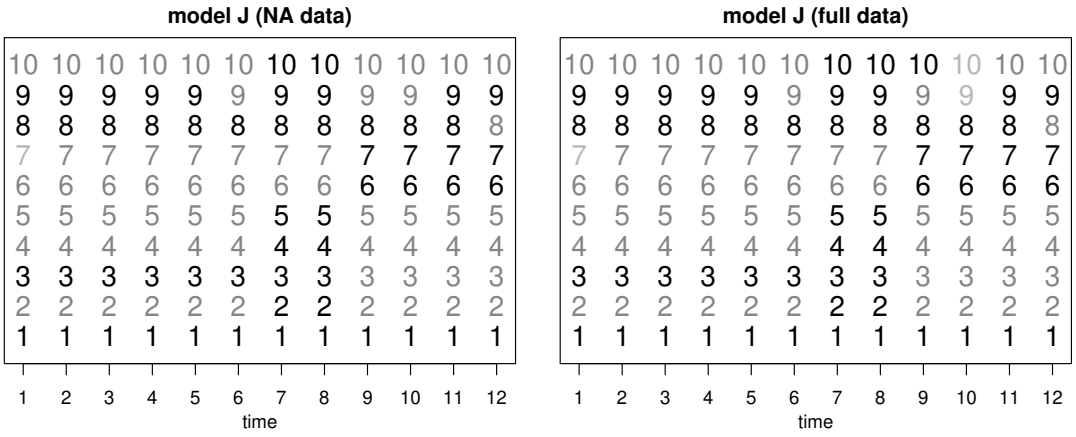

Figure 3.9: Clusters estimates produced by JDRPM fits, in the simulated data scenario, on a dataset with missing values. Time instants are annotated on the x axis, units are indicated vertically by their number, and colors represent the cluster label.

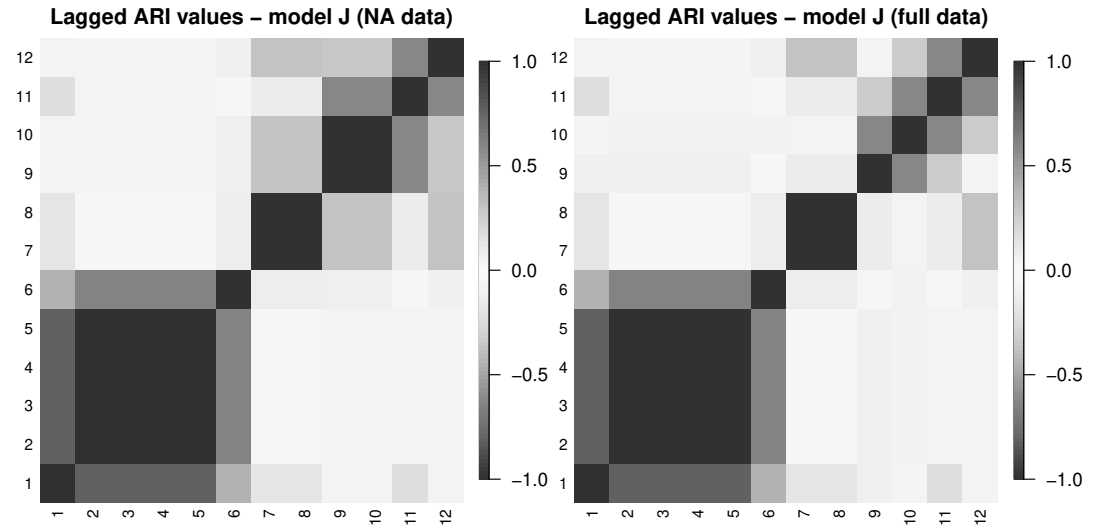

Figure 3.10: Lagged ARI values of JDRPM fits, in the simulated data scenario, on a dataset with missing values.

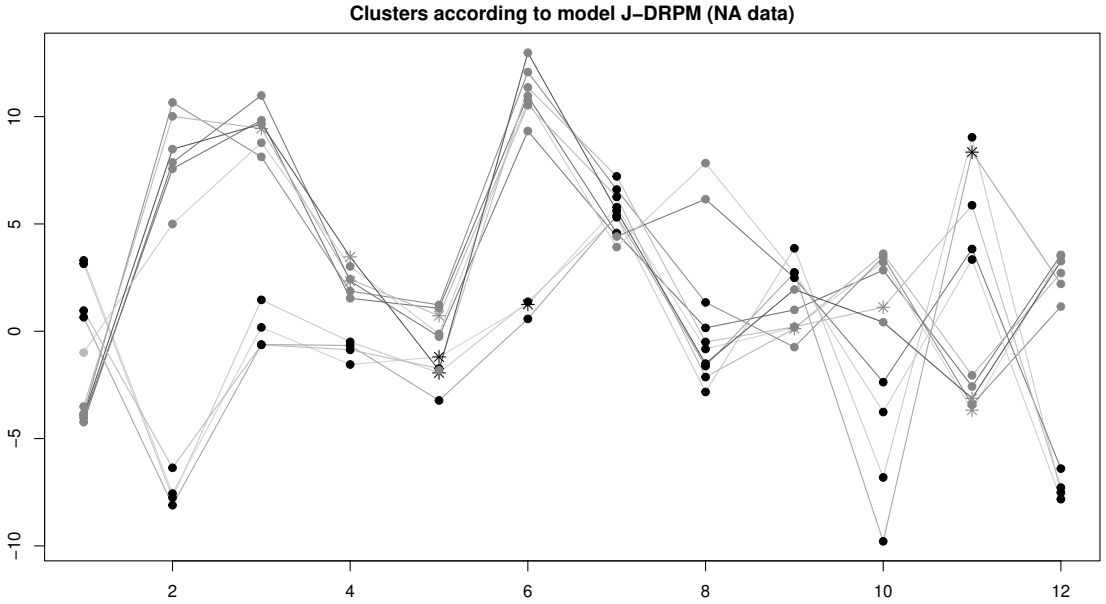

Figure 3.11: Visual representation of the clusters estimates produced by JDRPM fit, in the simulated data scenario, on a dataset with missing values. Cluster labels are represented as colored dots overlaid to the trend of the target variable, with special point markers devoted to data points corresponding to missing values.

From Figures 3.10, we observe a nearly identical temporal trend to that seen in the absence of missing data, indicating that JDRPM effectively captured a robust temporal dependency structure even when some data points were missing. Additionally, the clusters generated, as shown in Figure 3.11, appear remarkably similar. The only notable difference occurred around time $t = 10$, where the model now failed to identify the green cluster that characterized the final transition phase of units 9 and 10. This discrepancy may be attributed to the NA assignment of unit 9 at time 10, which likely removed critical information necessary for identifying

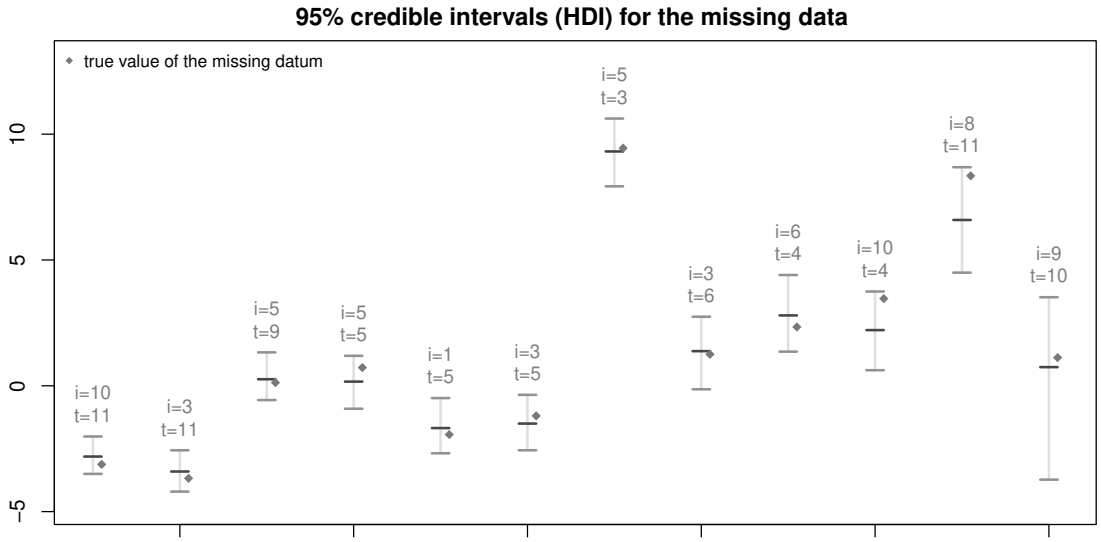

Figure 3.12: Credible intervals, computed with the highest posterior density (HPD) method at a 95% confidence, for the fitted values of the missing units in the JDRPM fit, in the simulated data scenario, on a dataset with missing values. In gray are reported the indexes of units i and time instants t which where missing, while green dots refer to the true values of the missing data.

that specific third cluster.

Finally, Figure 3.12 presents the 95% credible intervals for the fitted values corresponding to the missing data points. In nearly all cases, except for one, the true value falls within the credible interval, demonstrating the accuracy of JDRPM in providing reliable estimates of the target values, even in situations where no additional information was available from either space or covariates.

3.2.2 With spatial information

Table 3.4: Comparison of JDRPM fits, in the real-world scenario, on a complete dataset and on a dataset with missing values.

	MSE mean	MSE median	LPML	WAIC	exec. time
NA data	0.0160	0.0170	502.86	-1793.64	43m
full data	0.0131	0.0138	624.91	-1898.05	48m

The JDRPM demonstrates exhibits robust performance also in real-world scenario involving a dataset with missing values. Table 3.4 indicates a slight reduction in accuracy, which is expected due to the presence of missing data; however, the decline is not substantial. The fitted values are displayed in Figure 3.13, revealing how the estimation of the missing data becomes more challenging for the points that lie farther away from the main trajectory of the distribution. It is worth noting that the reported execution times may not fully reflect reality, as previously mentioned, due to my laptop's resources not being entirely devoted to the fitting process. In fact, the JDRPM fit with missing data ran faster than the JDRPM fit with complete data, which raises some eyebrows since we should typically expect

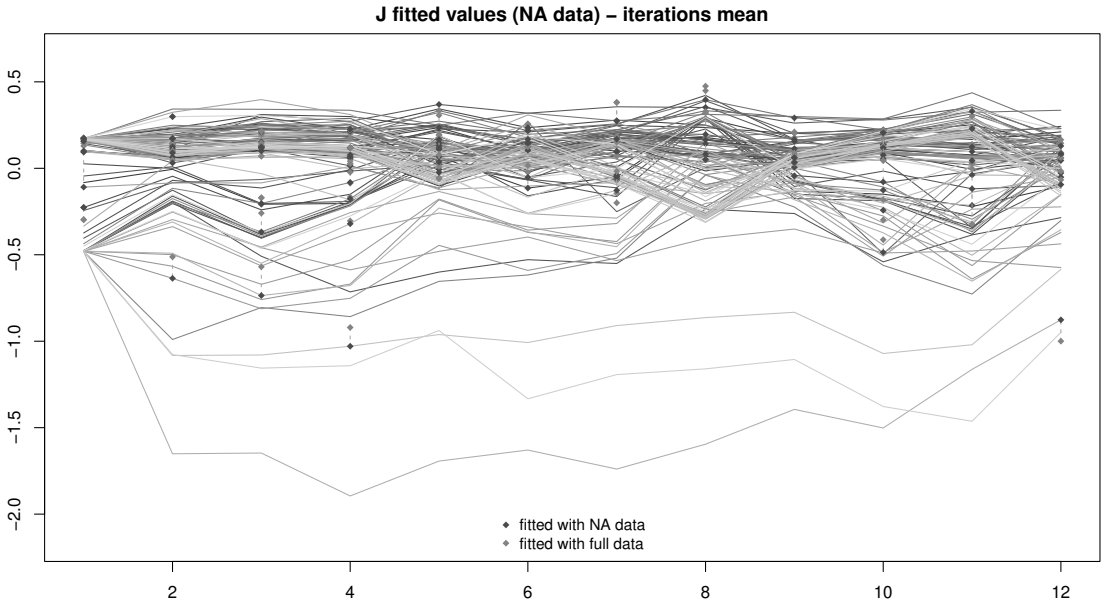

Figure 3.13: Fitted values of JDRPM fit, in the real-world scenario, on a dataset with missing values. Special square markers are devoted to the data points which were missing, highlighting the gaps between the fitted values on the full dataset (green) and the fitted values on the dataset with missing values (red).

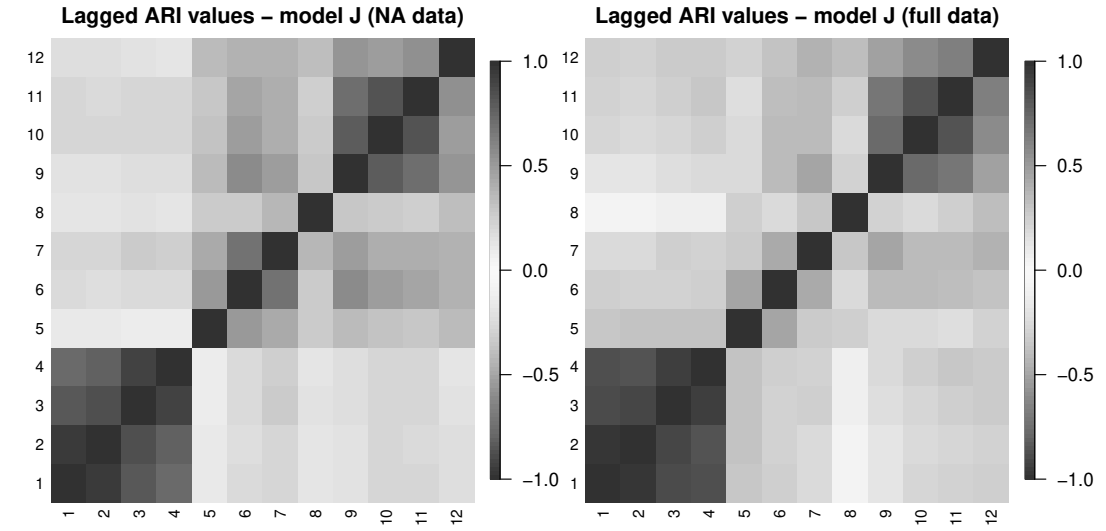

Figure 3.14: Lagged ARI values of JDRPM fits, in the real-world scenario, on a dataset with missing values.

additional computational demands when dealing with missing Y_{it} values due to their sampling in the MCMC algorithm. Again, for more accurate performance assessments we refer to Section 3.4.

The temporal trend remained consistent with what we observed in Section 3.1.2, as evidenced by Figure 3.14. Interestingly, the ARI plot for the JDRPM fit with missing data closely mirrors the original trend displayed by the CDRPM fit on the complete dataset; a similar pattern was also noted in the previous section regarding

fits in the simulated data scenario. To precisely evaluate clusters similarity, we computed the adjusted Rand index $\text{ARI}(\rho_{\text{JDRPM\_NA}}(t), \rho_{\text{JDRPM\_full}}(t))$ for each time point $t = 1, \dots, 12$. The results yielded a mean of 0.82 and a median of 0.86, indicating a strong level of agreement in the partitions despite the loss of a significant amount of data (121 points out of 1260 from the full dataset).

3.3 Effects of the covariates

We now conduct several experiments to explore the key advancement introduced by the JDRPM: the inclusion of covariates. Given their distinctly different purposes, we study separately the effects of including covariates in the likelihood and including covariates in the prior. Nevertheless, an analysis of the combined use of both information levels will be provided in Section 3.3.3. For the upcoming fits, all included covariates underwent the same time-wise correction applied to target variable, as outlined in Section 3.1.2.

3.3.1 Covariates in the likelihood

Following the discussion of the previous section, we can explore whether the inclusion of covariates in the likelihood can enhance accuracy in fits that deal with missing data. In fact, the main purpose of introducing the regression parameter $\boldsymbol{\beta}t$ was to improve the precision of the model's estimates for the target values Y_{it}, without significantly influencing the clusters generation. Therefore, the most natural application of this parameter arises when fitting models with missing values.

Table 3.5: Comparison of JDRPM fits, in the real-world scenario, with and without the inclusion of covariates in the likelihood, on a complete dataset and on a dataset with missing values.

	MSE mean	MSE median	LPML	WAIC	exec. time
full data	0.0131	0.0138	624.91	-1898.05	**48m**
full data + Xlk	**0.0112**	**0.0113**	**778.96**	**-2029.84**	56m
NA data	0.0160	0.0170	502.86	-1793.64	**43m**
NA data + Xlk	**0.0127**	**0.0130**	**625.81**	**1902.74**	58m

Indeed, after including multiple covariates in the likelihood and repeating the fit on the spatio-temporal dataset with missing values, we observed notable improvements. To effectively compare these enhanced results, we also performed the corresponding fit with covariates in the likelihood on the complete dataset, with the resulting cluster estimates displayed in Figure C.3. The results are summarized in Table 3.5, which also includes reference results from previous fits of Sections 3.1.2 and 3.2.2, which did not include the regressor component.

The inclusion of covariates in the likelihood clearly enhanced all fitting metrics. This demonstrates that incorporating covariates in the likelihood can effectively recover accuracy in the presence of missing values or to generally improve the

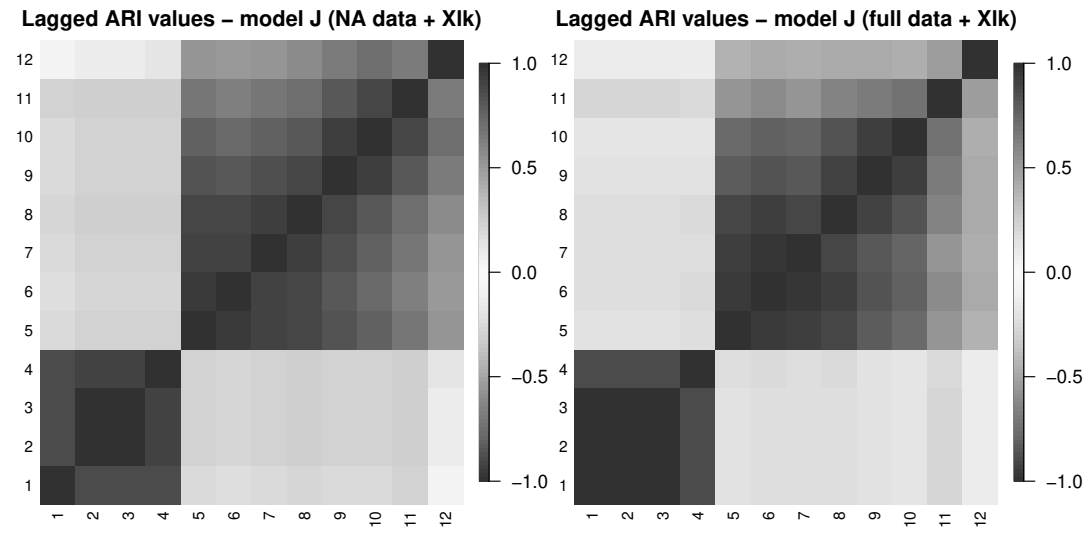

Figure 3.15: Lagged ARI values of JDRPM fits, in the real-world scenario, with covariates in the likelihood, on a dataset with missing values

estimates of the target variable Y_{it}. The regression vectors $\boldsymbol{\beta}_t$ exhibited favourable trace plots, as shown in Figures 3.16 and 3.17, confirming the correctness and effectiveness of the implementation. Additionally, the values of the regressors appear reasonable and interpretable. For instance, it is well established that higher altitudes correlate with lower air pollution levels, due to the scarcity of emission sources like industries and vehicles, stronger winds, and lower atmospheric pressure that facilitates air mixing. Consequently, the $\boldsymbol{\beta}_t$ component associated with `Altitude` hovers around negative values, indicating a reduction in PM_{10} concentrations. Conversely, the `LI_bovine` covariate, which represents the density of bovines per km^2 near the measuring station, tends to remain positive, reflecting the contribution of livestock industries to air pollutant emissions.

The generated partitions remained mostly unchanged. The spatio-temporal trend was similarly preserved, as shown in Figure 3.15, although a generally higher dependence was noted in the latter part of the time interval, after the correctly identified change point at $t = 4$.

The function which implements JDRPM's MCMC algorithm includes a parameter `beta_update_threshold`, defaulted to zero, that specifies the iteration after which the algorithm begins updating the $\boldsymbol{\beta}_t$ parameter. This addition, both harmless and straightforward, allows the model to prioritize the updating and refinement of more critical clustering parameters, such as $\mu^{\star}_{jt}$ and $\sigma^{2\star}_{jt}$, before turning its attention to updating the $\boldsymbol{\beta}_t$ parameter. Otherwise, without this adjustment, the early development of model parameters and cluster assignments could be skewed by inaccurate samples from the likelihood regressor, potentially compromising the overall performance of the model.

Figure 3.18 illustrates the fitted values from the JDRPM applied to the spatio-temporal dataset with missing values and incorporating covariates in likelihood. Visually, and as demonstrated by the improved MSEs, these fitted values more

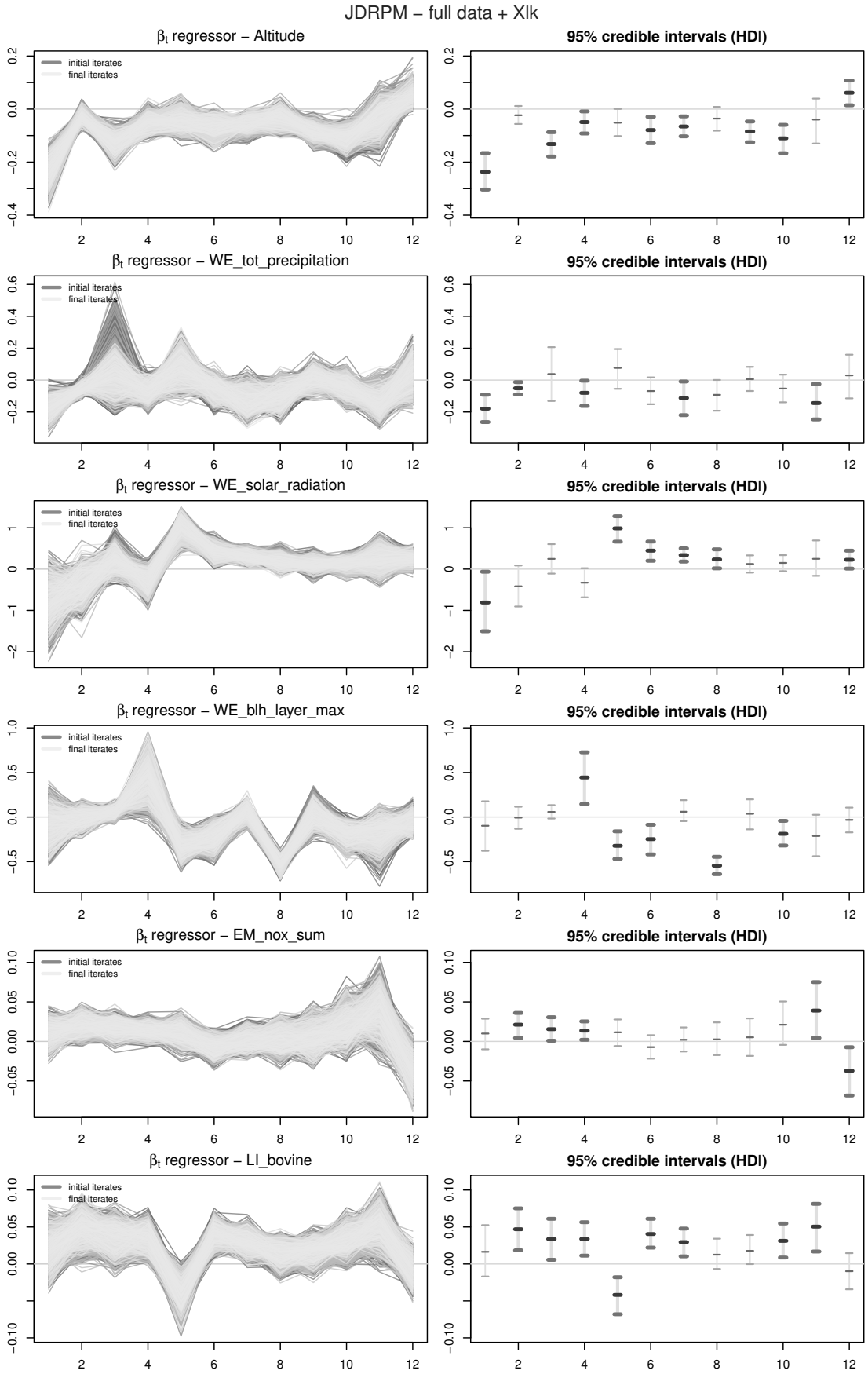

Figure 3.16: Regression vector $\boldsymbol{\beta}_t$ of JDRPM fit, in the real-world scenario, for the $p = 6$ covariates inserted in the likelihood, on the full spatio-temporal dataset, with trace plots (left) and 95% credible intervals (right) computed with the highest density interval (HDI) method.

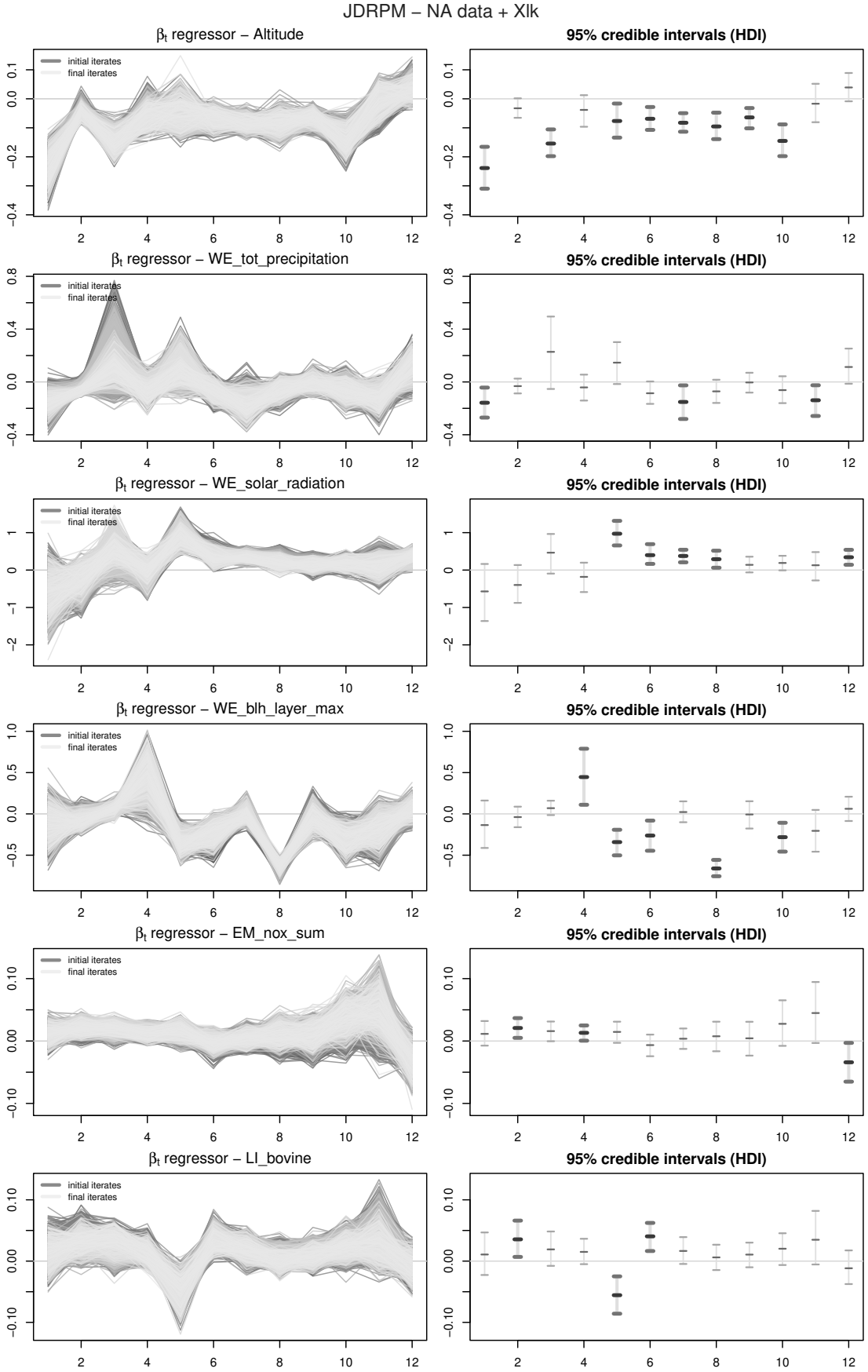

Figure 3.17: Regression vector $\boldsymbol{\beta}_t$ of JDRPM fit, in the real-world scenario, for the $p = 6$ covariates inserted in the likelihood, on the spatio-temporal dataset with missing values, with trace plots (left) and 95% credible intervals (right) computed with the highest density interval (HDI) method.

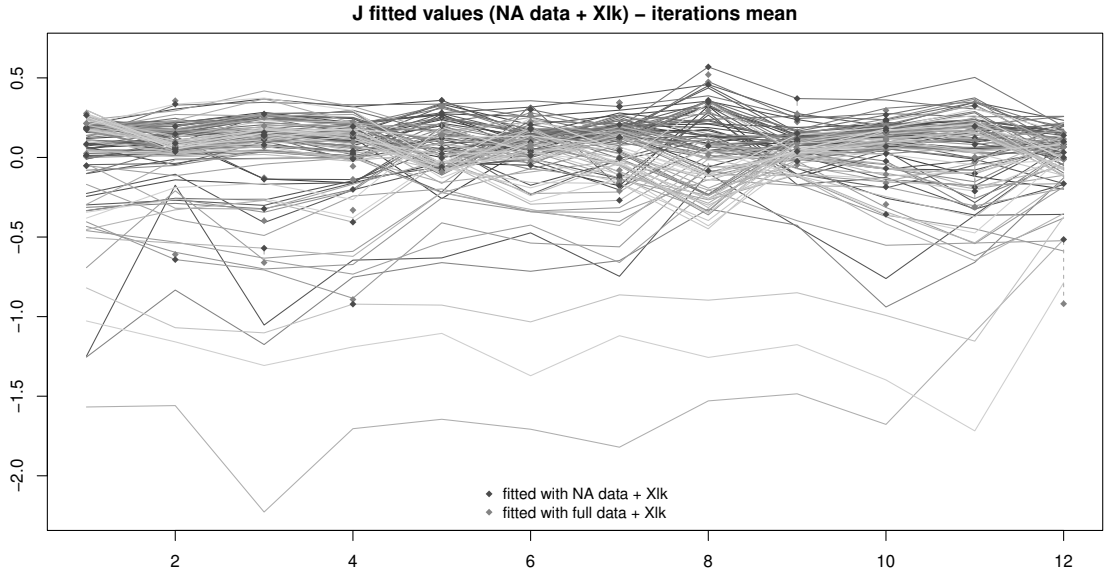

Figure 3.18: Target and fitted values of the JDRPM fits with target plus space values, on the NA and full dataset, to see the effects of the insertion of covariates in the likelihood.

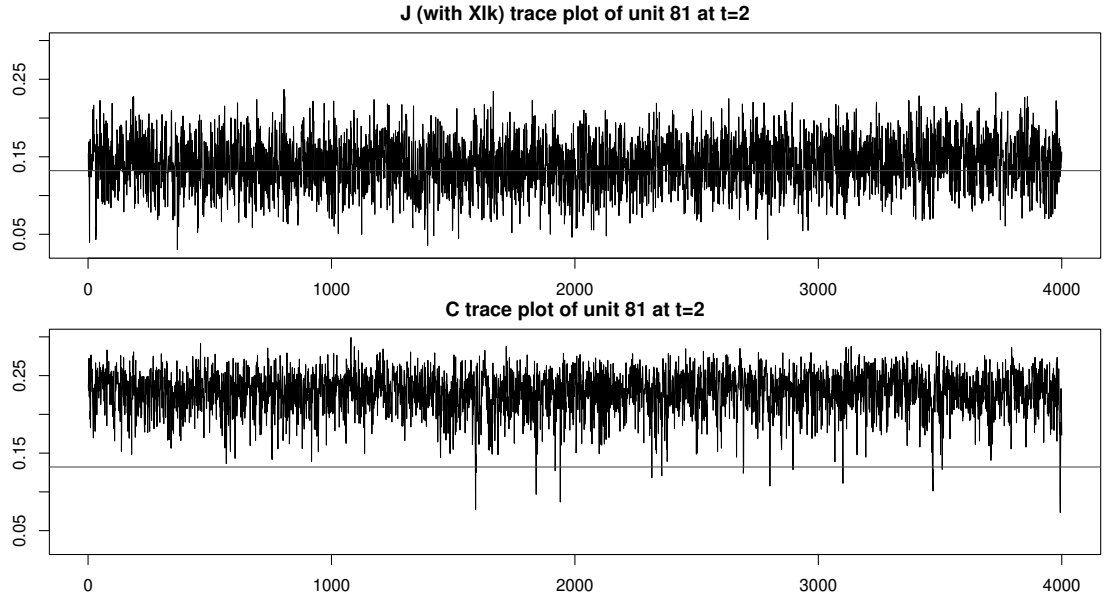

Figure 3.19: Trace plot of the fitted values of a specific unit i and time instant t, comparing the JDRPM fit with covariates in the likelihood to the standard spatially-informed CDRPM fit. The green line represents the true value of Y_{it}.

closely align with those of the real target variable. This is particularly evident when compared to the results in Figure 3.7, where both fits were performed without any "external suggestions" from covariates. Further evidence supporting the effectiveness of including covariates in the likelihood is provided in Figure 3.19, which displays the trace plot of the fitted values for a problematic unit and time in which both the standard JDRPM and CDRPM fits struggled to deliver accurate estimates. However, with the inclusion of covariates, these estimates have become more precise and are now closer to the actual associated Y_{it} value.

Overall, this analysis highlights how the addition of the regression parameter $\boldsymbol{\beta}_t$ can improve the accuracy of the results and partially support for the clustering process, as the contribution from the covariates in improving the Y_{it} estimates becomes evident in refining the update steps for the clustering parameters. In fact, as we saw in (1.10) and (1.11), the update rules of $\sigma^{2\star}_{jt}$ and $\mu^{\star}_{jt}$ are also influenced by a term involving $\boldsymbol{\beta}_t$.

3.3.2 Covariates in the prior

We now turn our attention to the inclusion of covariates in the prior. In deciding which covariates to incorporate, we focused on the factors that would most significantly influence PM_{10} concentrations. Ultimately, we selected the following three covariates:

- `WE_wind_speed_10m_max`. Wind speed is a key factor affecting air pollutant concentration levels. Its impact is twofold: on one hand, wind can disperse pollutants away from their sources, thereby reducing local concentrations; on the other hand, it can increase airborne contaminants by resuspending settled particles from surfaces like roads, soil, and buildings. This latter effect is particularly evident in dry and windy rural areas, making Lombardy region a relevant case study. The dataset also included wind speed at 100 m, a variable that however would be more suitable for broader analyses that track PM_{10} concentration trends across multiple regions or countries. In contrast, our approach focused on local dynamics and ground-level perspectives to cities in Lombardy, thus making the 10 m measurement more appropriate for our objectives.

- `WE_tot_precipitation`. Rain is well-known for its ability to enhance air quality by capturing aerosol particles and bringing them down to the ground. This process, often referred to as wet deposition, precipitation scavenging, or washout, is highly effective at reducing air pollutant concentrations. Consequently, this variable was considered highly relevant for inclusion in our analysis.

- `WE_blh_layer_max`. The boundary layer height (BLH) is another key factor influencing the dispersion of air contaminants. This variable defines the maximum altitude at which air mixing takes place. Typically, air cools as it rises in the atmosphere; however, there can be instances where warm air exists above colder air. At this boundary, mixing becomes inhibited, as the warm layer acts like a lid trapping the cooler air, and its associated pollutants, beneath it. This phenomenon leads to a deterioration in air quality, as pollution accumulates without a means of dispersal. Consequently, this covariate measures the maximum height of this problematic layer, with lower values indicating a higher expected concentration of pollutants due to restricted vertical mixing.

To conduct the JDRPM fit with covariates in the prior, we retained the same hyperparameters and MCMC configuration used in our earlier spatio-temporal

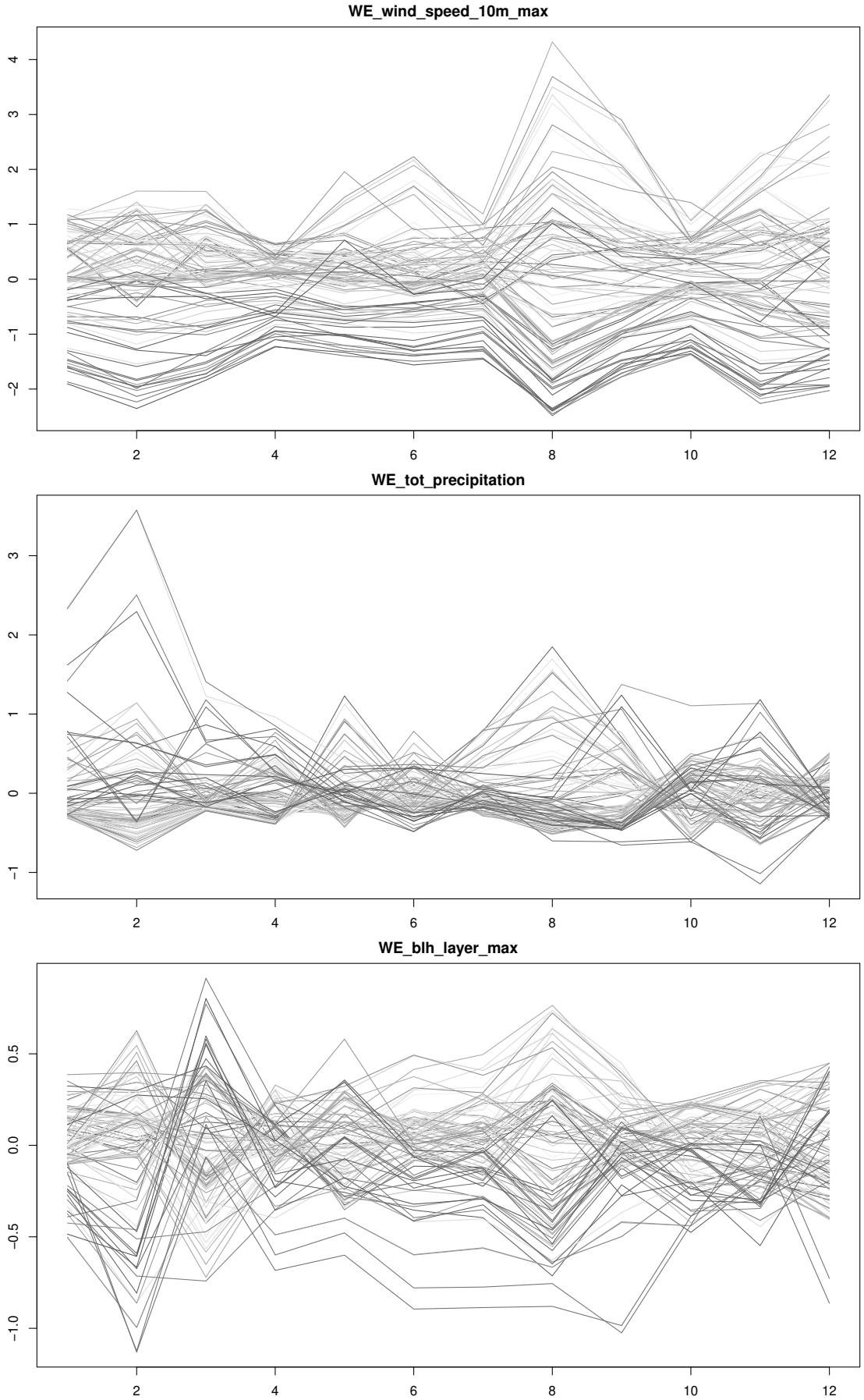

Figure 3.20: Covariates selected to be included in the prior. Coloring is based on the ranking of PM_{10} values of the units according to their median, from highest (red) to lowest (blue).

experiments described in Sections 3.1.2 and 3.2.2. For the similarity function we opted for g_4, the auxiliary similarity function, setting its parameters to $\mu_0 = 0$, $\lambda_0 = 1$, $a_0 = 7.5$, and $b_0 = 2$. This selection was based on experimental adjustments and especially on the standardization and centering process that was applied to covariates. In fact, as effectively illustrated in Figure 3.20, the trends of the covariates generally remained within the $[-1, 1]$ interval.

Table 3.6: Comparison between CDRPM and JDRPM fits and their associated algorithms, in the real-world scenario, with and without covariates in the prior.

	MSE mean	MSE median	LPML	WAIC	exec. time
CDRPM	0.0142	0.0149	694.81	-1768.42	1h38m
JDRPM	0.0131	0.0138	624.91	-1898.05	**48m**
JDRPM + Xcl	**0.0126**	**0.0135**	**677.71**	**-1969.76**	1h20m

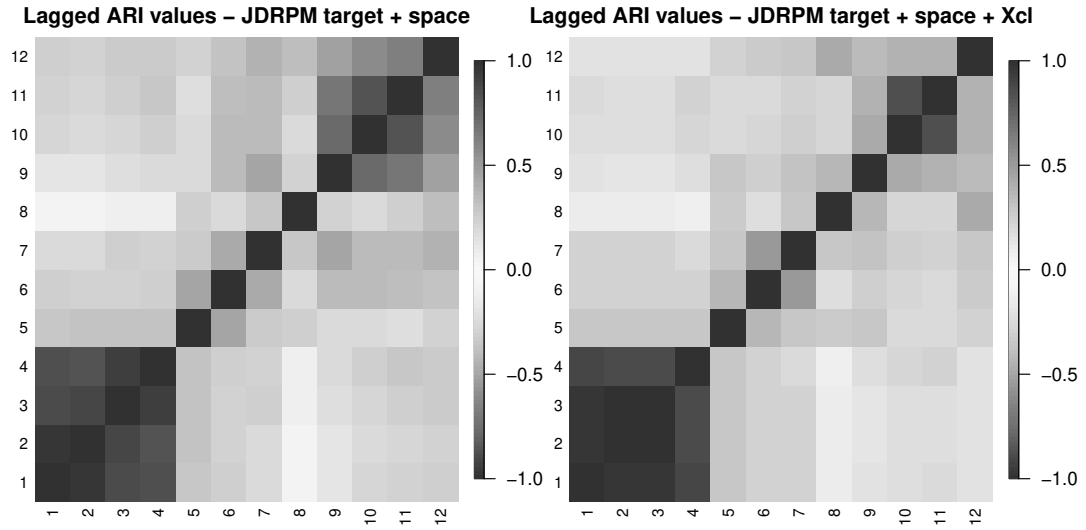

Figure 3.21: Lagged ARI values of CDRPM and JDRPM fits, in the real-world scenario, with covariates in the prior.

The results of this analysis are quite promising, as highlighted in Table 3.6, where we observe substantial improvements across all metrics when covariates are incorporated into the prior. The temporal trend of this latter fit is proposed in Figure 3.21. Although incorporating multiple covariates introduces the possibility of divergent "clustering suggestions," their contributions can still be effectively assessed. This is illustrated by complementing the partition representation with cluster-specific boxplots for the target variable PM_{10} and the three covariates considered in the analysis. Figure 3.22 provides a comparative overview of the fits reported in Table 3.6. This figure demonstrates how the JDRPM fit with covariates in the prior captured a more refined and coherent clustering structure compared to its two competitors.

The JDRPM fit with covariates in the prior, illustrated in panel (c), is the only model that demonstrates a clear separation among the covariates, particularly

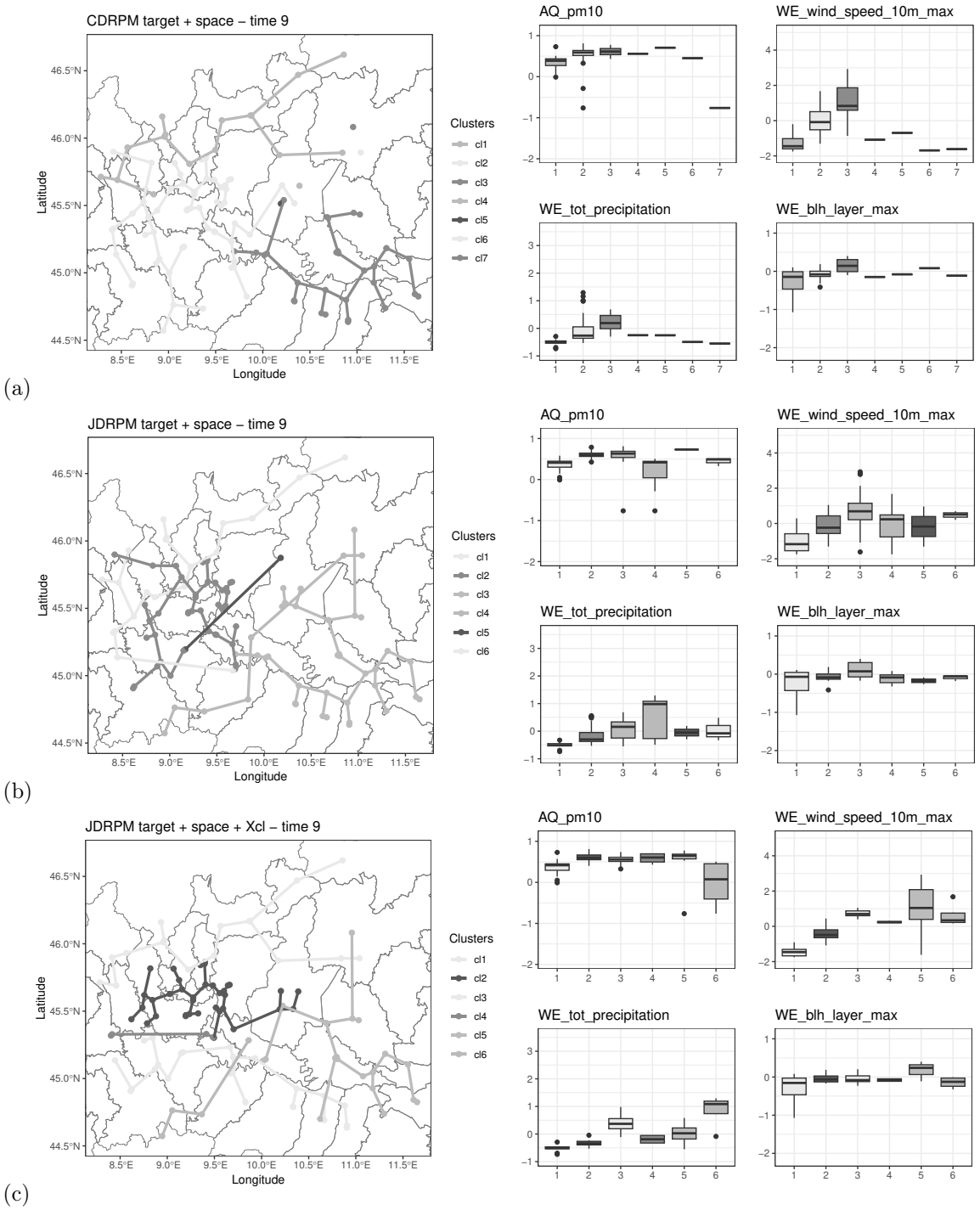

Figure 3.22: Visual representation of the clusters estimates produced by CDRPM and JDRPM fits, in the real-world scenario, exemplified by the case $t = 9$. The three panels refer to the standard spatially-informed fits of CDRPM (a) and JDRPM (b), along with the JDRPM with covariates in the prior (c).

regarding wind speed and total precipitation. A subtler separation also emerges for the BLH covariate, although somewhat obscured by the overall proximity of values across all the units, but evidenced by the disappearance of outliers present in cluster 2 in panels (a) and (b). These distinctions, supported by the improved

metrics, appear to contribute to a more accurate estimation of the clusters.

For instance, all models successfully identified the cluster extending over the mountain arch in the northern part of the map. This cluster is characterized by relatively low levels of PM_{10} and low values for the wind speed covariate. This is clearly depicted in panel (c), where cluster 1 is positioned at the bottom of the plot and is well-separated from the other clusters. In panels (a) and (b), the associated wind speed boxplots also place cluster 1 at the lower end of the scale; however, its values intersect with those of other clusters. This suggests that some units correctly assigned to cluster 1 by model (c) may have been misclassified by the other models.

Another notable improvement is observed in the identification of the most polluted cluster, depicted in dark red across all panels. While both spatially-informed models yielded smaller clusters, a singleton in panel (a) and a couple in panel (b), model (c) provided a more comprehensive analysis by identifying a larger and more spatially connected region of highly polluted units. This cluster is also characterized by the second lowest levels of wind speed and total precipitation, suggesting that these factors likely hindered pollutant dispersion, leading to these cities becoming the most polluted. Again, this insight was facilitated by the covariate contributions of model (c), which remained partially concealed in the purely spatially-informed fits presented in panels (a) and (b).

The impact of incorporating covariates in the prior is further illustrated in Figures 3.23 and 3.24, which compare the distribution of clusters with respect to the values of the `WE_wind_speed_10m_max` covariate. In these figures, colors represent cluster labels, so that units are ordered not by their conventional indexing $i = 1, \dots, 105$ but rather by the clusters sets $\{i : i \in S_{1t}\}, \dots, \{i : i \in S_{k_t t}\}$. While all models employed PM_{10} as the target variable, suggesting that the highest degree of separation should be observed there, we can expect that the inclusion of covariates would also reveal a clustering pattern within the auxiliary covariates included. Indeed, the distribution of clusters in the JDRPM fit with covariates exhibits a clearer distinction regarding the wind speed variable, while this separation appears more ambiguous in the CDRPM fit. The effects of including covariates are particularly evident at time points 8, 9, and 12. For instance, at $t = 12$, the red cluster identified by CDRPM in Figure 3.23 splits into red, green, and blue clusters that are more distinctly separated in the JDRPM informed with covariates shown in Figure 3.24. Additionally, when comparing this latter JDRPM fit with covariates to the standard spatially-informed JDRPM fit of Figure 3.25, we also observe a slight improvement.

It is important to note that the enhancement resulting from the inclusion of covariates could potentially have been more pronounced had we set a higher value for the parameter `cv_weight` in the Julia function implementing the MCMC algorithm. In this analysis, in fact, the covariate-informed fit was obtained with this parameter set to 0.2, to balance the total contribution of the covariates with that of the spatial information. Therefore, increasing the value of `cv_weight` would likely yield even clearer distinctions in this covariate separation analysis.

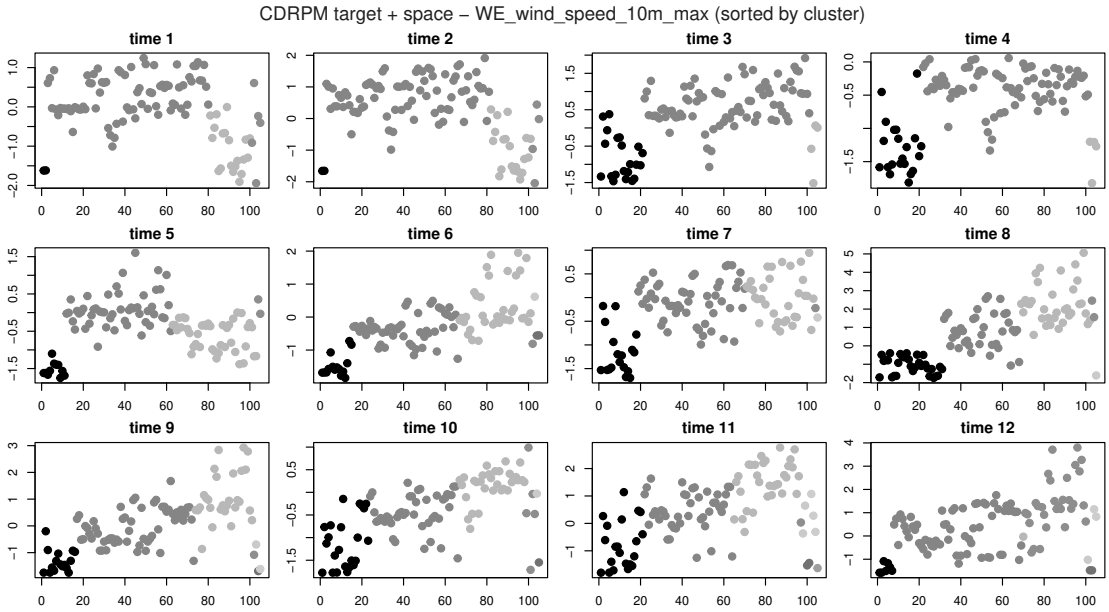

Figure 3.23: Distributions of clusters estimates with respect to the wind speed covariate, in the CDRPM spatially-informed fit.

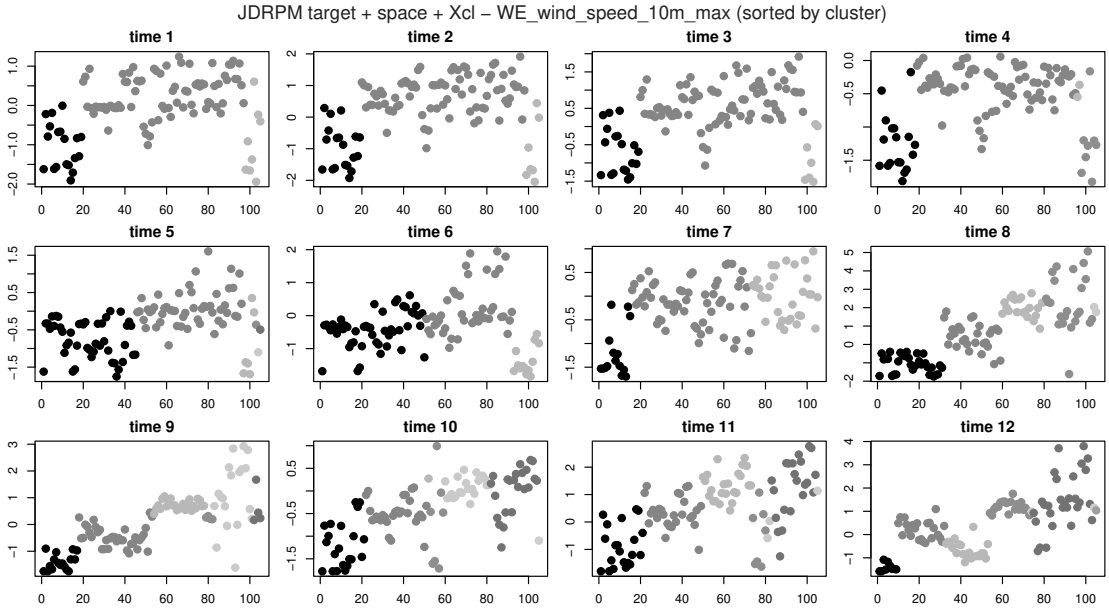

Figure 3.24: Distributions of clusters estimates with respect to the wind speed covariate, in the JDRPM spatially-informed fit with covariates in the prior.

3.3.3 Inference on a new location

We now conduct a final analysis that consolidates all the enhancements introduced by the JDRPM. In this analysis, we consider a spatio-temporal scenario in which a new unit is added at a new location, with the objective of inferring the values of its target variable time series. Alternatively, this scenario can be interpreted as removing all data entries from an existing unit within the dataset. In this context of kriging (Krige, 1951), we aim to evaluate the JDRPM's accuracy in

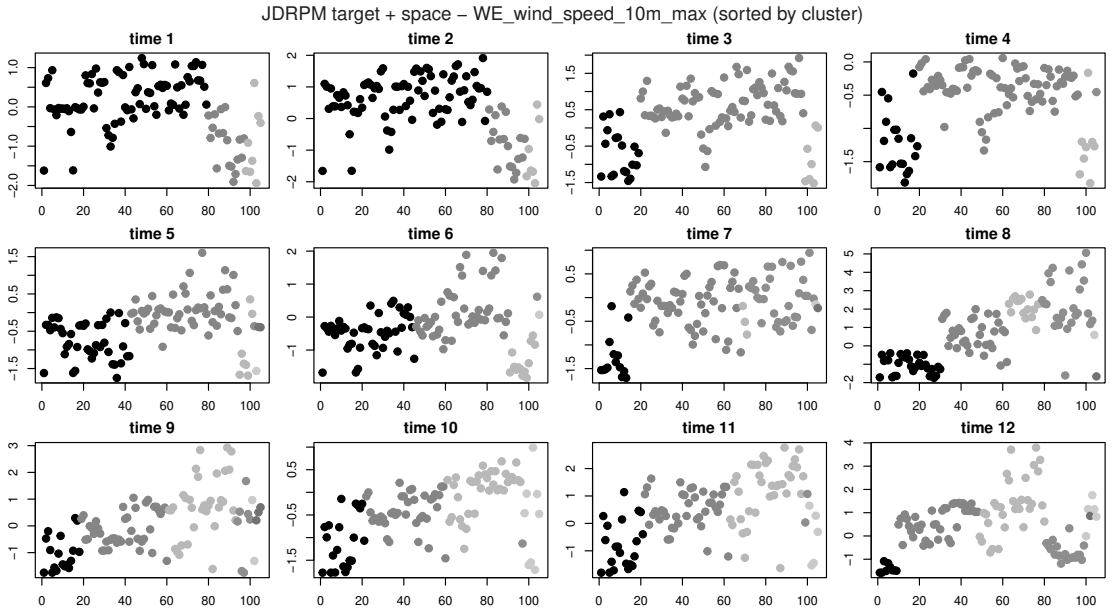

Figure 3.25: Distributions of clusters estimates with respect to the wind speed covariate, in the JDRPM spatially-informed fit.

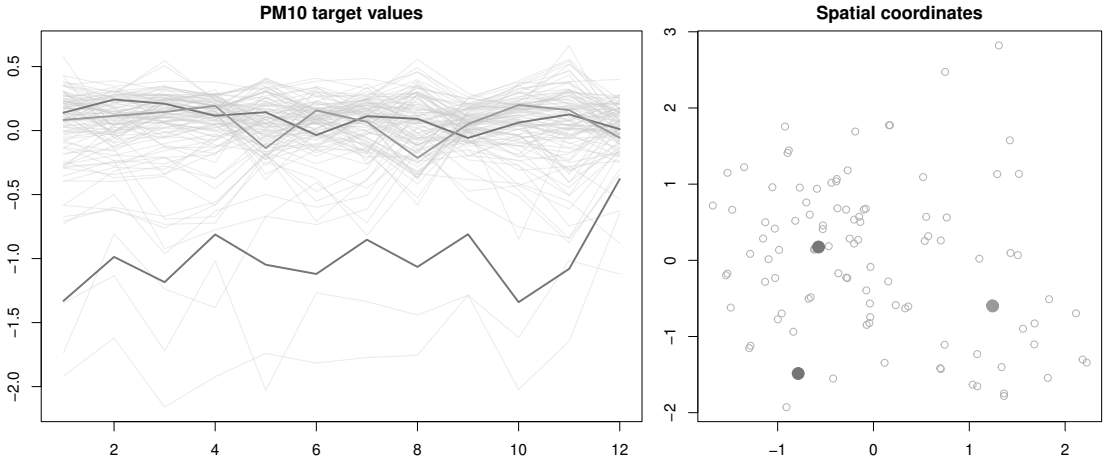

Figure 3.26: Representation of the three units selected for the kriging analysis, with their associated target variable time series (left) and spatial coordinates (right).

predicting the behavior of a unit for which sensors may be absent or inactive, with the expectation that the estimation accuracy will improve as model complexity increases. To assert this, we conducted an experiment in which all data entries of the response variable were to NA for three randomly selected units, represented in Figure 3.26. We performed multiple JDRPM fits with incremental levels of information: first with only the spatial information, then incorporating covariates in the likelihood, and finally including covariates also in the prior. We do not report the results from tests that included only covariates in the prior, as such an approach would be more aligned for clustering, rather than kriging. We used the same set of six covariates employed in Section 3.3.1 for the likelihood component, and the same set of three covariates used in Section 3.3.2 for the prior component.

Table 3.7 illustrates that the inclusion of covariates substantially improved the estimates for the missing units. The MSEs were calculated by taking both the mean and median of the fitted values from each model and comparing them to the true values of the missing units. Overall, the fit that incorporated covariates solely in the likelihood achieved the highest performance level. Notably, the base spatially-informed fit provided greater estimation accuracy for the fitted values associated with the green unit. In contrast, for the other units, the covariate-informed fits proved to be substantially more accurate. Figures 3.28 to 3.30 illustrate the 95% credible intervals of the estimated target values for the kriging units, derived from the three models examined.

Table 3.7: Comparison of JDRPM fits and their associated algorithms, in the kriging scenario.

		space	space+Xlk	space+Xlk+Xcl
unit 92 (red)	MSE mean	0.112452	**0.042037**	0.044957
	MSE median	0.111573	**0.041676**	0.045216
unit 61 (blue)	MSE mean	0.004117	**0.002449**	0.002527
	MSE median	0.004711	0.002547	**0.002534**
unit 44 (green)	MSE mean	**0.003919**	0.006368	0.005945
	MSE median	**0.003997**	0.006419	0.005950
	execution time	45m	**40m**	1h15m
	LPML	620.98	758.11	**791.86**
	WAIC	-1842.48	**-2041.95**	-1976.73

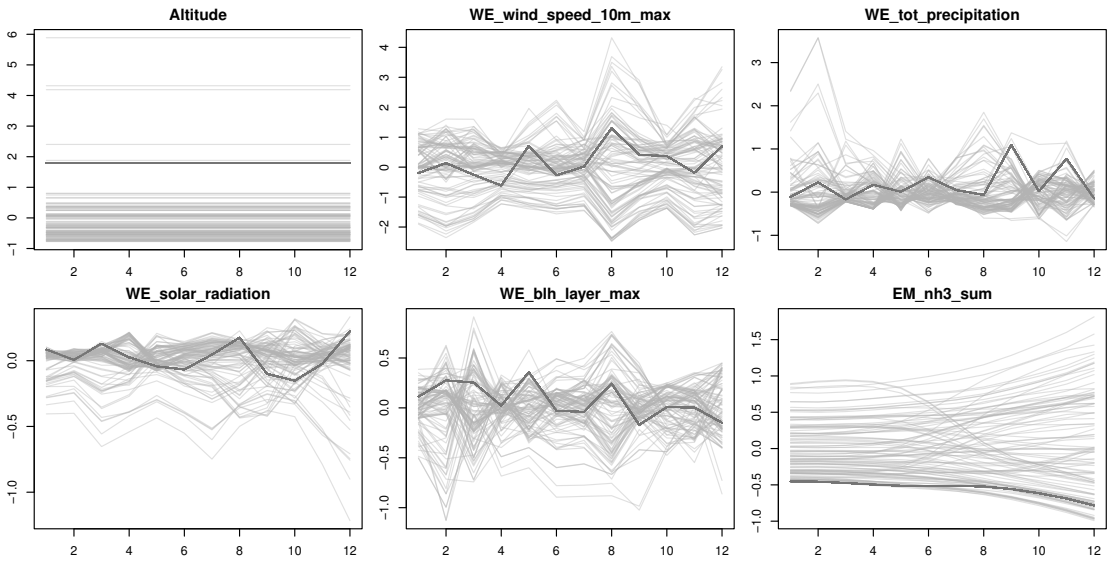

Figure 3.27: Covariates included in the likelihood, relative to unit 92, in the kriging analysis.

It is important to highlight that unit 92, marked in red in Figure 3.26, demonstrates significantly inferior fitted estimates when compared to other units. This discrepancy may stem from various factors. First, unit 92 is relatively isolated spatially, situated at a significant distance from its neighbouring units. Secondly, Figure

3.27 illustrates how unit 92 exhibits extreme values for the covariates `Altitude` and `EM_nh3_sum`. Thirdly, the clustering estimates shown in Figures C.1 through C.4 indicate that unit 92 is sometimes classified as a singleton. These factors suggests a distinctive behavior in the associated time series on PM_{10}, which may complicate estimation efforts within the kriging context.

According to (Quintana et al., 2015), the sole inclusion of covariates in the likelihood accounts only for their linear effects, as represented by the regressor term $\boldsymbol{\beta}_t$, resulting in a minimal impact on clusters estimates. In contrast, incorporating covariates solely in the prior captures all effects of the covariates, often leading to a greater number of smaller, more specific clusters, without necessarily improving the fitted estimates. A balanced approach can be achieved by incorporating covariates at both levels of information. This strategy allows for the linear effects to be considered in the likelihood, while also accommodating nonlinear effects in the clustering process. As a result, this dual approach can yield improved outcomes for both fitted values and cluster estimates.

3.4 Scaling performances

To rigorously assess whether the objective of faster execution times was achieved, we designed a series of experiments to compare the two models across different dataset sizes and varying levels of information.

Regarding information levels, CDRPM allowed clustering based solely on the target variable or with additional spatial information, while JDRPM expanded these options enabling the inclusion of covariates at both the likelihood and prior levels. We recall that, aside from the target variable which is of course always required, all other information levels are optional and independent, allowing flexible configurations such as fitting with covariates but without spatial information. However, with an additive perspective in mind, we conducted incremental experiments where we progressively inserted new information layers on top of each other. Consequently, we will compare fits starting with the target variable, followed by the addition of spatial information, the inclusion of covariates in the prior, and finally the inclusion of covariates also in the likelihood.

The different information levels affect the model complexity and therefore reflect into the computational load, however also the size of the testing dataset plays a significant role. To systematically explore this , we conducted the experiments across a "mesh" of dataset sizes, with both the number of units n and the time horizons T ranging through the set $\{10, 50, 100, 250\}$. As discussed in Section 2, the Julia implementation exhibited a slightly higher memory demand compared to the C implementation. As a consequence, when running the algorithms on the larger datasets, my system possibly ran out of RAM, requiring some data to be stored in the slower swap space on the disk and therefore leading to a drop in performance. As such, the extreme-sized experiments with n or T equal to 250 should be taken with a pinch of salt as they may reflect system hardware limitations rather than intrinsic model performance. For all the other experiments, on the other hand,

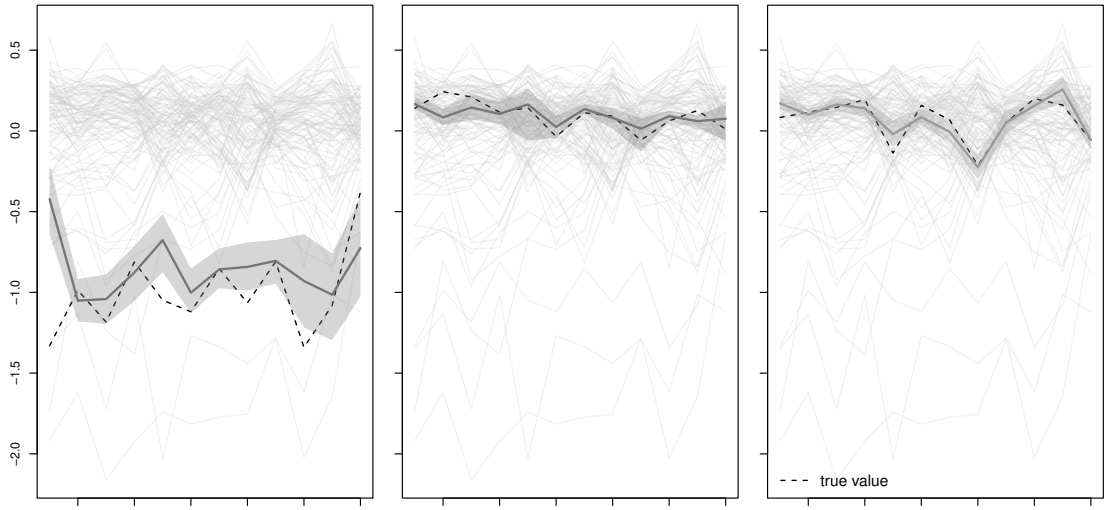

Figure 3.28: Kriging performances of JDRPM spatially-informed fit.

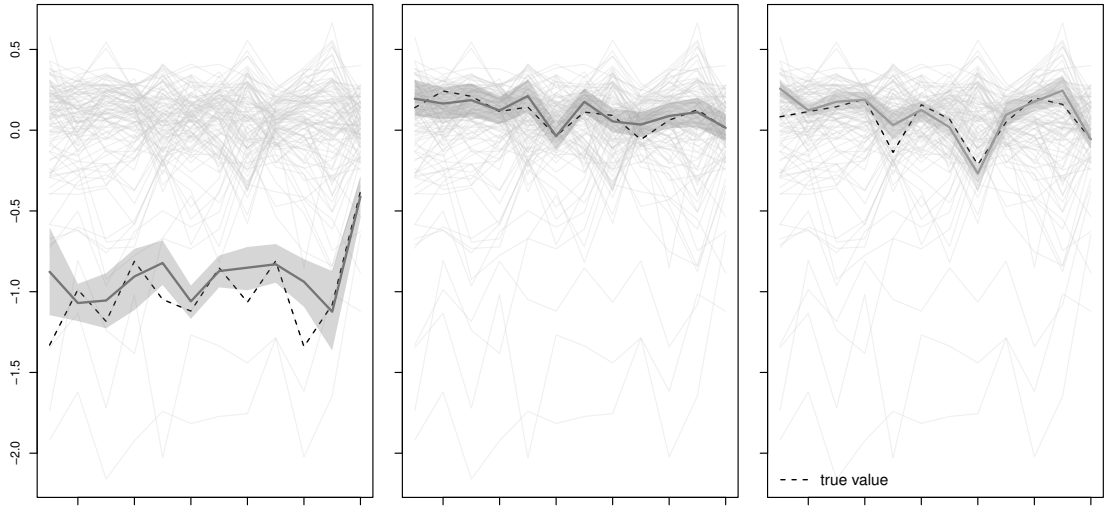

Figure 3.29: Kriging performances of JDRPM spatially-informed fit with covariates in the likelihood.

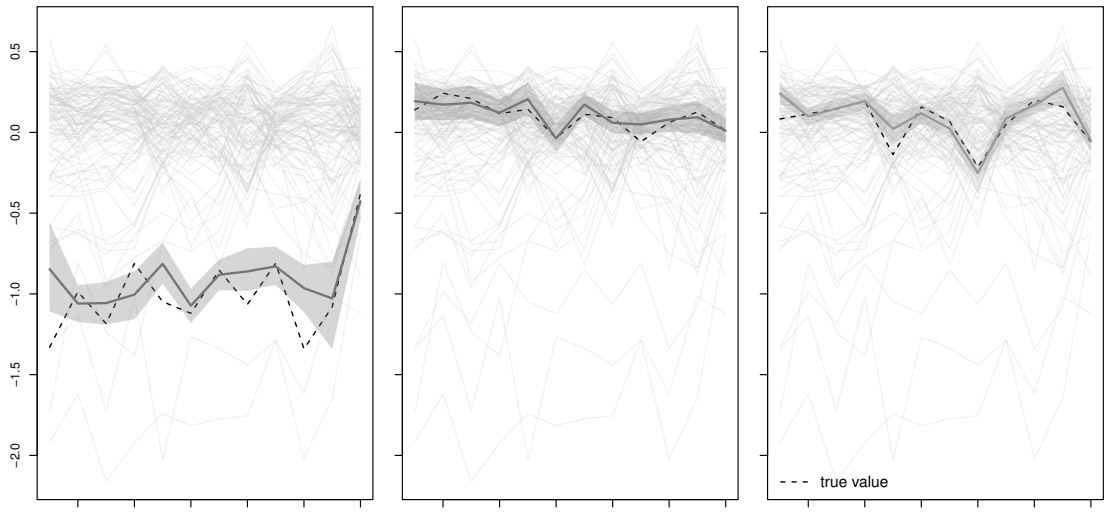

Figure 3.30: Kriging performances of JDRPM spatially-informed fit with covariates in the likelihood and in the prior.

the results should be highly accurate and reliably proving the JDRPM's improved performance.

In conducting the comparisons, we generated synthetic target data Y_{it} and spatial coordinates $\boldsymbol{s}_i$ according to the values of n and T. To measure the average execution time per iteration of each fit we defined the number of iterations to be inversely proportional to the size of the dataset, e.g. 10000 iterations in the case $(n, T) = (10, 10)$ and 16 iterations in the case $(n, T) = (250, 250)$. This ensured that each run lasted approximately the same amount of time. Moreover, each fit was repeated multiple times to record the minimum execution time observed. This practice is common in benchmarking and helps to eliminate bias attributable to the system computational demands and fluctuations to simulate the "ideal" testing environment in which all computational resources are devoted exclusively to the model fitting task.

As shown in Figure 3.31, the basic fit using only target values achieves significantly faster execution times in Julia, with speedups peaking around a 2x improvement. Similar performance gains are observed in the fits that incorporate spatial information, as illustrated in Figure 3.32. Therefore, particularly when examining the more reliable intermediate-sized tests, we can confidently conclude that the JDRPM algorithm implementation outperforms the CDRPM algorithm implementation with respect to execution speed.

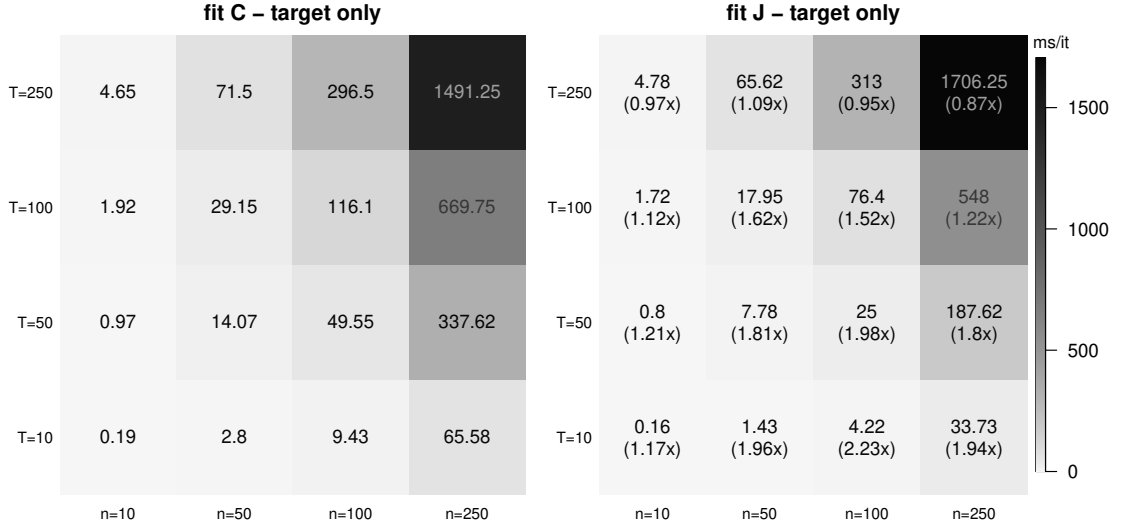

Figure 3.31: Execution times, measured in milliseconds per iteration, when fitting CDRPM and JDRPM in a simulated data scenario. In the JDRPM plot (right), in brackets, are reported the speedups relative to the CDRPM timings (left), where higher values indicate better performance.

In the analysis of fits involving covariates, we generated them by randomly creating matrices of dimensions $n \times p \times T$. For these experiments, we maintained a consistent value for p, the number of covariates, to avoid complications. In fact, the previous Figures 3.31 and 3.32 represented projections of three-dimensional data: n, T, and the execution time. If we extended the mesh construction to allow for varying p we would have dealt with four-dimensional data, or even five-dimensional if we considered separately covariates in the prior and in the likelihood. Therefore,

to preserve clarity and comprehensibility in our presentation, we fixed $p = 5$ for both covariates information levels. Nonetheless, a test with varying p for both prior and likelihood covariates, but fixed n and T, will be proposed in Figure 3.34.

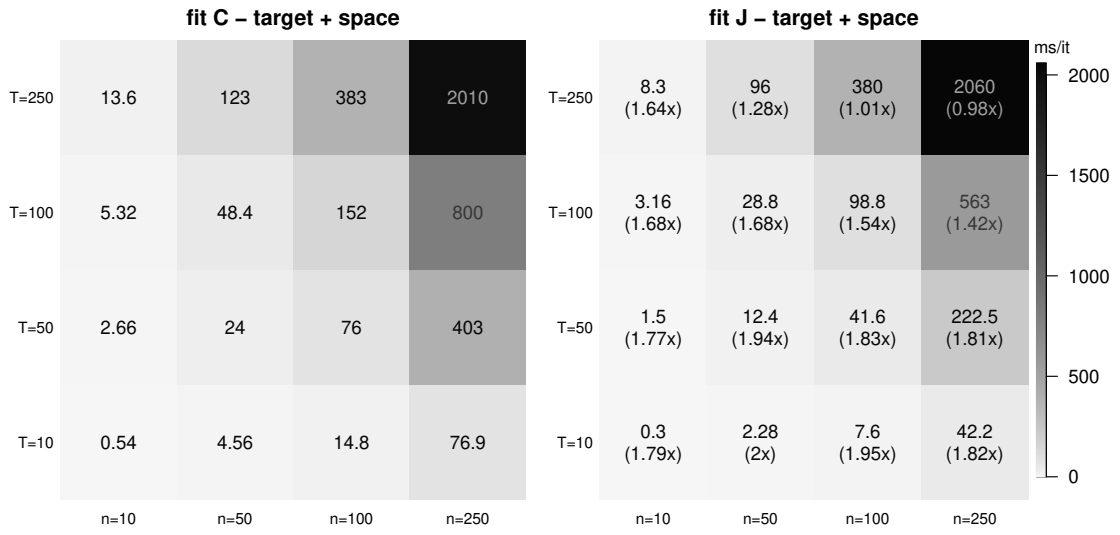

Figure 3.32: Execution times, measured in milliseconds per iteration, when fitting CDRPM and JDRPM in a real-world scenario. In the JDRPM plot (right), in brackets, are reported the speedups relative to the CDRPM timings (left), where higher values indicate better performance.

Figure 3.33 illustrates that fits incorporating covariates experienced a decrease in performance, which was expected due to the additional computational demands introduced by the new information layers. However, they maintained a satisfactory level of performance. As shown in Figure 3.35, some fits that included all information levels in Julia were surprisingly faster than a standard spatially-informed fit implemented in C.

Building on the encouraging results presented, we further investigated the model complexity at which the JDRPM implementation would reach the execution times provided by CDRPM. To conduct this analysis, we selected a moderately-sized dataset with $n = 50$ and $T = 50$, and used the performance metric from the CDRPM fit with spatial information as a reference; a value of 24 ms/iteration as retrieved by Figure 3.32. We then assessed the performance of JDRPM fits that included covariates at both likelihood and clustering levels, allowing p to vary independently in each information level to identify the degree of complexity at which the new implementation would align with the original one. The results of this analysis are summarized in Figure 3.34. Our experiments suggest that until that until we include $p_{\text{cl}} = 5$ covariates in the prior, we can expect JDRPM to outclass the CDRPM performance reference. This indicates that within the same amount of time in which CDRPM executes a spatially-informed fit, JDRPM can perform a fit including up to five covariates in the prior. Additionally, there is potential to include an indeterminate number of covariates in the likelihood, since the main performance drop appeared to associated with the increasing of p_{cl}, rather than of p_{lk}.

As in the previous tests of this section, this analysis was conducted with the

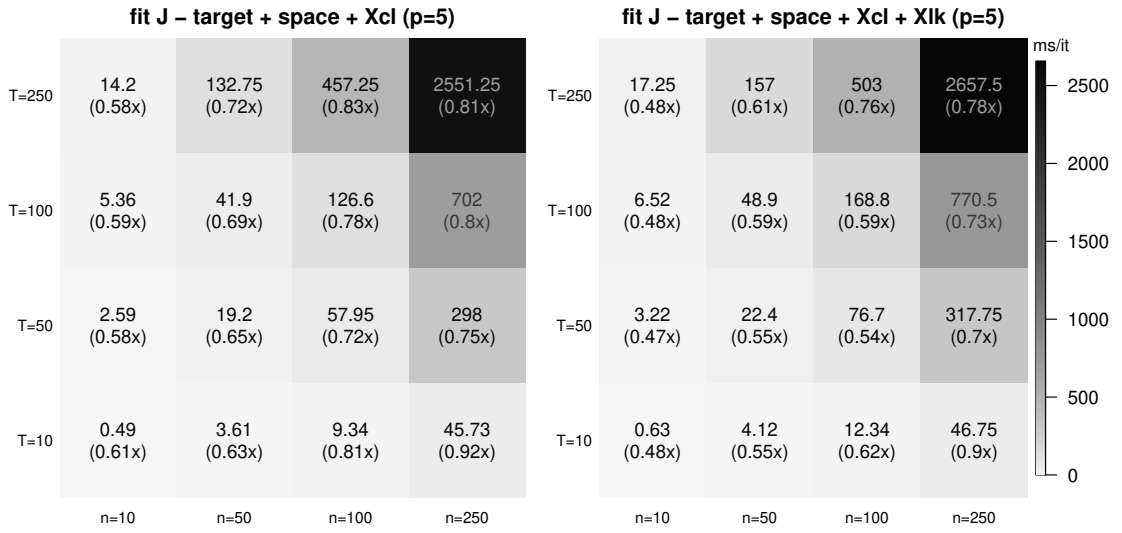

Figure 3.33: Execution times, measured in milliseconds per iteration, when fitting JDRPM in a real-world scenario, with a fixed number $p = 5$ of covariates in the prior (left) and in both the prior and the likelihood (right). In brackets are reported the speedups relative to the JDRPM timings of the fits with spatial information, with higher values still indicating better performance.

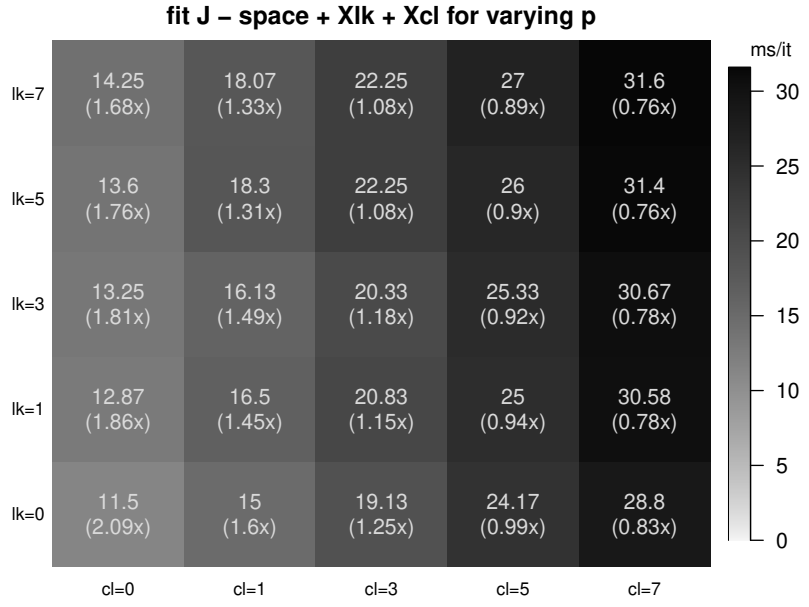

Figure 3.34: Execution times, measured in milliseconds per iteration, when fitting JDRPM in a real-world scenario, with a varying number of covariates in the likelihood (symbol lk on the y axis) and in the prior (symbol cl on the x axis). In brackets are reported the speedups relative to the CDRPM timing of the spatially-informed fit on the same $n = 50$, $T = 50$ dataset size, with higher values indicating better performance.

intention of dedicating all available computational resources to the fitting task; therefore, the results should be regarded as accurate. Notably, even in the noisier environment of the real-world experiments, a considerable speedup was observed, further proving the performance improvements achieved. The real-world experiments

were carried out on a dataset comprising $n = 105$ units and $T = 12$ time instants, with a summary of their results presented in Table 3.6. From this table, we note that the spatially-informed CDRPM fit required 1 hour and 38 minutes, while both JDRPM fits, with equivalent setup and with covariates in the prior, exhibited faster execution times. Remarkably, the equivalent JDRPM fit reduced the execution time by more than half, aligning with the measured speedup factor of 1.95x reported in Figure 3.32 when considering the closest corresponding case of $n = 100$ and $T = 10$. Additionally, the fit that included covariates in the prior demonstrated the expected speedup suggested by Figure 3.35, which we now discuss in detail.

Figure 3.35 encapsulates all the performance analyses conducted so far. It also offers an additional insight: the bottom right panel, corresponding to experiments on $n = 250$ units, reveals a convergence pattern in the speedup factors across all fits, denoting how all models tend to exhibit similar execution times regardless of the information levels included. This suggests that when applied to large-scale datasets, the performance bottleneck of JDRPM but also CDRPM shifts from the algorithmic complexity, that is, from the selection of desired information levels, to the limitations of available hardware resources.

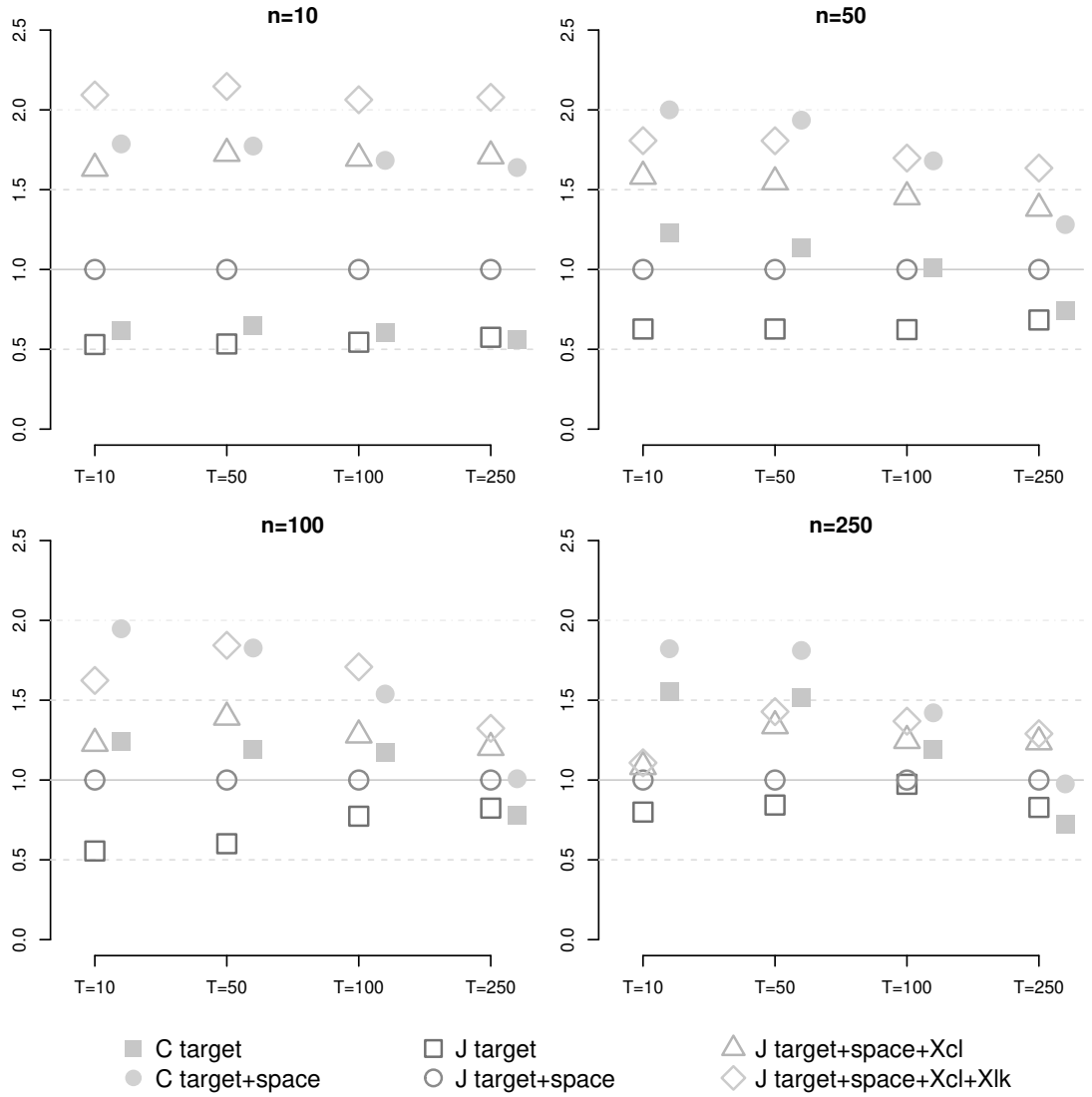

Figure 3.35: Visual representation of the performance of all the fits, for all the n and T cases, relatively to the JDRPM fit using target values and spatial information. Namely, the execution time per iteration metric of that fit has been taken as a reference, to which then all other fits have been compared to derive their speedup (or slowdown) factor. Points above the reference line indicate slower fits, while points below denote faster fits.

Chapter 4

Conclusion

And what in human reckoning seems still afar off, may by the Divine ordinance be close at hand, on the eve of its appearance. And so be it, so be it!

— Fëdor Dostoevskij, *Brothers Karamazov*

In conclusion, the JDRPM represents a significant enhancement over the original CDRPM. From a theoretical perspective, JDRPM retains the foundational structure of its predecessor while introducing the covariates in the prior and likelihood levels. Together with the reduction in the execution times, this is the core upgrade since it should help to yield more accurate and informed results in the partitions. Moreover, the modification on the variances, from a uniform law to an inverse gamma, possibly could enhance the quality of the posterior samples. This choice, in fact, restores conjugacy within the model, thereby improving the mixing properties of the Markov chain during the fitting process.

Despite these improvements, it is important to acknowledge potential drawbacks associated with the increased complexity of the model. The robustness of results may diminish as the intricacies of parameter selection—particularly concerning cohesion and similarity functions—can significantly influence cluster estimates. Striking an appropriate balance between these two sources of information may require empirical testing. In this context, Chapter 1 provides a comprehensive analysis of how tuning parameters for cohesion and similarity impact model performance.

Despite these improvements, it is important to acknowledge potential drawbacks associated with the increased complexity of the model. The robustness of the fits may diminish as the intricacies of parameters selection, particularly concerning the ones regulating cohesion and similarity functions, can significantly influence the cluster estimates. To this end, Chapter 1 provided a comprehensive analysis about how the possible choices on the parameters for cohesions and similarities reflect on their generated values. Moreover, in fits including both space and covariates information, reaching an appropriate balance between these two sources of information may require empirical testing. To address this balance, the Julia function `MCMC_fit` includes an optional argument, `cv_weight`, defaulted to 1, that allows to adjust the influence of covariate similarities.

This complexity is especially evident when defining the prior for the inverse gamma distribution, inherently more delicate than a simpler uniform, of the variance parameters. Other than conducting multiple experiments and studying the trace plots to asses a correct behaviour, a pragmatic approach to address this challenge could be in conducting an initial fit using the original CDRPM to see the expected range in which the variance samples tend to settle, and tune accordingly the inverse gamma parameters. For instance, in the spatio-temporal tests detailed in Section 3.1.2, we observed low variance estimates from the CDRPM fits. Consequently, we assigned an invGamma($a = 1.9, b = 0.4$) for λ^2 and τ_t^2, which has 90% of his density in the interval $[0.109151, 1.58222]$. For the more critical parameter $\sigma_{jt}^{2\star}$ we adopted a less informative prior invGamma($a = 0.01, b = 0.01$) which, despite being not always recommended (Andrew Gelman, 2004), proved to be effective and precise relative to sampled reference values from CDRPM. An alternative strategy, albeit less theoretically appealing, could involve truncating the inverse gamma distributions to mitigate the risk of sampling excessively high values when uninformative priors are inadequately adjusted by data. This adjustment can be seamlessly integrated into the Julia code by modifying `rand(InverseGamma(a,b))` to `rand(truncated(InverseGamma(a,b),l,u))`, where l and u define truncation bounds.

From a computational perspective, we successfully reduced execution times by up to 50% compared to the original implementation. Although this occurred with a slight increase in memory requirements, it is a trade-off that is surely manageable with the modern computing resources.

Looking ahead, there remains a wide opportunity for further enhancements, particularly in the usability front given the actual complexity of the model. While the current JDRPM implementation features basic logging capabilities, that allow for stepwise computation tracking, there is potential for more sophisticated profiling and monitoring tools that leverage Julia's flexibility. Possible suggestions could include heuristics about the initialization of the hyperparameters, based on the specific datasets at hand, or visualization tools, using Julia's robust plotting ecosystem, to provide real-time monitoring of the sampled parameters distributions and trace plots directly during execution. Moreover, implementing parallel processing with multiple chains, which is a common in technique implemented in many less heavy Bayesian models, could further enhance performance. Exploring GPU integration through packages within the `JuliaGPU` collection may also yield significant computational efficiencies.

In short, while the JDRPM's complexity may present certain challenges, it also lays the groundwork for significant methodological advancements and practical enhancements. These developments are expected to enhance the model's applicability and ease of use, for more effective research outcomes.

Appendix A

Theoretical details

A.1 Extended computations of the full conditionals

We propose here the extended computations which allowed to extract the full conditionals presented in Chapter 1. We report also the model graph of JDRPM to make it quickly accessible as a reference for the laws involved in the following computations.

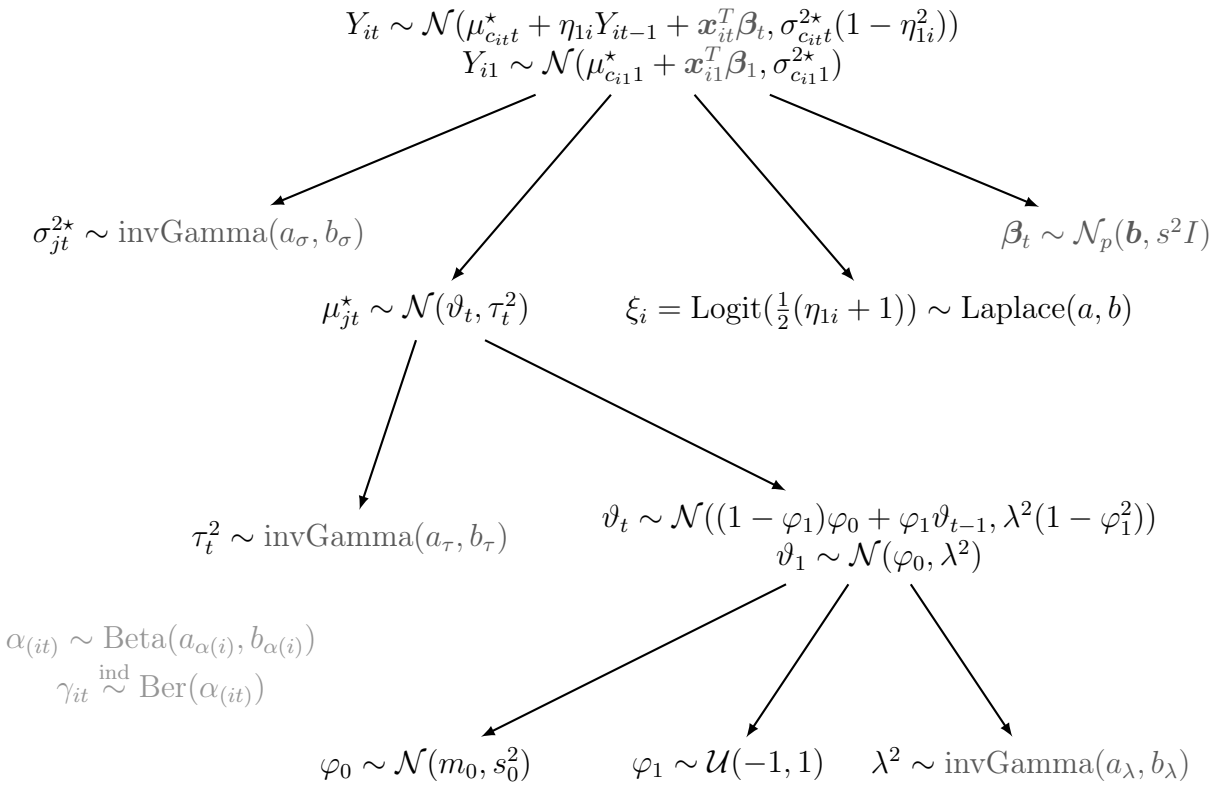

- update $\sigma^{2\star}_{jt}$. This full conditional derivation is characteristic of JDRPM only, since in CDRPM the variance had a uniform law and was therefore updated

through a Metropolis step.

for $t = 1$:

$$
\begin{aligned}
f(\sigma_{jt}^{2\star}|-) &\propto f(\sigma_{jt}^{2\star}) f(\{Y_{it} : c_{it} = j\}|\sigma_{jt}^{2\star}, -) \\
&= \mathcal{L}_{\text{invGamma}(a_\sigma, b_\sigma)}(\sigma_{jt}^{2\star}) \prod_{i \in S_{jt}} \mathcal{L}_{\mathcal{N}(\mu^\star_{c_{it}t} + \boldsymbol{x}_{it}^T \boldsymbol{\beta}_t, \sigma^{2\star}_{c_{it}1})}(Y_{it}) \\
&\propto \left[\left(\frac{1}{\sigma_{jt}^{2\star}} \right)^{a_\sigma + 1} \exp\left\{ -\frac{1}{\sigma_{jt}^{2\star}} b \right\} \right] \\
&\cdot \left[\prod_{i \in S_{jt}} \left(\frac{1}{\sigma_{jt}^{2\star}} \right)^{1/2} \exp\left\{ -\frac{1}{2\sigma_{jt}^{2\star}} (Y_{it} - \mu_{jt}^\star - \boldsymbol{x}_{it}^T \boldsymbol{\beta}_t)^2 \right\} \right] \\
&\propto \left(\frac{1}{\sigma_{jt}^{2\star}} \right)^{(a_\sigma + |S_{jt}|/2) + 1} \exp\left\{ -\frac{1}{\sigma_{jt}^{2\star}} \left(b_\sigma + \frac{1}{2} \sum_{i \in S_{jt}} (Y_{it} - \mu_{jt}^\star - \boldsymbol{x}_{it}^T \boldsymbol{\beta}_t)^2 \right) \right\}
\end{aligned}
$$

$$
\begin{aligned}
\implies f(\sigma_{jt}^{2\star}|-) &\propto \text{kernel of a invGamma}(a_{\sigma(\text{post})}, b_{\sigma(\text{post})}) \text{ with} \\
a_{\tau(\text{post})} &= a_\sigma + \frac{|S_{jt}|}{2} \\
b_{\tau(\text{post})} &= b_\sigma + \frac{1}{2} \sum_{i \in S_{jt}} (Y_{it} - \mu_{jt}^\star - \boldsymbol{x}_{it}^T \boldsymbol{\beta}_t)^2
\end{aligned} \tag{A.1}
$$

for $t > 1$:

$$
\begin{aligned}
f(\sigma_{jt}^{2\star}|-) &\propto f(\sigma_{jt}^{2\star}) f(\{Y_{it} : c_{it} = j\}|\sigma_{jt}^{2\star}, -) \\
&= \mathcal{L}_{\text{invGamma}(a_\sigma, b_\sigma)}(\sigma_{jt}^{2\star}) \prod_{i \in S_{jt}} \mathcal{L}_{\mathcal{N}(\mu^\star_{c_{it}t} + \eta_{1i} Y_{it-1} + \boldsymbol{x}_{it}^T \boldsymbol{\beta}_t, \sigma^{2\star}_{c_{it}1})}(Y_{it}) \\
&\propto \left[\left(\frac{1}{\sigma_{jt}^{2\star}} \right)^{a_\sigma + 1} \exp\left\{ -\frac{1}{\sigma_{jt}^{2\star}} b \right\} \right] \\
&\cdot \left[\prod_{i \in S_{jt}} \left(\frac{1}{\sigma_{jt}^{2\star}} \right)^{1/2} \exp\left\{ -\frac{1}{2\sigma_{jt}^{2\star}} (Y_{it} - \mu_{jt}^\star - \eta_{1i} Y_{it-1} - \boldsymbol{x}_{it}^T \boldsymbol{\beta}_t)^2 \right\} \right] \\
&\propto \left(\frac{1}{\sigma_{jt}^{2\star}} \right)^{(a_\sigma + |S_{jt}|/2) + 1} \\
&\cdot \exp\left\{ -\frac{1}{\sigma_{jt}^{2\star}} \left(b_\sigma + \frac{1}{2} \sum_{i \in S_{jt}} (Y_{it} - \eta_{1i} Y_{it-1} - \mu_{jt}^\star - \boldsymbol{x}_{it}^T \boldsymbol{\beta}_t)^2 \right) \right\}
\end{aligned}
$$

$$
\begin{aligned}
\implies f(\sigma_{jt}^{2\star}|-) &\propto \text{kernel of a invGamma}(a_{\sigma(\text{post})}, b_{\sigma(\text{post})}) \text{ with} \\
a_{\tau(\text{post})} &= a_\sigma + \frac{|S_{jt}|}{2} \\
b_{\tau(\text{post})} &= b_\sigma + \frac{1}{2} \sum_{i \in S_{jt}} (Y_{it} - \mu_{jt}^\star - \eta_{1i} Y_{it-1} - \boldsymbol{x}_{it}^T \boldsymbol{\beta}_t)^2
\end{aligned} \tag{A.2}
$$

- update $\mu^\star_{jt}$. This update rule is the same for both JDRPM and CDRPM.

  for $t = 1$:

$$
\begin{aligned}
f(\mu^\star_{jt}|-) &\propto f(\mu^\star_{jt}) f(\{Y_{it} : c_{it} = j\}|\mu^\star_{jt}, -) \\
&= \mathcal{L}_{\mathcal{N}(\vartheta_t, \tau_t^2)}(\mu^\star_{jt}) \prod_{i \in S_{jt}} \mathcal{L}_{\mathcal{N}(\mu^\star_{c_{it}t} + \boldsymbol{x}_{it}^T \boldsymbol{\beta}_t, \sigma^{2\star}_{c_{it}1})}(Y_{it}) \\
&\propto \exp\left\{ -\frac{1}{2\tau_t^2} (\mu^\star_{jt} - \vartheta_t)^2 \right\} \exp\left\{ -\frac{1}{2\sigma^{2\star}_{jt}} \left(\sum_{i \in S_{jt}} (\mu^\star_{jt} - (Y_{i1} - \boldsymbol{x}_{it}^T \boldsymbol{\beta}_t))^2 \right) \right\} \\
&\propto \exp\left\{ -\frac{1}{2\tau_t^2} (\mu^\star_{jt} - \vartheta_t)^2 \right\} \exp\left\{ -\frac{|S_{jt}|}{2\sigma^{2\star}_{jt}} \left(\mu^\star_{jt} - \frac{\text{SUM}_y}{|S_{jt}|} \right)^2 \right\} \\
&\text{where } \text{SUM}_y = \sum_{i \in S_{jt}} Y_{i1} - \boldsymbol{x}_{it}^T \boldsymbol{\beta}_t
\end{aligned}
$$

  $\implies f(\mu^\star_{jt}|-) \propto$ kernel of a $\mathcal{N}(\mu_{\mu^\star_{jt}(\text{post})}, \sigma^2_{\mu^\star_{jt}(\text{post})})$ with

$$
\begin{aligned}
\sigma^2_{\mu^\star_{jt}(\text{post})} &= \frac{1}{\frac{1}{\tau_t^2} + \frac{|S_{jt}|}{\sigma^{2\star}_{jt}}} \\
\mu_{\mu^\star_{jt}(\text{post})} &= \sigma^2_{\mu^\star_{jt}(\text{post})} \left(\frac{\vartheta_t}{\tau_t^2} + \frac{\text{SUM}_y}{\sigma^{2\star}_{jt}} \right)
\end{aligned} \tag{A.3}
$$

  for $t > 1$:

$$
\begin{aligned}
f(\mu^\star_{jt}|-) &\propto f(\mu^\star_{jt}) f(\{Y_{it} : c_{it} = j\}|\mu^\star_{jt}, -) \\
&= \mathcal{L}_{\mathcal{N}(\vartheta_1, \tau_t^2)}(\mu^\star_{jt}) \prod_{i \in S_{jt}} \mathcal{L}_{\mathcal{N}(\mu^\star_{c_{it}t} + \eta_{1i} Y_{it-1} + \boldsymbol{x}_{it}^T \boldsymbol{\beta}_t, \sigma^{2\star}_{c_{it}1})}(Y_{it}) \\
&\propto \exp\left\{ -\frac{1}{2\tau_t^2} (\mu^\star_{jt} - \vartheta_t)^2 \right\} \\
&\cdot \exp\left\{ -\frac{1}{2\sigma^{2\star}_{jt}} \left(\sum_{i \in S_{jt}} \frac{1}{1 - \eta_{1i}^2} \left(\mu^\star_{jt} - (Y_{it} - \eta_{1i} Y_{i,t-1} - \boldsymbol{x}_{it}^T \boldsymbol{\beta}_t) \right)^2 \right) \right\} \\
&\propto \exp\left\{ -\frac{1}{2\tau_t^2} (\mu^\star_{jt} - \vartheta_t)^2 \right\} \exp\left\{ -\frac{\text{SUM}_{e2}}{2\sigma^{2\star}_{jt}} \left(\mu^\star_{jt} - \frac{\text{SUM}_y}{\text{SUM}_{e2}} \right)^2 \right\} \\
&\text{where } \text{SUM}_y = \sum_{i \in S_{jt}} \frac{Y_{it} - \eta_{1i} Y_{i,t-1} - \boldsymbol{x}_{it}^T \boldsymbol{\beta}_t}{1 - \eta_{1i}^2}, \ \text{SUM}_{e2} = \sum_{i \in S_{jt}} \frac{1}{1 - \eta_{1i}^2}
\end{aligned}
$$

  $\implies f(\mu^\star_{jt}|-) \propto$ kernel of a $\mathcal{N}(\mu_{\mu^\star_{jt}(\text{post})}, \sigma^2_{\mu^\star_{jt}(\text{post})})$ with

$$
\begin{aligned}
\sigma^2_{\mu^\star_{jt}(\text{post})} &= \frac{1}{\frac{1}{\tau_t^2} + \frac{\text{SUM}_{e2}}{\sigma^{2\star}_{jt}}} \\
\mu_{\mu^\star_{jt}(\text{post})} &= \sigma^2_{\mu^\star_{jt}(\text{post})} \left(\frac{\vartheta_t}{\tau_t^2} + \frac{\text{SUM}_y}{\sigma^{2\star}_{jt}} \right)
\end{aligned} \tag{A.4}
$$

- update $\boldsymbol{\beta}_t$. This full conditional derivation is characteristic of JDRPM only, since the insertion of a regression term in the likelihood is a feature introduced

by our generalized model.

for $t = 1$:

$$
\begin{aligned}
f(\boldsymbol{\beta}_t|-) &\propto f(\boldsymbol{\beta}_t) f(\{Y_{1t}, \dots, Y_{nt}\}|\boldsymbol{\beta}_t, -) \\
&= \mathcal{L}_{\mathcal{N}(\boldsymbol{b}, s^2 I)}(\boldsymbol{\beta}_t) \prod_{i=1}^{n} \mathcal{L}_{\mathcal{N}(\mu^\star_{c_{it}t} + \boldsymbol{x}_{it}^T \boldsymbol{\beta}_t, \sigma^{2\star}_{c_{it}t})}(Y_{it}) \\
&\propto \exp\left\{ -\frac{1}{2} \left[(\boldsymbol{\beta}_t^T - \boldsymbol{b})^T \frac{1}{s^2} (\boldsymbol{\beta}_t - \boldsymbol{b}) \right] \right\} \\
&\cdot \exp\left\{ -\frac{1}{2} \sum_{i=1}^{n} (Y_{it} - \mu^\star_{c_{it}t} - \boldsymbol{x}_{it}^T \boldsymbol{\beta}_t)^2 \right\} \\
&\propto \exp\left\{ -\frac{1}{2} \left[\boldsymbol{\beta}_t^T \left(\frac{1}{s^2} I + \sum_{i=1}^{n} \frac{\boldsymbol{x}_{it} \boldsymbol{x}_{it}^T}{\sigma^{2\star}_{c_{it}t}} \right) \boldsymbol{\beta}_t \right.\right. \\
&\quad \left.\left. - \, 2 \left(\frac{\boldsymbol{b}}{s^2} + \sum_{i=1}^{n} \frac{(Y_{it} - \mu^\star_{c_{it}t}) \boldsymbol{x}_{it}}{\sigma^{2\star}_{c_{it}t}} \right) \cdot \boldsymbol{\beta}_t \right] \right\}
\end{aligned}
$$

$$
\begin{aligned}
&\implies f(\boldsymbol{\beta}_t|-) \propto \text{kernel of a } \mathcal{N}(\boldsymbol{b}_{(\text{post})}, A_{(\text{post})}) \text{ with} \\
&\quad A_{(\text{post})} = \left(\frac{1}{s^2} I + \sum_{i=1}^{n} \frac{\boldsymbol{x}_{it} \boldsymbol{x}_{it}^T}{\sigma^{2\star}_{c_{it}t}} \right)^{-1} \\
&\quad \boldsymbol{b}_{(\text{post})} = A_{(\text{post})} \left(\frac{\boldsymbol{b}}{s^2} + \sum_{i=1}^{n} \frac{(Y_{it} - \mu^\star_{c_{it}t}) \boldsymbol{x}_{it}}{\sigma^{2\star}_{c_{it}t}} \right) \\
&\iff f(\boldsymbol{\beta}_t|-) \propto \text{kernel of a } \mathcal{N}\text{Canon}(\boldsymbol{h}_{(\text{post})}, J_{(\text{post})}) \text{ with} \\
&\quad \boldsymbol{h}_{(\text{post})} = \left(\frac{\boldsymbol{b}}{s^2} + \sum_{i=1}^{n} \frac{(Y_{it} - \mu^\star_{c_{it}t}) \boldsymbol{x}_{it}}{\sigma^{2\star}_{c_{it}t}} \right) \\
&\quad J_{(\text{post})} = \left(\frac{1}{s^2} I + \sum_{i=1}^{n} \frac{\boldsymbol{x}_{it} \boldsymbol{x}_{it}^T}{\sigma^{2\star}_{c_{it}t}} \right)
\end{aligned} \tag{A.5}
$$

for $t > 1$:

$$
\begin{aligned}
f(\boldsymbol{\beta}_t|-) &\propto f(\boldsymbol{\beta}_t) f(\{Y_{1t}, \dots, Y_{nt}\}|\boldsymbol{\beta}_t, -) \\
&= \mathcal{L}_{\mathcal{N}(\boldsymbol{b}, s^2 I)}(\boldsymbol{\beta}_t) \prod_{i=1}^{n} \mathcal{L}_{\mathcal{N}(\mu^\star_{c_{it}t} + \eta_{1i} Y_{it-1} + \boldsymbol{x}_{it}^T \boldsymbol{\beta}_t, \sigma^{2\star}_{c_{it}t})}(Y_{it}) \\
&\propto \exp\left\{ -\frac{1}{2} \left[(\boldsymbol{\beta}_t^T - \boldsymbol{b})^T \frac{1}{s^2} (\boldsymbol{\beta}_t - \boldsymbol{b}) \right] \right\} \\
&\cdot \exp\left\{ -\frac{1}{2} \sum_{i=1}^{n} (Y_{it} - \mu^\star_{c_{it}t} - \eta_{1i} Y_{it-1} - \boldsymbol{x}_{it}^T \boldsymbol{\beta}_t)^2 \right\} \\
&\propto \exp\left\{ -\frac{1}{2} \left[\boldsymbol{\beta}_t^T \left(\frac{1}{s^2} I + \sum_{i=1}^{n} \frac{\boldsymbol{x}_{it} \boldsymbol{x}_{it}^T}{\sigma^{2\star}_{c_{it}t}} \right) \boldsymbol{\beta}_t \right.\right. \\
&\quad \left.\left. -2 \left(\frac{\boldsymbol{b}}{s^2} + \sum_{i=1}^{n} \frac{(Y_{it} - \mu^\star_{c_{it}t} - \eta_{1i} Y_{it-1}) \boldsymbol{x}_{it}}{\sigma^{2\star}_{c_{it}t}} \right) \cdot \boldsymbol{\beta}_t \right] \right\}
\end{aligned}
$$

$$
\begin{aligned}
&\implies f(\boldsymbol{\beta}_t|-) \propto \text{kernel of a } \mathcal{N}(\boldsymbol{b}_{(\text{post})}, A_{(\text{post})}) \text{ with} \\
&\quad A_{(\text{post})} = \left(\frac{1}{s^2} I + \sum_{i=1}^{n} \frac{\boldsymbol{x}_{it} \boldsymbol{x}_{it}^T}{\sigma^{2\star}_{c_{it}t}} \right)^{-1} \\
&\quad \boldsymbol{b}_{(\text{post})} = A_{(\text{post})} \left(\frac{\boldsymbol{b}}{s^2} + \sum_{i=1}^{n} \frac{(Y_{it} - \mu^{\star}_{c_{it}t} - \eta_{1i} Y_{it-1}) \boldsymbol{x}_{it}}{\sigma^{2\star}_{c_{it}t}} \right) \\
&\iff f(\boldsymbol{\beta}_t|-) \propto \text{kernel of a } \mathcal{N}\text{Canon}(\boldsymbol{h}_{(\text{post})}, J_{(\text{post})}) \text{ with} \\
&\quad \boldsymbol{h}_{(\text{post})} = \left(\frac{\boldsymbol{b}}{s^2} + \sum_{i=1}^{n} \frac{(Y_{it} - \mu^{\star}_{c_{it}t} - \eta_{1i} Y_{it-1}) \boldsymbol{x}_{it}}{\sigma^{2\star}_{c_{it}t}} \right) \\
&\quad J_{(\text{post})} = \left(\frac{1}{s^2} I + \sum_{i=1}^{n} \frac{\boldsymbol{x}_{it} \boldsymbol{x}_{it}^T}{\sigma^{2\star}_{c_{it}t}} \right)
\end{aligned} \tag{A.6}
$$

- update τ_t^2. This full conditional derivation is characteristic of JDRPM only, since in CDRPM the variance had a uniform law and was therefore updated through a Metropolis step.

$$
\begin{aligned}
f(\tau_t^2|-) &\propto f(\tau_t^2) f((\mu^{\star}_{1t}, \ldots, \mu^{\star}_{k_t t})|\tau_t^2, -) \\
&= \mathcal{L}_{\text{invGamma}(a_\tau, b_\tau)}(\tau_t^2) \prod_{j=1}^{k_t} \mathcal{L}_{\mathcal{N}(\vartheta_t, \tau_t^2)}(\mu^{\star}_{jt}) \\
&\propto \left[\left(\frac{1}{\tau_t^2} \right)^{a_\tau + 1} \exp\left\{ -\frac{b_\tau}{\tau_t^2} \right\} \right] \left[\prod_{j=1}^{k_t} \left(\frac{1}{\tau_t^2} \right)^{1/2} \exp\left\{ -\frac{1}{2\tau_t^2} (\mu^{\star}_{jt} - \vartheta_t)^2 \right\} \right] \\
&\propto \left(\frac{1}{\tau_t^2} \right)^{\left(\frac{k_t}{2} + a_\tau\right) + 1} \exp\left\{ -\frac{1}{\tau_t^2} \left(\frac{\sum_{j=1}^{k_t} (\mu^{\star}_{jt} - \vartheta_t)^2}{2} + b_\tau \right) \right\} \\
\implies f(\tau_t^2|-) &\propto \text{kernel of a invGamma}(a_{\tau(\text{post})}, b_{\tau(\text{post})}) \text{ with} \\
a_{\tau(\text{post})} &= \frac{k_t}{2} + a_\tau \\
b_{\tau(\text{post})} &= \frac{\sum_{j=1}^{k_t} (\mu^{\star}_{jt} - \vartheta_t)^2}{2} + b_\tau
\end{aligned} \tag{A.7}
$$

- update ϑ_t. This update rule is the same for both JDRPM and CDRPM.

$$
\begin{aligned}
&\text{for } t = T\text{:} \\
&\quad f(\vartheta_t|-) \propto f(\vartheta_t) f((\mu^{\star}_{1t}, \ldots, \mu^{\star}_{k_t t})|\vartheta_t, -) \\
&\qquad = \mathcal{L}_{\mathcal{N}((1-\varphi_1)\varphi_0 + \varphi_1 \vartheta_{t-1}, \lambda^2(1-\varphi_1^2))}(\vartheta_t) \prod_{j=1}^{k_t} \mathcal{L}_{\mathcal{N}(\vartheta_t, \tau_t^2)}(\mu^{\star}_{jt}) \\
&\qquad \propto \exp\left\{ -\frac{1}{2(\lambda^2(1-\varphi_1^2))} \Big(\vartheta_t - ((1-\varphi_1)\varphi_0 + \varphi_1 \vartheta_{t-1}) \Big)^2 \right\} \\
&\qquad \cdot \exp\left\{ -\frac{k_t}{2\tau_t^2} \left(\vartheta_t - \frac{\sum_{j=1}^{k_t} \mu^{\star}_{jt}}{k_t} \right) \right\}
\end{aligned}
$$

$$\begin{aligned}
&\implies f(\vartheta_t|-) \propto \text{kernel of a } \mathcal{N}(\mu_{\vartheta_t(\text{post})}, \sigma^2_{\vartheta_t(\text{post})}) \text{ with} \\
&\quad \sigma^2_{\vartheta_t(\text{post})} = \frac{1}{\frac{1}{\lambda^2(1-\varphi_1^2)} + \frac{k_t}{\tau_t^2}} \\
&\quad \mu_{\vartheta_t(\text{post})} = \sigma^2_{\vartheta_t(\text{post})} \left(\frac{\sum_{j=1}^{k_t} \mu^\star_{jt}}{\tau_t^2} + \frac{(1-\varphi_1)\varphi_0 + \varphi_1 \vartheta_{t-1}}{\lambda^2(1-\varphi_1^2)} \right)
\end{aligned} \tag{A.8}$$

for $1 < t < T$:

$$\begin{aligned}
f(\vartheta_t|-) &\propto \underbrace{f(\vartheta_t) f((\mu^\star_{1t}, \dots, \mu^\star_{k_t t})|\vartheta_t, -)}_{\text{as in the case } t=T} f(\vartheta_{t+1}|\vartheta_t, -) \\
&= \mathcal{L}_{\mathcal{N}(\mu_{\vartheta_t(\text{post})}, \sigma^2_{\vartheta_t(\text{post})})}(\vartheta_t) \mathcal{L}_{\mathcal{N}((1-\varphi_1)\varphi_0 + \varphi_1\vartheta_t, \lambda^2(1-\varphi_1^2))}(\vartheta_{t+1}) \\
&\propto \exp\left\{ -\frac{1}{2\sigma^2_{\vartheta_t(\text{post})}} \left(\vartheta_t - \mu_{\vartheta_t(\text{post})}\right)^2 \right\} \\
&\quad \cdot \exp\left\{ -\frac{1}{2\frac{\lambda^2(1-\varphi_1^2)}{\varphi_1^2}} \left(\vartheta_t - \frac{\vartheta_{t+1} - (1-\varphi_1)\varphi_0}{\varphi_1} \right)^2 \right\} \\
\implies f(\vartheta_t|-) &\propto \text{kernel of a } \mathcal{N}(\mu_{\vartheta_t(\text{post})}, \sigma^2_{\vartheta_t(\text{post})}) \text{ with} \\
\sigma^2_{\vartheta_t(\text{post})} &= \frac{1}{\frac{1+\varphi_1^2}{\lambda^2(1-\varphi_1^2)} + \frac{k_t}{\tau_t^2}} \\
\mu_{\vartheta_t(\text{post})} &= \sigma^2_{\vartheta_t(\text{post})} \left(\frac{\sum_{j=1}^{k_t} \mu^\star_{jt}}{\tau_t^2} + \frac{\varphi_1(\vartheta_{t-1} + \vartheta_{t+1}) + \varphi_0(1-\varphi_1)^2}{\lambda^2(1-\varphi_1^2)} \right)
\end{aligned} \tag{A.9}$$

for $t = 1$:

$$\begin{aligned}
f(\vartheta_t|-) &\propto f(\vartheta_t) f(\vartheta_{t+1}|\vartheta_t, -) f(\boldsymbol{\mu}^\star_t|\vartheta_t, -) \\
&= \mathcal{L}_{\mathcal{N}(\varphi_0, \lambda^2)}(\vartheta_t) \mathcal{L}_{\mathcal{N}((1-\varphi_1)\varphi_0 + \varphi_1\vartheta_{t-1}, \lambda^2(1-\varphi_1^2))}(\vartheta_{t+1}) \prod_{j=1}^{k_t} \mathcal{L}_{\mathcal{N}(\vartheta_t, \tau_t^2)}(\mu^\star_{jt}) \\
&\propto \exp\left\{ -\frac{1}{2\lambda^2} (\vartheta_t - \varphi_0)^2 \right\} \\
&\quad \cdot \exp\left\{ -\frac{1}{2\frac{\lambda^2(1-\varphi_1^2)}{\varphi_1^2}} \left(\vartheta_t - \frac{\vartheta_{t+1} - (1-\varphi_1)\varphi_0}{\varphi_1} \right)^2 \right\} \\
&\quad \cdot \exp\left\{ -\frac{k_t}{2\tau_t^2} \left(\vartheta_t - \frac{\sum_{j=1}^{k_t} \mu^\star_{jt}}{k_t} \right) \right\} \\
\implies f(\vartheta_t|-) &\propto \text{kernel of a } \mathcal{N}(\mu_{\vartheta_t(\text{post})}, \sigma^2_{\vartheta_t(\text{post})}) \text{ with} \\
\sigma^2_{\vartheta_t(\text{post})} &= \frac{1}{\frac{1}{\lambda^2} + \frac{\varphi_1^2}{\lambda^2(1-\varphi_1^2)} + \frac{k_t}{\tau_t^2}} \\
\mu_{\vartheta_t(\text{post})} &= \sigma^2_{\vartheta_t(\text{post})} \left(\frac{\varphi_0}{\lambda^2} + \frac{\varphi_1(\vartheta_{t+1} - (1-\varphi_1)\varphi_0)}{\lambda^2(1-\varphi_1^2)} + \frac{\sum_{j=1}^{k_t} \mu^\star_{jt}}{\tau_t^2} \right)
\end{aligned} \tag{A.10}$$

- update φ_0. This update rule is also the same for both JDRPM and CDRPM.

$$
\begin{aligned}
f(\varphi_0|-) &\propto f(\varphi_0) f((\vartheta_1,\dots,\vartheta_T)|\varphi_0,-) \\
&= \mathcal{L}_{\mathcal{N}(m_0,s_0^2)}(\varphi_0)\mathcal{L}_{\mathcal{N}(\varphi_0,\lambda^2)}(\vartheta_1)\prod_{t=2}^{T}\mathcal{L}_{\mathcal{N}((1-\varphi_1)\varphi_0+\varphi_1\vartheta_{t-1},\lambda^2(1-\varphi_1^2))}(\vartheta_t) \\
&\propto \exp\left\{\left\{-\frac{1}{2s_0^2}(\varphi_0-m_o)^2\right\}\right\}\exp\left\{\left\{-\frac{1}{2\lambda^2}(\varphi_0-\vartheta_1)^2\right\}\right\} \\
&\cdot \exp\left\{\left\{-\frac{1}{2\frac{\lambda^2(1-\varphi_1^2)}{(T-1)(1-\varphi_1)^2}}\left(\varphi_0-\frac{(1-\varphi_1)(\mathrm{SUM}_t)}{(T-1)(1-\varphi_1)^2}\right)^2\right\}\right\} \\
&\text{where } \mathrm{SUM}_t = \sum_{t=2}^{T}(\vartheta_t-\varphi_1\vartheta_{t-1}) \\
\implies f(\varphi_0|-) &\propto \text{kernel of a } \mathcal{N}(\mu_{\varphi_0(\mathrm{post})},\sigma^2_{\varphi_0(\mathrm{post})}) \text{ with} \\
\sigma^2_{\varphi_0(\mathrm{post})} &= \frac{1}{\frac{1}{s_0^2}+\frac{1}{\lambda^2}+\frac{(T-1)(1-\varphi_1)^2}{\lambda^2(1-\varphi_1^2)}} \\
\mu_{\varphi_0(\mathrm{post})} &= \sigma^2_{\varphi_0(\mathrm{post})}\left(\frac{m_0}{s_0^2}+\frac{\vartheta_1}{\lambda^2}+\frac{1-\varphi_1}{\lambda^2(1-\varphi_1^2)}\mathrm{SUM}_t\right)
\end{aligned}
\tag{A.11}
$$

- update λ^2. This full conditional derivation is characteristic of JDRPM only, since in CDRPM the variance had a uniform law and was therefore updated through a Metropolis step.

$$
\begin{aligned}
f(\lambda^2|-) &\propto f(\lambda^2) f(\vartheta_1,\dots,\vartheta_T|\lambda^2,-) \\
&= \mathcal{L}_{\mathrm{invGamma}(a_\lambda,b_\lambda)}(\lambda^2)\mathcal{L}_{\mathcal{N}(\varphi_0,\lambda^2)}(\vartheta_1)\prod_{t=2}^{T}\mathcal{L}_{\mathcal{N}((1-\varphi_1)\varphi_0+\varphi_1\vartheta_{t-1},\lambda^2(1-\varphi_1^2))}(\vartheta_t) \\
&\propto \left[\left(\frac{1}{\lambda_t^2}\right)^{a_\lambda+1}\exp\left\{-\frac{b_\lambda}{\lambda^2}\right\}\right]\left[\left(\frac{1}{\lambda^2}\right)^{1/2}\exp\left\{-\frac{1}{2\lambda^2}(\vartheta_1-\varphi_0)^2\right\}\right] \\
&\cdot \left[\prod_{t=2}^{T}\left(\frac{1}{\lambda^2}\right)^{1/2}\exp\left\{-\frac{1}{2\lambda^2}\left(\vartheta_t-(1-\varphi_1)\varphi_0-\varphi_1\vartheta_{t-1}\right)^2\right\}\right] \\
&\propto \left(\frac{1}{\lambda^2}\right)^{\left(\frac{T}{2}+a_\lambda\right)+1} \\
&\cdot \exp\left\{-\frac{1}{\lambda^2}\left(\frac{(\vartheta_1-\varphi_0)^2}{2}+\sum_{t=2}^{T}\frac{\left(\vartheta_t-(1-\varphi_1)\varphi_0-\varphi_1\vartheta_{t-1}\right)^2}{2}+b_\lambda\right)\right\} \\
\implies f(\lambda^2|-) &\propto \text{kernel of a } \mathrm{invGamma}(a_{\lambda(\mathrm{post})},b_{\lambda(\mathrm{post})}) \text{ with} \\
a_{\lambda(\mathrm{post})} &= \frac{T}{2}+a_\lambda \\
b_{\lambda(\mathrm{post})} &= \frac{(\vartheta_1-\varphi_0)^2}{2}+\sum_{t=2}^{T}\frac{\left(\vartheta_t-(1-\varphi_1)\varphi_0-\varphi_1\vartheta_{t-1}\right)^2}{2}+b_\lambda
\end{aligned}
\tag{A.12}
$$

- update α. This update rule is the same for both JDRPM and CDRPM.

if global α: prior is $\alpha \sim \text{Beta}(a_\alpha, b_\alpha)$

$$\begin{aligned} f(\alpha|-) &\propto f(\alpha) f((\gamma_{11}, \ldots, \gamma_{1T}, \ldots, \gamma_{n1}, \ldots, \gamma_{nT})|\alpha) \\ &\propto \alpha^{a_\alpha - 1}(1-\alpha)^{b_\alpha - 1} \prod_{i=1}^{n}\prod_{t=1}^{T} \alpha^{\gamma_{it}}(1-\alpha)^{1-\gamma_{it}} \\ &= \alpha^{(a_\alpha + \sum_{i=1}^{n}\sum_{t=1}^{T}\gamma_{it}) - 1}(1-\alpha)^{(b_\alpha + nT - \sum_{i=1}^{n}\sum_{t=1}^{T}\gamma_{it}) - 1} \\ \implies f(\alpha|-) &\propto \text{kernel of a Beta}(a_{\alpha(\text{post})}, b_{\alpha(\text{post})}) \text{ with} \\ a_{\alpha(\text{post})} &= a_\alpha + \sum_{i=1}^{n}\sum_{t=1}^{T}\gamma_{it} \quad b_{\alpha(\text{post})} = b_\alpha + nT - \sum_{i=1}^{n}\sum_{t=1}^{T}\gamma_{it} \end{aligned} \tag{A.13}$$

if time specific α: prior is $\alpha_t \sim \text{Beta}(a_\alpha, b_\alpha)$

$$\begin{aligned} f(\alpha_t|-) &\propto f(\alpha_t) f((\gamma_{1t}, \ldots, \gamma_{nt})|\alpha_t) \\ &\propto \alpha_t^{a_\alpha - 1}(1-\alpha_t)^{b_\alpha - 1} \prod_{i=1}^{n} \alpha_t^{\gamma_{it}}(1-\alpha_t)^{1-\gamma_{it}} \\ &= \alpha_t^{(a_\alpha + \sum_{i=1}^{n}\gamma_{it}) - 1}(1-\alpha_t)^{(b_\alpha + n - \sum_{i=1}^{n}\gamma_{it}) - 1} \\ \implies f(\alpha_t|-) &\propto \text{kernel of a Beta}(a_{\alpha(\text{post})}, b_{\alpha(\text{post})}) \text{ with} \\ a_{\alpha(\text{post})} &= a_\alpha + \sum_{i=1}^{n}\gamma_{it} \quad b_{\alpha(\text{post})} = b_\alpha + n - \sum_{i=1}^{n}\gamma_{it} \end{aligned} \tag{A.14}$$

if unit specific α: prior is $\alpha_i \sim \text{Beta}(a_{\alpha i}, b_{\alpha i})$

$$\begin{aligned} f(\alpha_i|-) &\propto f(\alpha_i) f((\gamma_{i1}, \ldots, \gamma_{iT})|\alpha_i) \\ &\propto \alpha_i^{a_{\alpha i} - 1}(1-\alpha_i)^{b_{\alpha i} - 1} \prod_{t=1}^{T} \alpha_i^{\gamma_{it}}(1-\alpha_i)^{1-\gamma_{it}} \\ &= \alpha_{it}^{(a_{\alpha i} + \sum_{t=1}^{T}\gamma_{it}) - 1}(1-\alpha_{it})^{(b_{\alpha i} + T - \sum_{t=1}^{T}\gamma_{it}) - 1} \\ \implies f(\alpha_i|-) &\propto \text{kernel of a Beta}(a_{\alpha(\text{post})}, b_{\alpha(\text{post})}) \text{ with} \\ a_{\alpha(\text{post})} &= a_{\alpha i} + \sum_{t=1}^{T}\gamma_{it} \quad b_{\alpha(\text{post})} = b_{\alpha i} + T - \sum_{t=1}^{T}\gamma_{it} \end{aligned} \tag{A.15}$$

if time and unit specific α: prior is $\alpha_{it} \sim \text{Beta}(a_{\alpha_i}, b_{\alpha_i})$

$$\begin{aligned} f(\alpha_{it}|-) &\propto f(\alpha_{it}) f(\gamma_{it}|\alpha_{it}) \\ &\propto \alpha_{it}^{a-1}(1-\alpha_{it})^{b-1}\alpha_{it}^{\gamma_{it}}(1-\alpha_{it})^{1-\gamma_{it}} \\ &= \alpha_i^{(a+\gamma_{it})-1}(1-\alpha_i)^{(b+1-\gamma_{it})-1} \\ \implies f(\alpha_{it}|-) &\propto \text{kernel of a Beta}(a_{\alpha(\text{post})}, b_{\alpha(\text{post})}) \text{ with} \\ a_{\alpha(\text{post})} &= a_{\alpha i} + \gamma_{it} \quad b_{\alpha(\text{post})} = b_{\alpha i} + 1 - \gamma_{it} \end{aligned} \tag{A.16}$$

- update a missing observation Y_{it}. This full conditional derivation is characteristic of JDRPM only, since the handling of missing data feature introduced by our generalized model.

for $t = 1$:

$$
\begin{aligned}
f(Y_{it}|-) &\propto f(Y_{it}) f(Y_{it+1}|Y_{it}, -) \\
&= \mathcal{L}_{\mathcal{N}(\mu^{\star}_{c_{it}t} + \boldsymbol{x}_{it}^T \boldsymbol{\beta}_t, \sigma^{2\star}_{c_{it}t})}(Y_{it}) \\
&\cdot \mathcal{L}_{\mathcal{N}(\mu^{\star}_{c_{it+1}t+1} + \eta_{1i} Y_{it} + \boldsymbol{x}_{it+1}^T \boldsymbol{\beta}_{t+1}, \sigma^{2\star}_{c_{it+1}t+1}(1-\eta_{1i}^2))}(Y_{it+1}) \\
&\propto \exp\left\{ -\frac{1}{2\sigma^{2\star}_{c_{it}t}} (Y_{it} - \mu^{\star}_{c_{it}t} - \boldsymbol{x}_{it}^T \boldsymbol{\beta}_t)^2 \right\} \\
&\cdot \exp\left\{ -\frac{1}{2\sigma^{2\star}_{c_{it+1}t+1}(1-\eta_{1i}^2)} (Y_{it+1} - \mu^{\star}_{c_{it+1}t+1} - \eta_{1i} Y_{it} - \boldsymbol{x}_{it+1}^T \boldsymbol{\beta}_{t+1})^2 \right\} \\
&= \exp\left\{ -\frac{1}{2\sigma^{2\star}_{c_{it}t}} \left(Y_{it} - (\mu^{\star}_{c_{it}t} + \boldsymbol{x}_{it}^T \boldsymbol{\beta}_t) \right)^2 \right\} \\
&\cdot \exp\left\{ -\frac{\eta_{1i}^2}{2\sigma^{2\star}_{c_{it+1}t+1}(1-\eta_{1i}^2)} \left(Y_{it} - \frac{Y_{it+1} - \mu^{\star}_{c_{it+1}t+1} - \boldsymbol{x}_{it+1}^T \boldsymbol{\beta}_{t+1}}{\eta_{1i}} \right)^2 \right\}
\end{aligned}
$$

$$
\begin{aligned}
\implies f(Y_{it}|-) &\propto \mathcal{N}(\mu_{Y_{it}(\text{post})}, \sigma^2_{Y_{it}(\text{post})}) \text{ with} \\
\sigma^2_{Y_{it}(\text{post})} &= \frac{1}{\frac{1}{\sigma^{2\star}_{c_{it}t}} + \frac{\eta_{1i}^2}{2\sigma^{2\star}_{c_{it+1}t+1}(1-\eta_{1i}^2)}} \\
\mu_{Y_{it}(\text{post})} &= \sigma^2_{Y_{it}(\text{post})} \left(\frac{\mu^{\star}_{c_{it}t} + \boldsymbol{x}_{it}^T \boldsymbol{\beta}_t}{\sigma^{2\star}_{c_{it}t}} + \frac{\eta_{1i}(Y_{it+1} - \mu^{\star}_{c_{it+1}t+1} - \boldsymbol{x}_{it+1}^T \boldsymbol{\beta}_{t+1})}{\sigma^{2\star}_{c_{it+1}t+1}(1-\eta_{1i}^2)} \right)
\end{aligned}
\tag{A.17}
$$

for $1 < t < T$:

$$
\begin{aligned}
f(Y_{it}|-) &\propto f(Y_{it}) f(Y_{it+1}|Y_{it}, -) \\
&= \mathcal{L}_{\mathcal{N}(\mu^{\star}_{c_{it}t} + \eta_{1i} Y_{it-1} + \boldsymbol{x}_{it}^T \boldsymbol{\beta}_t, \sigma^{2\star}_{c_{it}t})}(Y_{it}) \\
&\cdot \mathcal{L}_{\mathcal{N}(\mu^{\star}_{c_{it+1}t+1} + \eta_{1i} Y_{it} + \boldsymbol{x}_{it+1}^T \boldsymbol{\beta}_{t+1}, \sigma^{2\star}_{c_{it+1}t+1}(1-\eta_{1i}^2))}(Y_{it+1}) \\
&\propto \exp\left\{ -\frac{1}{2\sigma^{2\star}_{c_{it}t}(1-\eta_{1i}^2)} (Y_{it} - \mu^{\star}_{c_{it}t} - \eta_{1i} Y_{it-1} - \boldsymbol{x}_{it}^T \boldsymbol{\beta}_t)^2 \right\} \\
&\cdot \exp\left\{ -\frac{1}{2\sigma^{2\star}_{c_{it+1}t+1}(1-\eta_{1i}^2)} (Y_{it+1} - \mu^{\star}_{c_{it+1}t+1} - \eta_{1i} Y_{it} - \boldsymbol{x}_{it+1}^T \boldsymbol{\beta}_{t+1})^2 \right\} \\
&= \exp\left\{ -\frac{1}{2\sigma^{2\star}_{c_{it}t}(1-\eta_{1i}^2)} \left(Y_{it} - (\mu^{\star}_{c_{it}t} + \eta_{1i} Y_{it-1} + \boldsymbol{x}_{it}^T \boldsymbol{\beta}_t) \right)^2 \right\} \\
&\cdot \exp\left\{ -\frac{\eta_{1i}^2}{2\sigma^{2\star}_{c_{it+1}t+1}(1-\eta_{1i}^2)} \left(Y_{it} - \frac{Y_{it+1} - \mu^{\star}_{c_{it+1}t+1} - \boldsymbol{x}_{it+1}^T \boldsymbol{\beta}_{t+1}}{\eta_{1i}} \right)^2 \right\}
\end{aligned}
$$

$$
\implies f(Y_{it}|-) \propto \mathcal{N}(\mu_{Y_{it}(\text{post})}, \sigma^2_{Y_{it}(\text{post})}) \text{ with}
$$

$$\sigma^2_{Y_{it}(\text{post})} = \frac{1-\eta_{1i}^2}{\frac{1}{\sigma^{2\star}_{c_{it}t}} + \frac{\eta_{1i}^2}{\sigma^{2\star}_{c_{it+1}t+1}}}$$
$$\mu_{Y_{it}(\text{post})} = \sigma^2_{Y_{it}(\text{post})} \left(\frac{\mu^\star_{c_{it}t} + \eta_{1i} Y_{it-1} + \boldsymbol{x}_{it}^T \boldsymbol{\beta}_t}{\sigma^{2\star}_{c_{it}t}(1-\eta_{1i}^2)} + \frac{\eta_{1i}(Y_{it+1} - \mu^\star_{c_{it+1}t+1} - \boldsymbol{x}_{it+1}^T \boldsymbol{\beta}_{t+1})}{\sigma^{2\star}_{c_{it+1}t+1}(1-\eta_{1i}^2)} \right) \tag{A.18}$$

$$\begin{aligned} &\text{for } t = T\text{:} \\ &\quad f(Y_{it}|-) \propto f(Y_{it}) \\ &\qquad\qquad = \mathcal{L}_{\mathcal{N}(\mu^\star_{c_{it}t} + \eta_{1i} Y_{it-1} + \boldsymbol{x}_{it}^T \boldsymbol{\beta}_t, \sigma^{2\star}_{c_{it}t}(1-\eta_{1i}^2))}(Y_{it}) \\ &\implies f(Y_{it}|-) \text{ is just the likelihood of } Y_{it} \end{aligned} \tag{A.19}$$

Appendix B

Computational details

B.1 Implementation of the MCMC algorithm

We now present the code from the `MCMC_fit` function which implements the JDRPM algorithm. We report exclusively the functional part of the implementation, omitting setup lines related to function definitions, variable preallocations, and input argument checks. This inclusion allows readers to appreciate the ease, clarity, and elegance of the Julia language in translating the mathematical formulations into code. As such, we hope that Julia will emerge as the natural choice in the statistical and scientific computing fields, offering them a refreshing approach.

In addition to the points discussed in Chapter 2, we note that the productivity granted by the Julia language is not only derived from its extensive ecosystem of packages and documentation, but also from an active online forum (`https://discourse.julialang.org`), where I personally posed some questions and received valuable answers during the development of this thesis.

Listing 3: Julia code that implements JDRPM's MCMC algorithm.

```
############# start MCMC algorithm #############
println(replace(string(now()),"T" => " ")[1:end-4])
println("Starting MCMC algorithm")

t_start = now()
progresso = Progress(round(Int64(draws)),
      showspeed=true,
      output=stdout, # default is stderr, which turns out in orange color on R
      dt=1, # every how many seconds update the feedback
      barlen=0 # no progress bar
      )

@inbounds for i in 1:draws
   ############# sample the missing values #############
   # from the "update rho" section onwards also the Y[j,t] will be needed (to
   ↪  compute weights, update laws, etc)
   # so we need now to simulate the values for the data which are missing (from
   ↪  their full conditional)
   if Y_has_NA
      # we have to use the missing_idxs to remember which units and at which
      ↪  times had a missing value,
```

```
    # in order to simulate just them and instead use the given value for the
    ↪ other units and times
    for (j,t) in missing_idxs
        # Problem: if when filling a NA we occur in another NA value? eg when
        ↪ we also need Y[j,t±1]
        # I decided here to set that value to 0, if occurs, since anyway target
        ↪ should be centered
        # so it seems a reasonable patch
        # We could have decided to ignore this computation and just use the
        ↪ likelihood as proposal
        # filling distribution, but this would have just worked in the Y[j,t+1]
        ↪ case so the general
        # problem would have still been there

        c_it = Si_iter[j,t]
        Xlk_term_t = (lk_xPPM ? dot(view(Xlk_covariates,j,:,t), beta_iter[t]) :
        ↪ 0)
        aux1 = eta1_iter[j]^2

        if t==1
            c_itp1 = Si_iter[j,t+1]
            Xlk_term_tp1 = (lk_xPPM ? dot(view(Xlk_covariates,j,:,t+1),
            ↪ beta_iter[t+1]) : 0)

            sig2_post = 1 / (1/sig2h_iter[c_it,t] +
            ↪ aux1/(sig2h_iter[c_itp1,t+1]*(1-aux1)))
            mu_post = sig2_post * (
                (1/sig2h_iter[c_it,t])*(muh_iter[c_it,t] + Xlk_term_t) +
                (eta1_iter[j]/(sig2h_iter[c_itp1,t+1]*(1-aux1)))*((ismissing(Y[j,t+1])
                ↪ ? 0 : Y[j,t+1]) - muh_iter[c_itp1,t+1] - Xlk_term_tp1)
                )

            Y[j,t] = rand(Normal(mu_post,sqrt(sig2_post)))

        elseif 1<t<T
            c_itp1 = Si_iter[j,t+1]
            Xlk_term_tp1 = (lk_xPPM ? dot(view(Xlk_covariates,j,:,t+1),
            ↪ beta_iter[t+1]) : 0)

            sig2_post = (1-aux1) / (1/sig2h_iter[c_it,t] +
            ↪ aux1/sig2h_iter[c_itp1,t+1])
            mu_post = sig2_post * (
                (1/(sig2h_iter[c_it,t]*(1-aux1)))*(muh_iter[c_it,t] +
                ↪ eta1_iter[j]*(ismissing(Y[j,t-1]) ? 0 : Y[j,t-1]) +
                ↪ Xlk_term_t) +
                (eta1_iter[j]/(sig2h_iter[c_itp1,t+1]*(1-aux1)))*((ismissing(Y[j,t+1])
                ↪ ? 0 : Y[j,t+1]) - muh_iter[c_itp1,t+1] - Xlk_term_tp1)
                )

            Y[j,t] = rand(Normal(mu_post,sqrt(sig2_post)))

        else # t==T
            Y[j,t] = rand(Normal(
                muh_iter[c_it,t] + eta1_iter[j]*(ismissing(Y[j,t-1]) ? 0 :
                ↪ Y[j,t-1]) + Xlk_term_t,
                sqrt(sig2h_iter[c_it,t]*(1-aux1))
                ))
        end
    end
end
```

```
for t in 1:T
   ############# update gamma #############
   for j in 1:n
      if t==1
         gamma_iter[j,t] = 0
         # at the first time units get reallocated
      else
         # we want to find rho_t^{R_t(-j)} ...
         indexes = findall_faster(jj -> jj != j && gamma_iter[jj, t] == 1,
         ↪  1:n)
         Si_red = Si_iter[indexes, t]
         copy!(Si_red1, Si_red)
         push!(Si_red1, Si_iter[j,t]) # ... and rho_t^R_t(+j)}

         # get also the reduced spatial info if sPPM model
         if sPPM
            sp1_red = @view sp1[indexes]
            sp2_red = @view sp2[indexes]
         end
         # and the reduced covariates info if cl_xPPM model
         if cl_xPPM
            Xcl_covariates_red = @view Xcl_covariates[indexes,:,t]
         end

         # compute n_red's and nclus_red's and relabel
         n_red = length(Si_red) # = "n" relative to here, i.e. the
         ↪  sub-partition size
         n_red1 = length(Si_red1)
         relabel!(Si_red,n_red)
         relabel!(Si_red1,n_red1)
         nclus_red = isempty(Si_red) ? 0 : maximum(Si_red) # = number of
         ↪  clusters
         nclus_red1 = maximum(Si_red1)

         # save the label of the current working-on unit j
         j_label = Si_red1[end]

         # compute also nh_red's
         nh_red .= 0
         nh_red1 .= 0
         for jj in 1:n_red
            nh_red[Si_red[jj]] += 1 # = numerosities for each cluster label
            nh_red1[Si_red1[jj]] += 1
         end
         nh_red1[Si_red1[end]] += 1 # account for the last added unit j, not
         ↪  included in the above loop

         # start computing weights
         lg_weights .= 0

         # unit j can enter an existing cluster...
         for k in 1:nclus_red

            # filter the indexes of the units of label k
            aux_idxs = findall(Si_red .== k)
            lC .= 0.
            if sPPM
               copy!(s1o, sp1_red[aux_idxs])
               copy!(s2o, sp2_red[aux_idxs])
               copy!(s1n,s1o); push!(s1n, sp1[j])
               copy!(s2n,s2o); push!(s2n, sp2[j])
```

```
            spatial_cohesion!(spatial_cohesion_idx, s1o, s2o,
            ↪  sp_params_struct, true, M_dp, S,1,false,lC)
            spatial_cohesion!(spatial_cohesion_idx, s1n, s2n,
            ↪  sp_params_struct, true, M_dp, S,2,false,lC)
         end

         lS .= 0.
         if cl_xPPM
            for p in 1:p_cl
               if isa(first(Xcl_covariates[j,p,t]),Real) # numerical
               ↪  covariate
                  copy!(Xo, @view Xcl_covariates_red[aux_idxs,p])
                  copy!(Xn, Xo); push!(Xn,Xcl_covariates[j,p,t])

                  if covariate_similarity_idx == 4
                     covariate_similarity!(covariate_similarity_idx, Xo,
                     ↪  cv_params_sim4[p], Rs[p,t],
                     ↪  true,1,true,lS,cv_weight)
                     covariate_similarity!(covariate_similarity_idx, Xn,
                     ↪  cv_params_sim4[p], Rs[p,t],
                     ↪  true,2,true,lS,cv_weight)
                  else
                     covariate_similarity!(covariate_similarity_idx, Xo,
                     ↪  cv_params, Rs[p,t], true,1,true,lS,cv_weight)
                     covariate_similarity!(covariate_similarity_idx, Xn,
                     ↪  cv_params, Rs[p,t], true,2,true,lS,cv_weight)
                  end
               else # categorical covariate
                  copy!(Xo_cat, @view Xcl_covariates_red[aux_idxs,p])
                  copy!(Xn_cat, Xo_cat);
                  ↪  push!(Xn_cat,Xcl_covariates[j,p,t])

                  covariate_similarity!(covariate_similarity_idx, Xo_cat,
                  ↪  cv_params, Rs[p,t], true,1,true,lS,cv_weight)
                  covariate_similarity!(covariate_similarity_idx, Xn_cat,
                  ↪  cv_params, Rs[p,t], true,2,true,lS,cv_weight)
               end
            end
         end

         lg_weights[k] = log(nh_red[k]) + lC[2] - lC[1] + lS[2] - lS[1]
      end

      # ... or unit j can create a singleton
      lC .= 0.
      if sPPM
         spatial_cohesion!(spatial_cohesion_idx, SVector(sp1[j]),
         ↪  SVector(sp2[j]), sp_params_struct, true, M_dp, S,2,false,lC)
      end
      lS .= 0.
      if cl_xPPM
         for p in 1:p_cl
            if covariate_similarity_idx == 4
               covariate_similarity!(covariate_similarity_idx,
               ↪  SVector(Xcl_covariates[j,p,t]), cv_params_sim4[p],
               ↪  Rs[p,t], true, 2,true,lS,cv_weight)
            else
               covariate_similarity!(covariate_similarity_idx,
               ↪  SVector(Xcl_covariates[j,p,t]), cv_params, Rs[p,t],
               ↪  true, 2,true,lS,cv_weight)
            end
         end
```

```
        end
        lg_weights[nclus_red+1] = log_Mdp + lC[2] + lS[2]

        # now use the weights towards sampling the new gamma_jt
        max_ph = maximum(@view lg_weights[1:(nclus_red+1)])
        sum_ph = 0.0

        # exponentiate...
        for k in 1:(nclus_red+1)
            # for numerical purposes we subract max_ph
           lg_weights[k] = exp(lg_weights[k] - max_ph)
           sum_ph += lg_weights[k]
        end
        # ... and normalize
        lg_weights ./= sum_ph

        # compute probh
        probh::Float64 = 0.0
        if time_specific_alpha==false && unit_specific_alpha==false
           probh = alpha_iter / (alpha_iter + (1 - alpha_iter) *
           ↪  lg_weights[j_label])
        elseif time_specific_alpha==true && unit_specific_alpha==false
           probh = alpha_iter[t] / (alpha_iter[t] + (1 - alpha_iter[t]) *
           ↪  lg_weights[j_label])
        elseif time_specific_alpha==false && unit_specific_alpha==true
           probh = alpha_iter[j] / (alpha_iter[j] + (1 - alpha_iter[j]) *
           ↪  lg_weights[j_label])
        elseif time_specific_alpha==true && unit_specific_alpha==true
           probh = alpha_iter[j,t] / (alpha_iter[j,t] + (1 -
           ↪  alpha_iter[j,t]) * lg_weights[j_label])
        end

        # compatibility check for gamma transition
        if gamma_iter[j, t] == 0
           # we want to find rho_(t-1)^{R_t(+j)} ...
           indexes = findall_faster(jj -> jj==j || gamma_iter[jj, t]==1,
           ↪  1:n)
           Si_comp1 = @view Si_iter[indexes, t-1]
           Si_comp2 = @view Si_iter[indexes, t] # ... and rho_t^R_t(+j)}

           rho_comp = compatibility(Si_comp1, Si_comp2)
           if rho_comp == 0
              probh = 0.0
           end
        end
        # sample the new gamma
        gt = rand(Bernoulli(probh))
        gamma_iter[j, t] = gt
     end
  end # for j in 1:n

  ############## update rho #############
  # we only update the partition for the units which can move (i.e. with
  ↪  gamma_jt=0)
  movable_units = findall(gamma_iter[:,t] .== 0) # fast

  for j in movable_units
     # remove unit j from the cluster she is currently in

     if nh[Si_iter[j,t],t] > 1 # unit j does not belong to a singleton
     ↪  cluster
        nh[Si_iter[j,t],t] -= 1
```

```
   # no nclus_iter[t] change since j's cluster is still alive
else # unit j belongs to a singleton cluster
   j_label = Si_iter[j,t]
   last_label = nclus_iter[t]

   if j_label < last_label
      # here we enter if j_label is not the last label, so we need to
      # relabel clusters in order to then remove j's cluster
      # eg: units 1 2 3 4 5 j 7 -> units 1 2 3 4 5 j 7
      #     label 1 1 2 2 2 3 4    label 1 1 2 2 2 4 3

      # swap cluster labels...
      for jj in 1:n
         if Si_iter[jj, t] == last_label
            Si_iter[jj, t] = j_label
         end
      end
      Si_iter[j, t] = last_label
      # ... and cluster-specific parameters
      sig2h_iter[j_label, t], sig2h_iter[last_label, t] =
      ↪  sig2h_iter[last_label, t], sig2h_iter[j_label, t]
      muh_iter[j_label, t], muh_iter[last_label, t] =
      ↪  muh_iter[last_label, t], muh_iter[j_label, t]
      nh[j_label, t] = nh[last_label, t]
      nh[last_label, t] = 1

   end
   # remove the j-th observation and the last cluster (being j in a
   ↪  singleton)
   nh[last_label, t] -= 1
   nclus_iter[t] -= 1
end

# setup probability weights towards the sampling of rho_jt
ph .= 0.0
resize!(ph,nclus_iter[t]+1)
copy!(rho_tmp, @view Si_iter[:,t])

# compute nh_tmp (numerosities for each cluster label)
copy!(nh_tmp, @view nh[:,t])
# unit j contribute is already absent from the change we did above
nclus_temp = 0

# we now simulate the unit j to be assigned to one of the existing
↪  clusters...
for k in 1:nclus_iter[t]
   rho_tmp[j] = k
   indexes = findall(gamma_iter[:,t+1] .== 1) # fast
   # we check the compatibility between rho_t^{h=k,R_(t+1)} ...
   Si_comp1 = @view rho_tmp[indexes]
   Si_comp2 = @view Si_iter[indexes,t+1] # and rho_(t+1)^{R_(t+1)}
   rho_comp = compatibility(Si_comp1, Si_comp2)

   if rho_comp != 1
      ph[k] = log(0) # assignment to cluster k is not compatible
   else
      # update params for "rho_jt = k" simulation
      nh_tmp[k] += 1
      nclus_temp = count(a->(a>0), nh_tmp)

      lPP .= 0.
      for kk in 1:nclus_temp
```

```
            aux_idxs = findall(rho_tmp .== kk)
            if sPPM
               copy!(s1n, @view sp1[aux_idxs])
               copy!(s2n, @view sp2[aux_idxs])
               spatial_cohesion!(spatial_cohesion_idx, s1n, s2n,
               ↪  sp_params_struct, true, M_dp, S,1,true,lPP)
            end
            if cl_xPPM
               for p in 1:p_cl
                  Xn_view = @view Xcl_covariates[aux_idxs,p,t]
                  if covariate_similarity_idx == 4
                     covariate_similarity!(covariate_similarity_idx,
                     ↪  Xn_view, cv_params_sim4[p], Rs[p,t],
                     ↪  true,1,true,lPP,cv_weight)
                  else
                     covariate_similarity!(covariate_similarity_idx,
                     ↪  Xn_view, cv_params, Rs[p,t],
                     ↪  true,1,true,lPP,cv_weight)
                  end
               end
            end
            lPP[1] += log_Mdp + lgamma(nh_tmp[kk])
         end

         if t==1
            ph[k] = loglikelihood(Normal(
               muh_iter[k,t] + (lk_xPPM ? dot(view(Xlk_covariates,j,:,t),
               ↪  beta_iter[t]) : 0),
               sqrt(sig2h_iter[k,t])),
               Y[j,t]) + lPP[1]
         else
            ph[k] = loglikelihood(Normal(
               muh_iter[k,t] + eta1_iter[j]*Y[j,t-1] + (lk_xPPM ?
               ↪  dot(view(Xlk_covariates,j,:,t), beta_iter[t]) : 0),
               sqrt(sig2h_iter[k,t]*(1-eta1_iter[j]^2))),
               Y[j,t]) + lPP[1]
         end

         # restore params after "rho_jt = k" simulation
         nh_tmp[k] -= 1
      end
   end

   # ... plus the case of being assigned to a new (singleton for now)
   ↪  cluster
   k = nclus_iter[t]+1
   rho_tmp[j] = k
   # declare (for later scope accessibility) the new params here
   muh_draw = 0.0; sig2h_draw = 0.0

   indexes = findall(gamma_iter[:,t+1] .== 1)
   Si_comp1 = @view rho_tmp[indexes]
   Si_comp2 = @view Si_iter[indexes,t+1]
   rho_comp = compatibility(Si_comp1, Si_comp2)

   if rho_comp != 1
      ph[k] = log(0) # assignment to a new cluster is not compatible
   else
      # sample new params for this new cluster
      muh_draw = rand(Normal(theta_iter[t], sqrt(tau2_iter[t])))
      sig2h_draw = rand(InverseGamma(sig2h_priors[1],sig2h_priors[2]))
```

```
        # update params for "rho_jt = k" simulation
        nh_tmp[k] += 1
        nclus_temp = count(a->(a>0), nh_tmp)

        lPP .= 0.
        for kk in 1:nclus_temp
            aux_idxs = findall(rho_tmp .== kk) # fast
            if sPPM
                copy!(s1n, @view sp1[aux_idxs])
                copy!(s2n, @view sp2[aux_idxs])
                spatial_cohesion!(spatial_cohesion_idx, s1n, s2n,
                ↪  sp_params_struct, true, M_dp, S,1,true,lPP)
            end
            if cl_xPPM
                for p in 1:p_cl
                    Xn_view = @view Xcl_covariates[aux_idxs,p,t]
                    if covariate_similarity_idx == 4
                        covariate_similarity!(covariate_similarity_idx, Xn_view,
                        ↪  cv_params_sim4[p], Rs[p,t],
                        ↪  true,1,true,lPP,cv_weight)
                    else
                        covariate_similarity!(covariate_similarity_idx, Xn_view,
                        ↪  cv_params, Rs[p,t], true,1,true,lPP,cv_weight)
                    end
                end
            end
            lPP[1] += log_Mdp + lgamma(nh_tmp[kk])
        end

        if t==1
            ph[k] = loglikelihood(Normal(
                muh_draw + (lk_xPPM ? dot(view(Xlk_covariates,j,:,t),
                ↪  beta_iter[t]) : 0),
                sqrt(sig2h_draw)),
                Y[j,t]) + lPP[1]
        else
            ph[k] = loglikelihood(Normal(
                muh_draw + eta1_iter[j]*Y[j,t-1] + (lk_xPPM ?
                ↪  dot(view(Xlk_covariates,j,:,t), beta_iter[t]) : 0),
                sqrt(sig2h_draw*(1-eta1_iter[j]^2))),
                Y[j,t]) + lPP[1]
        end

        # restore params after "rho_jt = k" simulation
        nh_tmp[k] -= 1
    end

    # now exponentiate the weights...
    max_ph = maximum(ph)
    sum_ph = 0.0
    for k in eachindex(ph)
        # for numerical purposes we subract max_ph
        ph[k] = exp(ph[k] - max_ph)
        sum_ph += ph[k]
    end
    # ... and normalize them
    ph ./= sum_ph

    # now sample the new label Si_iter[j,t]
    u = rand(Uniform(0,1))
    cph = cumsum(ph)
    cph[end] = 1 # fix numerical problems of having sums like 0.999999etc
```

```
        new_label = 0
        for k in eachindex(ph)
            if u <= cph[k]
                new_label = k
                break
            end
        end

        if new_label <= nclus_iter[t]
            # we enter an existing cluster
            Si_iter[j, t] = new_label
            nh[new_label, t] += 1
        else
            # we create a new singleton cluster
            nclus_iter[t] += 1
            cl_new = nclus_iter[t]
            Si_iter[j, t] = cl_new
            nh[cl_new, t] = 1
            muh_iter[cl_new, t] = muh_draw
            sig2h_iter[cl_new, t] = sig2h_draw
        end

        # now we need to relabel after the possible mess created by the
        ↪  sampling
        # eg: (before sampling)  (after sampling)
        #     units j 2 3 4 5 ->  units j 2 3 4 5
        #    labels 1 1 1 2 2    labels 3 1 1 2 2
        # the after case has to be relabelled
        Si_tmp = @view Si_iter[:,t]

        relabel_full!(Si_tmp,n,Si_relab, nh_reorder, old_lab)
        # - Si_relab gives the relabelled partition
        # - nh_reorder gives the numerosities of the relabelled partition, ie
        ↪  "nh_reorder[k] = #(units of new cluster k)"
        # - old_lab tells "the index in position i (which before was cluster i)
        ↪  is now called cluster old_lab[i]"
        # eg:             Original labels (Si): 4 2 1 1 1 3 1 4 5
        #          Relabeled groups (Si_relab): 1 2 3 3 3 4 3 1 5
        # Reordered cluster sizes (nh_reorder): 2 1 4 1 1 0 0 0 0
        #                 Old labels (old_lab): 4 2 1 3 5 0 0 0 0

        # now fix everything (morally permute params)
        Si_iter[:,t] = Si_relab
        # discard the zeros at the end of the auxiliary vectors nh_reorde and
        ↪  old_lab
        copy!(muh_iter_copy, muh_iter)
        copy!(sig2h_iter_copy, sig2h_iter)
        len = findlast(x -> x != 0, nh_reorder)
        for k in 1:nclus_iter[t]
            muh_iter[k,t] = muh_iter_copy[old_lab[k],t]
            sig2h_iter[k,t] = sig2h_iter_copy[old_lab[k],t]
            nh[k,t] = nh_reorder[k]
        end

    end # for j in movable_units

    ############# update muh #############
    if t==1
        for k in 1:nclus_iter[t]
            sum_Y = 0.0
            for j in 1:n
                if Si_iter[j,t]==k
```

```
            sum_Y += Y[j,t] - (lk_xPPM ? dot(view(Xlk_covariates,j,:,t),
            ↪  beta_iter[t]) : 0.0)
         end
      end
      sig2_star = 1 / (1/tau2_iter[t] + nh[k,t]/sig2h_iter[k,t])
      mu_star = sig2_star * (theta_iter[t]/tau2_iter[t] +
      ↪  sum_Y/sig2h_iter[k,t])

      muh_iter[k,t] = rand(Normal(mu_star,sqrt(sig2_star)))
   end

else # t>1
   for k in 1:nclus_iter[t]
      sum_Y = 0.0
      sum_e2 = 0.0
      for j in 1:n
         if Si_iter[j,t]==k
            aux1 = 1 / (1-eta1_iter[j]^2)
            sum_e2 += aux1
            sum_Y += (Y[j,t] - eta1_iter[j]*Y[j,t-1] - (lk_xPPM ?
            ↪  dot(view(Xlk_covariates,j,:,t), beta_iter[t]) : 0.0)) *
            ↪  aux1
         end
      end
      sig2_star = 1 / (1/tau2_iter[t] + sum_e2/sig2h_iter[k,t])
      mu_star = sig2_star * (theta_iter[t]/tau2_iter[t] +
      ↪  sum_Y/sig2h_iter[k,t])

      muh_iter[k,t] = rand(Normal(mu_star,sqrt(sig2_star)))
   end
end

############## update sigma2h ##############
if t==1
   for k in 1:nclus_iter[t]
      a_star = sig2h_priors[1] + nh[k,t]/2
      sum_Y = 0.0
      S_kt = findall(Si_iter[:,t] .== k)
      for j in S_kt
         sum_Y += (Y[j,t] - muh_iter[k,t] - (lk_xPPM ?
         ↪  dot(view(Xlk_covariates,j,:,t), beta_iter[t]) : 0.0))^2
      end

      b_star = sig2h_priors[2] + sum_Y/2
      sig2h_iter[k,t] = rand(InverseGamma(a_star, b_star))
   end

else # t>1
   for k in 1:nclus_iter[t]
      a_star = sig2h_priors[1] + nh[k,t]/2
      sum_Y = 0.0
      S_kt = findall(Si_iter[:,t] .== k)
      for j in S_kt
         sum_Y += (Y[j,t] - muh_iter[k,t] - eta1_iter[j]*Y[j,t-1] -
         ↪  (lk_xPPM ? dot(view(Xlk_covariates,j,:,t), beta_iter[t]) :
         ↪  0.0))^2
      end

      b_star = sig2h_priors[2] + sum_Y/2
      sig2h_iter[k,t] = rand(InverseGamma(a_star, b_star))
   end
end
```

```
############# update beta #############
if lk_xPPM && i>=beta_update_threshold
   if t==1
      sum_Y = zeros(p_lk)
      A_star = I(p_lk)/s2_beta
      for j in 1:n
         X_jt = @view Xlk_covariates[j,:,t]
         sum_Y += (Y[j,t] - muh_iter[Si_iter[j,t],t]) * X_jt /
         ↪  sig2h_iter[Si_iter[j,t],t]
         A_star += (X_jt * X_jt') / sig2h_iter[Si_iter[j,t],t]
      end
      b_star = beta0/s2_beta + sum_Y
      A_star = Symmetric(A_star)
      # Symmetric is needed for numerical problems
      # but A_star is indeed symm and pos def (by construction) so there
      ↪  is no problem
      beta_iter[t] = rand(MvNormalCanon(b_star, A_star))
      # this is the quicker and more accurate method

      # old method with the MvNormal and the inversion required
      # Am1_star = inv(A_star)
      # beta_iter[t] = rand(MvNormal(inv(Symmetric(A_star))*b_star,
      ↪  inv(Symmetric(A_star))))
   else
      sum_Y = zeros(p_lk)
      A_star = I(p_lk)/s2_beta
      for j in 1:n
         X_jt = @view Xlk_covariates[j,:,t]
         sum_Y += (Y[j,t] - muh_iter[Si_iter[j,t],t] -
         ↪  eta1_iter[j]*Y[j,t-1]) * X_jt / sig2h_iter[Si_iter[j,t],t]
         A_star += (X_jt * X_jt') / sig2h_iter[Si_iter[j,t],t]
      end
      b_star = beta0/s2_beta + sum_Y
      A_star = Symmetric(A_star)
      beta_iter[t] = rand(MvNormalCanon(b_star, A_star))
   end
end

############# update theta #############
aux1::Float64 = 1 / (lambda2_iter*(1-phi1_iter^2))
kt = nclus_iter[t]
sum_mu=0.0
for k in 1:kt
   sum_mu += muh_iter[k,t]
end

if t==1
   sig2_post = 1 / (1/lambda2_iter + phi1_iter^2*aux1 + kt/tau2_iter[t])
   mu_post = sig2_post * (phi0_iter/lambda2_iter + sum_mu/tau2_iter[t] +
   ↪  (phi1_iter*(theta_iter[t+1] - (1-phi1_iter)*phi0_iter))*aux1)

   theta_iter[t] = rand(Normal(mu_post, sqrt(sig2_post)))

elseif t==T
   sig2_post = 1 / (aux1 + kt/tau2_iter[t])
   mu_post = sig2_post * (sum_mu/tau2_iter[t] + ((1- phi1_iter)*phi0_iter
   ↪  + phi1_iter*theta_iter[t-1])*aux1)

   theta_iter[t] = rand(Normal(mu_post, sqrt(sig2_post)))

else # 1<t<T
```

```
      sig2_post = 1 / ((1+phi1_iter^2)*aux1 + kt/tau2_iter[t])
      mu_post = sig2_post * (sum_mu/tau2_iter[t] +
      ↪  (phi1_iter*(theta_iter[t-1]+theta_iter[t+1]) +
      ↪  phi0_iter*(1-phi1_iter)^2)*aux1)

      theta_iter[t] = rand(Normal(mu_post, sqrt(sig2_post)))
   end

   ############# update tau2 #############
   kt = nclus_iter[t]
   aux1 = 0.0
   for k in 1:kt
      aux1 += (muh_iter[k,t] - theta_iter[t])^2
   end
   a_star_tau = tau2_priors[1] + kt/2
   b_star_tau = tau2_priors[2] + aux1/2
   tau2_iter[t] = rand(InverseGamma(a_star_tau, b_star_tau))

end # for t in 1:T

############# update eta1 #############
# the input argument eta1_priors[2] is already the std dev
if update_eta1
   for j in 1:n
      eta1_old = eta1_iter[j]
      eta1_new = rand(Normal(eta1_old,eta1_priors[2])) # proposal value

      if (-1 <= eta1_new <= 1)
         ll_old = 0.0
         ll_new = 0.0
         for t in 2:T
            # likelihood contribution
            ll_old += loglikelihood(Normal(
               muh_iter[Si_iter[j,t],t] + eta1_old*Y[j,t-1] + (lk_xPPM ?
               ↪  dot(view(Xlk_covariates,j,:,t), beta_iter[t]) : 0),
               sqrt(sig2h_iter[Si_iter[j,t],t]*(1-eta1_old^2))
               ), Y[j,t])
            ll_new += loglikelihood(Normal(
               muh_iter[Si_iter[j,t],t] + eta1_new*Y[j,t-1] + (lk_xPPM ?
               ↪  dot(view(Xlk_covariates,j,:,t), beta_iter[t]) : 0),
               sqrt(sig2h_iter[Si_iter[j,t],t]*(1-eta1_new^2))
               ), Y[j,t])
         end
         logit_old = aux_logit(eta1_old)
         logit_new = aux_logit(eta1_new)

         # prior contribution
         ll_old += -log(2*eta1_priors[1]) -1/eta1_priors[1]*abs(logit_old)
         ll_new += -log(2*eta1_priors[1]) -1/eta1_priors[1]*abs(logit_new)

         ll_ratio = ll_new-ll_old
         u = rand(Uniform(0,1))
         if (ll_ratio > log(u))
            eta1_iter[j] = eta1_new # accept the candidate
            acceptance_ratio_eta1 += 1
         end
      end
   end
end

############# update alpha #############
if update_alpha
```

```
    if time_specific_alpha==false && unit_specific_alpha==false
       # a scalar
       sumg = sum(@view gamma_iter[:,1:T])
       a_star = alpha_priors[1] + sumg
       b_star = alpha_priors[2] + n*T - sumg
       alpha_iter = rand(Beta(a_star, b_star))

    elseif time_specific_alpha==true && unit_specific_alpha==false
       # a vector in time
       for t in 1:T
          sumg = sum(@view gamma_iter[:,t])
          a_star = alpha_priors[1] + sumg
          b_star = alpha_priors[2] + n - sumg
          alpha_iter[t] = rand(Beta(a_star, b_star))
       end

    elseif time_specific_alpha==false && unit_specific_alpha==true
       # a vector in units
       for j in 1:n
          sumg = sum(@view gamma_iter[j,1:T])
          a_star = alpha_priors[1,j] + sumg
          b_star = alpha_priors[2,j] + T - sumg
          alpha_iter[j] = rand(Beta(a_star, b_star))
       end
    elseif time_specific_alpha==true && unit_specific_alpha==true
       # a matrix
       for j in 1:n
          for t in 1:T
             sumg = gamma_iter[j,t] # nothing to sum in this case
             a_star = alpha_priors[1,j] + sumg
             b_star = alpha_priors[2,j] + 1 - sumg
             alpha_iter[j,t] = rand(Beta(a_star, b_star))
          end
       end
    end
end

############# update phi0 #############
aux1 = 1/lambda2_iter
aux2 = 0.0
for t in 2:T
    aux2 += theta_iter[t] - phi1_iter*theta_iter[t-1]
end
sig2_post = 1 / ( 1/phi0_priors[2] + aux1 * (1 +
↪  (T-1)*(1-phi1_iter)/(1+phi1_iter)) )
mu_post = sig2_post * ( phi0_priors[1]/phi0_priors[2] + theta_iter[1]*aux1 +
↪  aux1/(1+phi1_iter)*aux2 )
phi0_iter = rand(Normal(mu_post, sqrt(sig2_post)))

############# update phi1 #############
# the input argument phi1_priors is already the std dev
if update_phi1
    phi1_old = phi1_iter
    phi1_new = rand(Normal(phi1_old, phi1_priors)) # proposal value

    if (-1 <= phi1_new <= 1)
       ll_old = 0.0; ll_new = 0.0
       for t in 2:T
          # likelihood contribution
          ll_old += loglikelihood(Normal(
             (1-phi1_old)*phi0_iter + phi1_old*theta_iter[t-1],
             sqrt(lambda2_iter*(1-phi1_old^2))
```

```
            ), theta_iter[t])
         ll_new += loglikelihood(Normal(
            (1-phi1_new)*phi0_iter + phi1_new*theta_iter[t-1],
            sqrt(lambda2_iter*(1-phi1_new^2))
            ), theta_iter[t])
      end

      # prior contribution
      ll_old += loglikelihood(Uniform(-1,1), phi1_old)
      ll_new += loglikelihood(Uniform(-1,1), phi1_new)

      ll_ratio = ll_new-ll_old
      u = rand(Uniform(0,1))
      if (ll_ratio > log(u))
         phi1_iter = phi1_new # accept the candidate
         acceptance_ratio_phi1 += 1
      end
   end
end

############# update lambda2 #############
aux1 = 0.0
for t in 2:T
   aux1 += (theta_iter[t] - (1-phi1_iter)*phi0_iter -
   ↪  phi1_iter*theta_iter[t-1])^2
end
a_star_lambda2 = lambda2_priors[1] + T/2
b_star_lambda2 = lambda2_priors[2] + ((theta_iter[1] - phi0_iter)^2 + aux1) /
↪  2
lambda2_iter = rand(InverseGamma(a_star_lambda2,b_star_lambda2))

############# save MCMC iterates #############
if i>burnin && i%thin==0
   Si_out[:,:,i_out] = Si_iter[:,1:T]
   gamma_out[:,:,i_out] = gamma_iter[:,1:T]
   if time_specific_alpha==false && unit_specific_alpha==false
      # for each iterate, a scalar
      alpha_out[i_out] = alpha_iter
   elseif time_specific_alpha==true && unit_specific_alpha==false
      # for each iterate, a vector in time
      alpha_out[:,i_out] = alpha_iter[1:T]
   elseif time_specific_alpha==false && unit_specific_alpha==true
      # for each iterate, a vector in units
      alpha_out[:,i_out] = alpha_iter
   elseif time_specific_alpha==true && unit_specific_alpha==true
      # for each iterate, a matrix
      alpha_out[:,:,i_out] = alpha_iter[:,1:T]
   end
   for t in 1:T
      for j in 1:n
         sigma2h_out[j,t,i_out] = sig2h_iter[Si_iter[j,t],t]
         muh_out[j,t,i_out] = muh_iter[Si_iter[j,t],t]
      end
   end
   eta1_out[:,i_out] = eta1_iter
   if lk_xPPM
      for t in 1:T
         beta_out[t,:,i_out] = beta_iter[t]
      end
   end
   theta_out[:,i_out] = theta_iter[1:T]
   tau2_out[:,i_out] = tau2_iter[1:T]
```

```
      phi0_out[i_out] = phi0_iter
      phi1_out[i_out] = phi1_iter
      lambda2_out[i_out] = lambda2_iter

      ############# save fitted values and metrics #############
      for j in 1:n
         for t in 1:T
            muh_jt = muh_iter[Si_iter[j,t],t]
            sig2h_jt = sig2h_iter[Si_iter[j,t],t]
            X_lk_term = lk_xPPM ? dot(view(Xlk_covariates,j,:,t), beta_iter[t])
            ↪  : 0.0

            if t==1
               llike[j,t,i_out] = logpdf(Normal(
                  muh_jt + X_lk_term,
                  sqrt(sig2h_jt)
                  ), Y[j,t])
               fitted[j,t,i_out] = muh_jt + X_lk_term
            else # t>1
               llike[j,t,i_out] = logpdf(Normal(
                  muh_jt + eta1_iter[j]*Y[j,t-1] + X_lk_term,
                  sqrt(sig2h_jt*(1-eta1_iter[j]^2))
                  ), Y[j,t])
               fitted[j,t,i_out] = muh_jt + eta1_iter[j]*Y[j,t-1] + X_lk_term
            end

            mean_likelhd[j,t] += exp(llike[j,t,i_out])
            mean_loglikelhd[j,t] += llike[j,t,i_out]
            CPO[j,t] += exp(-llike[j,t,i_out])
         end
      end

      i_out += 1
   end

next!(progresso)

end # for i in 1:draws

println("\ndone!")
t_end = now()
println("Elapsed time: ",
↪  Dates.canonicalize(Dates.CompoundPeriod(t_end-t_start)))

############# compute LPML and WAIC #############
for j in 1:n
   for t in 1:T
      LPML += log(CPO[j,t])
   end
end
LPML -= n*T*log(nout) # scaling factor
LPML = -LPML # fix sign
println("LPML: ", LPML, " (the higher the better)")

# adjust mean variables
mean_likelhd ./= nout
mean_loglikelhd./= nout
for j in 1:n
   for t in 1:T
      WAIC += 2*mean_loglikelhd[j,t] - log(mean_likelhd[j,t])
   end
end
```

```
WAIC *= -2
println("WAIC: ", WAIC, " (the lower the better)")

if update_eta1 @printf "acceptance ratio eta1: %.2f%%\n"
↪  acceptance_ratio_eta1/(n*draws) *100 end
if update_phi1 @printf "acceptance ratio phi1: %.2f%%"
↪  acceptance_ratio_phi1/draws*100 end
println()

if perform_diagnostics
   chn = Chains(
      hcat(lambda2_out,phi0_out,tau2_out',theta_out',eta1_out',alpha_out'),
      ["lambda2","phi0",
      [string("tau2_t", i) for i in 1:T]...,
      [string("theta_t", i) for i in 1:T]...,
      [string("eta1_j", i) for i in 1:n]...,
      [string("alpha_t", i) for i in 1:T]...,
      ]
   )
   ss = DataFrame(summarystats(chn))
   println("\nDiagnostics:")
   @show ss[!,[1,4,5,6,7]];
   if logging CSV.write(log_file,ss[!,[1,4,5,6,7]]) end
end

close(log_file)

if simple_return
   return Si_out, LPML, WAIC
else
   return Si_out, Int.(gamma_out), alpha_out, sigma2h_out, muh_out, include_eta1
   ↪  ? eta1_out : NaN,
      lk_xPPM ? beta_out : NaN, theta_out, tau2_out, phi0_out, include_phi1 ?
      ↪  phi1_out : NaN, lambda2_out,
      fitted, llike, LPML, WAIC
end
```

B.2 Interface

We now provide some technical details regarding the overall implementation design. The fitting algorithm was written in Julia, but its primary intended use is within the R programming environment. This choice reflects R's current status as the leading language for statistical analysis.

To achieve this integration, we relied on the `JuliaConnectoR` library (Lenz et al., 2022) in R, which enables interaction between the two languages. This library allows to load the Julia project `JDRPM`, which contains the functionalities, including code and package dependencies, required for the implementation of the JDRPM algorithm. Through `JuliaConnectoR` we can pass data and parameters from R to Julia, run the fitting algorithm, and convert the output back into R structures. The design of this workflow is illustrated in Listing 4.

Listing 4: Overview of the R and Julia integration process for running the JDRPM algorithm.

```
############# Requirements #############
# install the required pacakge
install.packages("JuliaConnectoR")

############# Setup #############
# load the package
library(JuliaConnectoR)
# check it returns TRUE
juliaSetupOk()

# load the Package manager on Julia
juliaEval("using Pkg")
# enter into the JDRPM project
juliaEval("Pkg.activate(\"<path/to/where/you/stored/JDRPM>\")")

# downloads and install, only once, all the depdendencies
juliaEval("Pkg.instantiate()")
# now, as a check, this should print the list of packages that JDRPM uses,
# such as Distributions, Statistics, LinearAlgebra, SpecialFunctions, etc.
juliaEval("Pkg.status()")

# locate the "main" file
module = normalizePath("<path/to/where/you/stored/JDRPM>/src/JDRPM.jl")
# load the "main" file into a callable R object
module_JDRPM = juliaImport(juliaCall("include", module))

############# Fit #############
# perform the fit
out = module_JDRPM$MCMC_fit(...)

# convert the output to R structures
rout = juliaGet(out)
names(rout)  = c("Si","gamma","alpha", "sigma2h", "muh", "eta1","beta","theta",
↪  "tau2", "phi0", "phi1","lambda2","fitted","llike","lpml","waic")

# and reshape it to uniform to the DRPM output form
rout$Si = aperm(rout$Si, c(2, 1, 3))
rout$gamma = aperm(rout$gamma, c(2, 1, 3))
rout$sigma2h = aperm(rout$sigma2h, c(2, 1, 3))
rout$muh = aperm(rout$muh, c(2, 1, 3))
rout$fitted = aperm(rout$fitted, c(2, 1, 3))
rout$llike = aperm(rout$llike, c(2, 1, 3))
rout$alpha = aperm(rout$alpha, c(2, 1))
rout$theta = aperm(rout$theta, c(2, 1))
rout$tau2 = aperm(rout$tau2, c(2, 1))
rout$eta1 = aperm(rout$eta1, c(2, 1))
rout$phi0 = matrix(rout$phi0, ncol = 1)
rout$phi1 = matrix(rout$phi1, ncol = 1)
rout$lambda2 = matrix(rout$lambda2, ncol = 1)
# this reshape works in the case of full model fit, but in the case of special
# fitting options (e.g. unit_specific_alpha=true) it needs to be adjusted
```

In terms of the user interface and feedback provided by the function, we aimed to enhance the friendliness and informativeness compared to the original C implementation. Notable improvements include the ability to perform convergence

diagnostics, on a subset of the sampled parameters, and the real-time progress monitoring, which updates every second, to display the estimated remaining time for completing the fit. These features further exemplify the ease of use inherent in Julia: they were implemented with just a few additional lines of code, leveraging the Julia packages `MCMCChains` (Ge et al., 2018) and `ProgressMeter`.

Listing 5: Feedback from the JDRPM implementation.

```
# if verbose=true this initial parameter section is also printed
Parameters:
sig2h ∼ invGamma(0.01, 0.01)
Logit(1/2(eta1+1)) ∼ Laplace(0, 0.9)
tau2 ∼ invGamma(1.9, 0.4)
phi0 ∼ Normal(μ=0.0, σ=10.0)
lambda2 ∼ invGamma(1.9, 0.4)
alpha ∼ Beta(2.0, 2.0)

- using seed 111.0 -
fitting 110000 total iterates (with burnin=90000, thinning=5)
thus producing 4000 valid iterates in the end

on n=105 subjects
for T=12 time instants

[✓] with space? true (cohesion 3.0)
[✓] with covariates in the likelihood? true (p=6)
[✓] with covariates in the clustering process? true (p=3, similarity 4.0)
[✓] are there missing data in Y? true

2024-10-30 13:50:23
Starting MCMC algorithm
Progress 100% Time: 1:15:45 (41.33 ms/it)

done!
Elapsed time 1 hour, 15 minutes, 45 seconds, 920 milliseconds
LPML: 791.8603234076745 (the higher the better)
WAIC: -1976.7279705951883 (the lower the better)
acceptance ratio eta1: 52.18%
acceptance ratio phi1: 35.04%

# if perform_diagnostics=true this final diagnostics section is also printed
Diagnostics:
ss[!, [1, 4, 5, 6, 7]] = 143×5 DataFrame
 Row | parameters  mcse         ess_bulk   ess_tail   rhat
     | Symbol      Float64      Float64    Float64    Float64
-----------------------------------------------------------------
   1 | lambda2     0.000817173  4243.04    3970.25    0.999769
   2 | phi0        0.00218706   3533.95    3675.99    1.00018
   3 | tau2_t1     0.00540064   3716.56    3645.99    0.999968
         ⋮
  14 | tau2_t12    0.00259168   3965.77    3655.55    0.999951
  15 | theta_t1    0.00404988   3603.34    3765.78    0.999834
         ⋮
  26 | theta_t12   0.00337843   3588.83    3907.13    0.999866
  27 | eta1_j1     0.0112187     451.588   1107.96    1.00163
```

```
        ⋮
131 | eta1_j105   0.00328424   1539.36    2194.83    1.00002
132 | alpha_t1    0.000213087  3774.24    3920.48    1.00044
        ⋮
143 | alpha_t12   0.00266005    541.427   1867.54    1.0084
```

All codes and insights related to JDRPM's MCMC algorithm implementation, along with the experiments conducted throughout this work, are available at `https://github.com/federicomor/Tesi/tree/main/src/JDRPM`.

Appendix C

Further plots

We now present the visualization of the clusters estimates for the fits analysed in the experiments of Chapter 3.

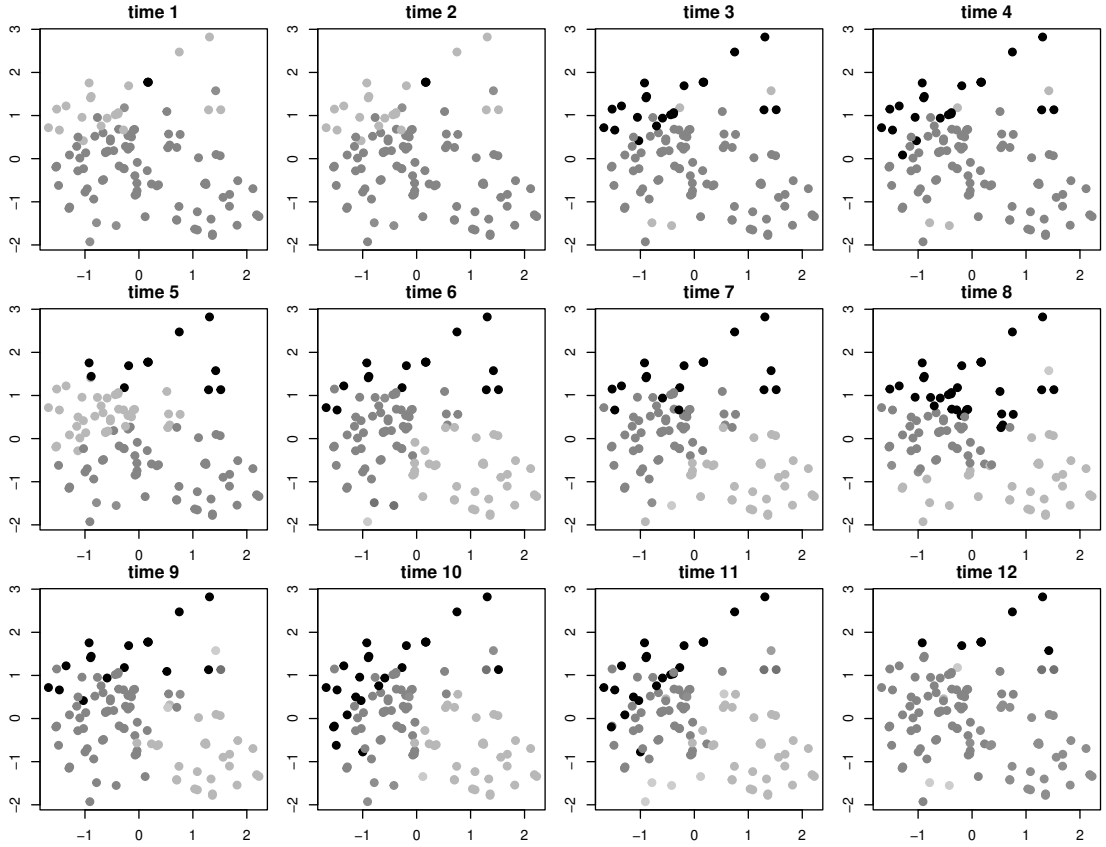

Figure C.1: Clusters estimates produced by CDRPM fit, in the real-world scenario.

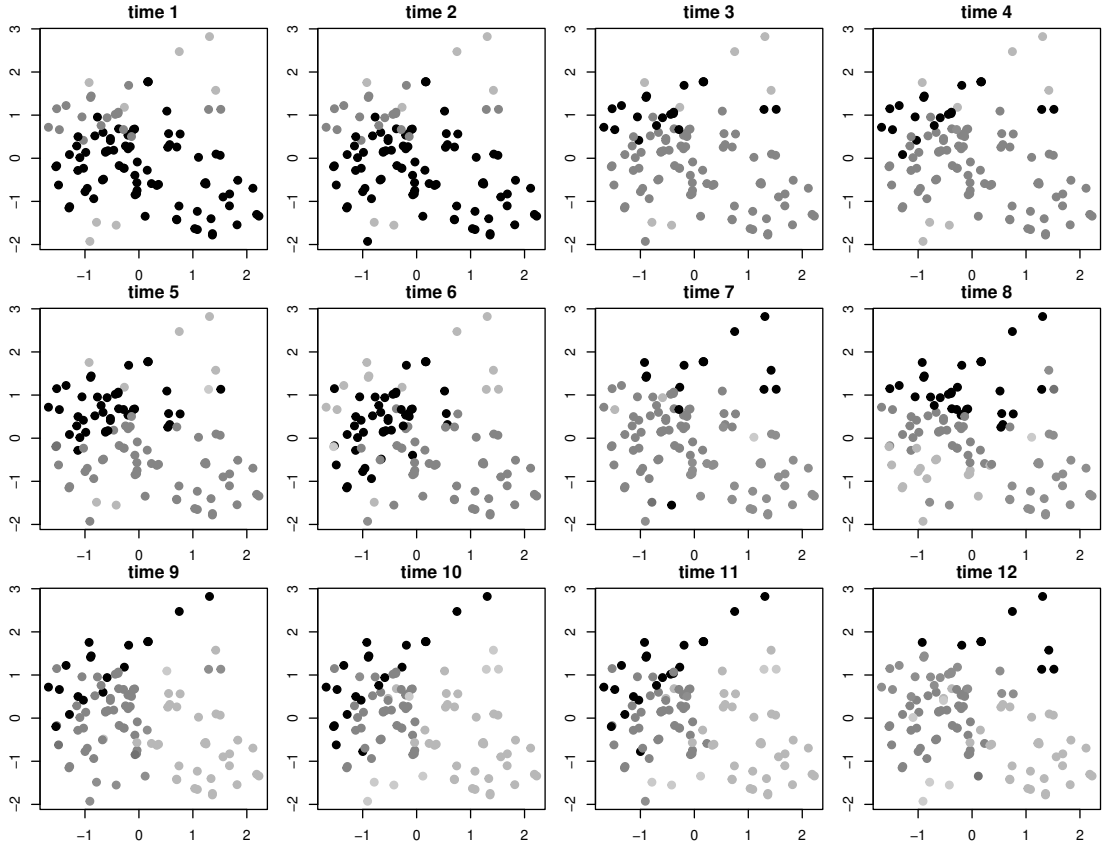

Figure C.2: Clusters estimates produced by JDRPM fit, in the real-world scenario.

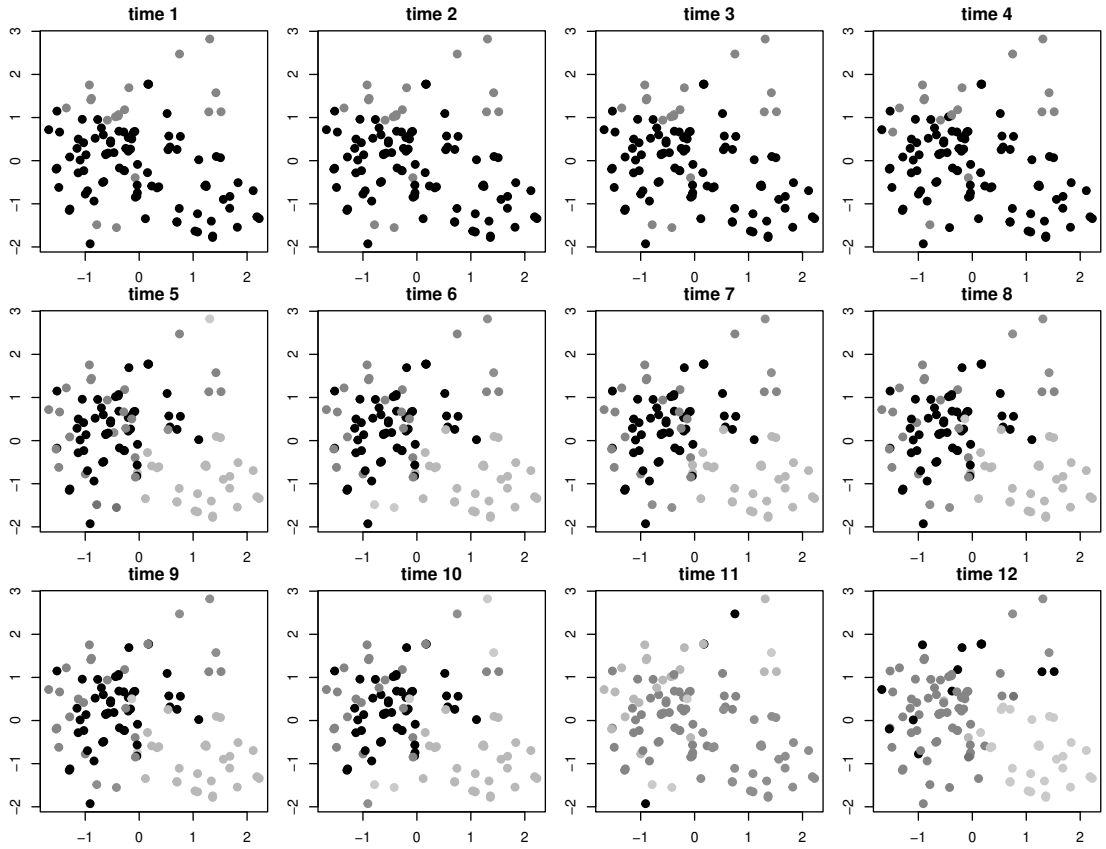

Figure C.3: Clusters estimates produced by JDRPM fit, in the real-world scenario, with covariates in the likelihood.

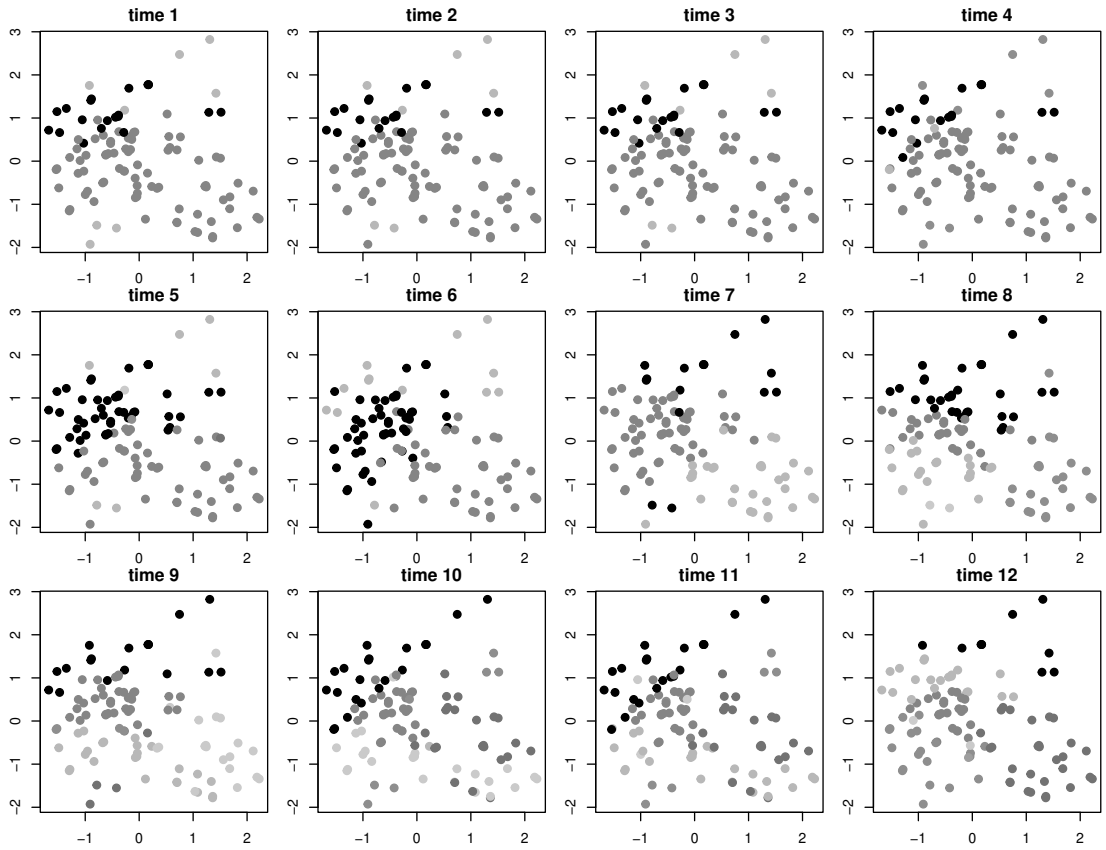

Figure C.4: Clusters estimates produced by JDRPM fit, in the real-world scenario, with covariates in the prior.

Bibliography

Aldous, David J. (1985). "Exchangeability and related topics". In: *École d'Été de Probabilités de Saint-Flour XIII — 1983*. Ed. by P. L. Hennequin. Berlin, Heidelberg: Springer Berlin Heidelberg, pp. 1–198. ISBN: 978-3-540-39316-0 (cit. on p. 6).

Antoniano Villalobos, Isadora and Stephen Walker (Aug. 2015). "A Nonparametric Model for Stationary Time Series". In: *Journal of Time Series Analysis* 63. DOI: 10.1111/jtsa.12146 (cit. on p. 7).

Besançon, Mathieu, Theodore Papamarkou, David Anthoff, Alex Arslan, Simon Byrne, Dahua Lin, and John Pearson (2021). "Distributions.jl: Definition and Modeling of Probability Distributions in the JuliaStats Ecosystem". In: *Journal of Statistical Software* 98.16, pp. 1–30. ISSN: 1548-7660. DOI: 10.18637/jss.v098.i16 (cit. on p. 29).

Bezanson, Jeff, Alan Edelman, Stefan Karpinski, and Viral B Shah (2017). "Julia: A fresh approach to numerical computing". In: *SIAM Review* 59.1, pp. 65–98. DOI: 10.1137/141000671 (cit. on p. 29).

Blackwell, David and James B. MacQueen (1973). "Ferguson Distributions Via Polya Urn Schemes". In: *The Annals of Statistics* 1.2, pp. 353–355. DOI: 10.1214/aos/1176342372 (cit. on p. 6).

Böhning, Dankmar (Aug. 2007). "Finite Mixture and Markov Switching Models by S. Frühwirth-Schnatter". In: *Biometrics* 63.3, pp. 971–972. ISSN: 0006-341X. DOI: 10.1111/j.1541-0420.2007.00856_6.x. eprint: https://academic.oup.com/biometrics/article-pdf/63/3/971/52454335/biometrics_63_3_971.pdf (cit. on pp. 2, 5).

Bouveyron, Charles, Gilles Celeux, T. Brendan Murphy, and Adrian E. Raftery (2019). *Model-Based Clustering and Classification for Data Science: With Applications in R*. Cambridge Series in Statistical and Probabilistic Mathematics. Cambridge University Press (cit. on pp. 2, 5).

Caron, François, Willie Neiswanger, Frank Wood, Arnaud Doucet, and Manuel Davy (Jan. 2017). "Generalized Pólya urn for time-varying Pitman-Yor processes". In: *Journal of Machine Learning Research* 18.1, pp. 836–867. ISSN: 1532-4435 (cit. on p. 7).

Chen, Jiahao and Jarrett Revels (Aug. 2016). "Robust benchmarking in noisy environments". In: *arXiv e-prints*, arXiv:1608.04295. arXiv: 1608.04295 [cs.PF] (cit. on p. 31).

Christensen, Ronald, Wesley Johnson, Adam Branscum, and Timothy Hanson (2010). *Bayesian ideas and data analysis. An introduction for scientists and statisticians*. CRC Press. DOI: 10.1201/9781439894798 (cit. on p. 15).

David B. Dahl, Devin J. Johnson and Peter Müller (2022). "Search Algorithms and Loss Functions for Bayesian Clustering". In: *Journal of Computational and Graphical Statistics* 31.4, pp. 1189–1201. DOI: 10.1080/10618600.2022.2069779 (cit. on p. 37).

De Blasi, Pierpaolo, Stefano Favaro, Antonio Lijoi, Ramses H. Mena, Igor Prunster, and Matteo Ruggiero (Feb. 2015). "Are Gibbs-Type Priors the Most Natural Generalization of the Dirichlet Process?" In: *IEEE Trans. Pattern Anal. Mach. Intell.* 37.2, pp. 212–229. ISSN: 0162-8828. DOI: 10.1109/TPAMI.2013.217 (cit. on pp. 8, 19).

De Iorio, Maria, Stefano Favaro, Alessandra Guglielmi, and Lifeng Ye (Oct. 2019). *Bayesian nonparametric temporal dynamic clustering via autoregressive Dirichlet priors*. DOI: 10.48550/arXiv.1910.10443 (cit. on p. 7).

De Iorio, Maria and Athanasios Kottas (2018). "Modeling for Dynamic Ordinal Regression Relationships: An Application to Estimating Maturity of Rockfish in California". In: *Journal of the American Statistical Association* 113.521, pp. 68–80. DOI: 10.1080/01621459.2017.1328357 (cit. on p. 7).

Denison, D. and C Holmes (Apr. 2001). "Bayesian Partitioning for Estimating Disease Risk". In: *Biometrics* 57, pp. 143–9. DOI: 10.1111/j.0006-341X.2001.00143.x (cit. on p. 18).

Duncan, Earl (2016). *Deriving the Full Conditionals*. BRAG: Bayesian Research & Application Group. URL: https://bragqut.wordpress.com/wp-content/uploads/2018/04/deriving-the-full-conditionals.pdf (cit. on p. 12).

Ester, Martin, Hans-Peter Kriegel, Jörg Sander, and Xiaowei Xu (1996). "A density-based algorithm for discovering clusters in large spatial databases with noise". In: *Proceedings of the Second International Conference on Knowledge Discovery and Data Mining*. KDD'96. Portland, Oregon: AAAI Press, pp. 226–231 (cit. on p. 1).

Fassò, A., J. Rodeschini, A. Fusta Moro, Q. Shaboviq, P. Maranzano, M. Cameletti, F. Finazzi, N. Golini, R. Ignaccolo, and P. Otto (2023). *AgrImOnIA: Open Access dataset correlating livestock and air quality in the Lombardy region, Italy (3.0.0)*. DOI: https://doi.org/10.5281/zenodo.7956006 (cit. on pp. v, vii, 40, 45).

Ferguson, Thomas S. (1973). "A Bayesian Analysis of Some Nonparametric Problems". In: *The Annals of Statistics* 1.2, pp. 209–230. DOI: 10.1214/aos/1176342360 (cit. on p. 6).

Franzén, Jessica (2008). "Bayesian Cluster Analysis : Some Extensions to Non-standard Situations". In: URL: https://api.semanticscholar.org/CorpusID:12397258 (cit. on pp. 2, 6).

Ge, Hong, Kai Xu, and Zoubin Ghahramani (2018). "Turing: a language for flexible probabilistic inference". In: *International Conference on Artificial Intelligence and Statistics, AISTATS 2018, 9-11 April 2018, Playa Blanca, Lanzarote, Canary Islands, Spain*, pp. 1682–1690. URL: http://proceedings.mlr.press/v84/ge18b.html (cit. on p. 100).

Gelman, A., J.B. Carlin, H.S. Stern, and D.B. Rubin (2003). *Bayesian Data Analysis, Second Edition*. Chapman & Hall/CRC Texts in Statistical Science. Taylor & Francis. ISBN: 9781420057294. DOI: 10.1201/9780429258480 (cit. on pp. 2, 7).

Gelman, Andrew (Jan. 2004). "Prior Distributions for Variance Parameters in Hierarchical Models". In: *Economics and Econometrics Research Institute (EERI), EERI Research Paper Series* 1 (cit. on p. 72).

Gelman, Andrew, Jessica Hwang, and Aki Vehtari (July 2013). "Understanding predictive information criteria for Bayesian models". In: *Statistics and Computing* 24. DOI: 10.1007/s11222-013-9416-2 (cit. on p. 15).

Geman, Stuart and Donald Geman (Nov. 1984). "Geman, D.: Stochastic relaxation, Gibbs distribution, and the Bayesian restoration of images. IEEE Trans. Pattern Anal. Mach. Intell. PAMI-6(6), 721-741". In: *IEEE Trans. Pattern Anal. Mach. Intell.* 6, pp. 721–741. DOI: 10.1109/TPAMI.1984.4767596 (cit. on p. 12).

Gormley, Isobel, Thomas Murphy, and Adrian Raftery (Oct. 2022). "Model-Based Clustering". In: *Annual Review of Statistics and Its Application* 10. DOI: 10.1146/annurev-statistics-033121-115326 (cit. on p. 1).

Gower, J. C. (1971). "A General Coefficient of Similarity and Some of Its Properties". In: *Biometrics* 27.4, pp. 857–871. ISSN: 0006341X, 15410420. URL: http://www.jstor.org/stable/2528823 (cit. on p. 23).

Grazian, Clara (Mar. 2023). "A review on Bayesian model-based clustering". In: DOI: 10.48550/arXiv.2303.17182 (cit. on pp. 2, 5, 6).

Grün, Bettina (July 2018). *Model-based Clustering*. DOI: 10.48550/arXiv.1807.01987 (cit. on pp. 2, 5).

Gutiérrez, Luis, Ramsés H. Mena, and Matteo Ruggiero (2016). "A time dependent Bayesian nonparametric model for air quality analysisa". In: *Computational Statistics & Data Analysis* 95.C, pp. 161–175. DOI: 10.1016/j.csda.2015.10.00. URL: https://ideas.repec.org/a/eee/csdana/v95y2016icp161-175.html (cit. on p. 7).

Hartigan, J. A. and M. A. Wong (1979). "Algorithm AS 136: A K-Means Clustering Algorithm". In: *Journal of the Royal Statistical Society. Series C (Applied Statistics)* 28.1, pp. 100–108. ISSN: 00359254, 14679876. URL: http://www.jstor.org/stable/2346830 (visited on 11/04/2024) (cit. on p. 1).

Hubert, Lawrence J. and Phipps Arabie (1985). "Comparing partitions". In: *Journal of Classification* 2, pp. 193–218. URL: https://api.semanticscholar.org/CorpusID:189915041 (cit. on p. 37).

Jain, Anil K. and Richard C. Dubes (1988). *Algorithms for clustering data*. Prentice-Hall, Inc. URL: http://portal.acm.org/citation.cfm?id=46712 (cit. on p. 1).

Jo, Seongil, Jaeyong Lee, Peter Müller, Fernando A. Quintana, and Lorenzo Trippa (2017). "Dependent Species Sampling Models for Spatial Density Estimation". In: *Bayesian Analysis* 12, pp. 379–406. URL: https://api.semanticscholar.org/CorpusID:52028880 (cit. on p. 7).

Kalli, Maria and Jim Griffin (Jan. 2018). "Bayesian nonparametric vector autoregressive models". In: *Journal of Econometrics* 203. DOI: 10.1016/j.jeconom.2017.11.009 (cit. on p. 7).

Kaufman, Leonard and Peter Rousseeuw (Jan. 1990). *Finding Groups in Data: An Introduction To Cluster Analysis*. ISBN: 0-471-87876-6. DOI: 10.2307/2532178 (cit. on p. 1).

Krige, Daniel G (1951). "A statistical approach to some basic mine valuation problems on the Witwatersrand". In: *Journal of the Southern African Institute of Mining and Metallurgy* 52.6, pp. 119–139 (cit. on p. 60).

Lawson, C. L., R. J. Hanson, D. R. Kincaid, and F. T. Krogh (Sept. 1979). "Basic Linear Algebra Subprograms for Fortran Usage". In: *ACM Trans. Math. Softw.* 5.3, pp. 308–323. ISSN: 0098-3500. DOI: 10.1145/355841.355847 (cit. on p. 29).

Lenz, Stefan, Maren Hackenberg, and Harald Binder (2022). "The JuliaConnectoR: A Functionally-Oriented Interface for Integrating Julia in R". In: *Journal of Statistical Software* 101.6, pp. 1–24. DOI: 10.18637/jss.v101.i06 (cit. on pp. 37, 98).

Lin, Dahua, John Myles White, Simon Byrne, Douglas Bates, Andreas Noack, John Pearson, Alex Arslan, Kevin Squire, David Anthoff, Theodore Papamarkou, Mathieu Besançon, Jan Drugowitsch, Moritz Schauer, and other contributors (July 2019). *JuliaStats/Distributions.jl: a Julia package for probability distributions and associated functions*. DOI: 10.5281/zenodo.2647458 (cit. on p. 29).

McLachlan, Geoffrey J and Thriyambakam Krishnan (2008). *The EM algorithm and extensions*. John Wiley & Sons. DOI: 10.1002/9780470191613 (cit. on pp. 2, 5).

Metropolis, Nicholas, Arianna W. Rosenbluth, Marshall N. Rosenbluth, Augusta H. Teller, and Edward Teller (June 1953). "Equation of State Calculations by Fast Computing Machines". In: *The Journal of Chemical Physics* 21.6, pp. 1087–1092. DOI: 10.1063/1.1699114 (cit. on p. 12).

Müller, Peter, Fernando A. Quintana, and Gary Rosner (Mar. 2011). "A Product Partition Model With Regression on Covariates". In: *Journal of computational and graphical statistics: a joint publication of American Statistical Association, Institute of Mathematical Statistics, Interface Foundation of North America* 20, pp. 260–278. DOI: 10.1198/jcgs.2011.09066 (cit. on p. 19).

Ng, See, Thriyambakam Krishnan, and G. Mclachlan (Jan. 2004). "The EM algorithm". In: *Handbook of Computational Statistics: Concepts and Methods*. DOI: 10.1007/978-3-642-21551-3_6 (cit. on pp. 2, 5).

Nieto-Barajas, Luis E., Peter Müller, Yuan Ji, Yiling Lu, and Gordon B. Mills (Jan. 2012). "A Time-Series DDP for Functional Proteomics Profiles". In: *Biometrics* 68.3, pp. 859–868. ISSN: 0006-341X. DOI: 10.1111/j.1541-0420.2011.01724.x (cit. on p. 7).

Page, Garrit L., Fernando A. Quintana, and David B. Dahl (2022). "Dependent Modeling of Temporal Sequences of Random Partitions". In: *Journal of Computational and Graphical Statistics* 31.2, pp. 614–627. DOI: 10.1080/10618600.2021.1987255 (cit. on pp. v, vii, 3, 7–12, 17, 37, 38, 42).

Page, Garritt L. and Fernando A. Quintana (Sept. 2018). "Calibrating covariate informed product partition models". In: *Statistics and Computing* 28, pp. 1–23. DOI: 10.1007/s11222-017-9777-z (cit. on pp. 19, 23).

— (2016). "Spatial Product Partition Models". In: *Bayesian Analysis* 11.1, pp. 265–298. DOI: 10.1214/15-BA971 (cit. on pp. 18, 19, 24).

Quintana, Fernando A., Peter Müller, and Ana Luisa Papoila (2015). "Cluster-Specific Variable Selection for Product Partition Models". In: *Scandinavian Journal of Statistics* 42.4, pp. 1065–1077. DOI: 10.1111/sjos.12151 (cit. on pp. 19, 63).

R Core Team (2024). *R: A Language and Environment for Statistical Computing*. R Foundation for Statistical Computing. Vienna, Austria. URL: https://www.R-project.org/ (cit. on p. 37).

Robert, Christian and George Casella (Nov. 2000). "Monte Carlo Statistical Method". In: *Technometrics* 42. DOI: 10.2307/1270959 (cit. on pp. 2, 7).

Tanner, Martin A. and Wing Hung Wong (1987). "The Calculation of Posterior Distributions by Data Augmentation". In: *Journal of the American Statistical Association* 82.398, pp. 528–540. ISSN: 01621459. URL: http://www.jstor.org/stable/2289457 (cit. on p. 12).

Teh, Yee Whye (2010). "Dirichlet Process". In: *Encyclopedia of Machine Learning*. Ed. by Claude Sammut and Geoffrey I. Webb. Boston, MA: Springer US, pp. 280–287. ISBN: 978-0-387-30164-8. DOI: 10.1007/978-0-387-30164-8_219 (cit. on p. 6).

Wade, Sara (Mar. 2023). "Bayesian cluster analysis". In: *Philosophical transactions. Series A, Mathematical, physical, and engineering sciences* 381, p. 20220149. DOI: 10.1098/rsta.2022.0149 (cit. on pp. 2, 5).

Acknowledgements

"This is to be my haven for many long years, my niche which I enter with such a mistrustful, such a painful sensation... And who knows? Maybe when I come to leave it many years hence I may regret it!"

— Fëdor Dostoevskij, *The House of the Dead*

I would like to thank my advisors Alessandra Guglielmi and Alessandro Carminati, primarily for having made me feel, during the entire course of the thesis, in a very calm, lovely atmosphere, in which I have been able to feel perfectly at ease (which is notoriously a NP-hard problem). The epigraphs of my beloved author Dostoevskij and the title inspired by the Star Wars films, as well as some poetic licenses and easter eggs scattered across the chapters (which they have kindly allowed me to keep) I think prove this feeling of sweet but respectful confidence.

I thank professor Alessandra Guglielmi for having guided me through the fog of uncertainty and puzzlement often associated to the thesis or in general to the final period of university. From the beginning she demonstrated a genuine interest in the topic of the thesis and a confidence in my chances of carrying it out.

I thank Alessandro Carminati for having assisted me in many of the most critical phases of the thesis. His action always precise and effective has been necessary to solve the various theoretical puddles in which I got stuck. Moreover, we share the same passion for Julia and, I believe, the delight for having overthrown the not-so-missed C of the old model implementation.

I thank my family for having helped and supported me during all these years of university, and my friends and fellows who have always and wisely brought to light my highest potential and resources. The passion for solving problems, inventing creative solutions, getting lost in calculations, wandering through the magical world of the most advanced mathematics, sharing doubts and reasonings: all this has always found in you a wonderful and unforeseen companion.

I also thank all the boys and girls I had the pleasure of working and playing with in the various summer camps, for consistently reminding me of the cheerful and mild spirit with which all the various challenges can be faced.

And finally, I thank all the cats and kittens that I met, also quite literally, during my journey, which through a tender meow or a kind rub have always managed to enlighten the various days.

Ringraziamenti

> *"Ecco il mio ponte d'approdo per molti lunghi anni, il mio angoletto, nel quale faccio il mio ingresso con una sensazione così diffidente, così morbosa... Ma chi lo sa? Forse, quando tra molti anni mi toccherà abbandonarlo, magari potrei anche rimpiangerlo!"*
>
> — Fëdor Dostoevskij, *Memorie da una casa di morti*

Vorrei ringraziare innanzitutto i miei relatori Alessandra Guglielmi e Alessandro Carminati, principalmente per avermi fatto sentire, durante l'intero svolgimento della tesi, in un clima molto tranquillo, sereno, in cui ho avuto modo di trovarmi pienamente a mio agio. Le epigrafi del mio caro autore Dostoevskij e il titolo ispirato alla saga di Star Wars, nonché alcune licenze poetiche sparse nei vari capitoli (che loro mi hanno gentilmente concesso di tenere) credo dimostrino questa atmosfera di piacevole ma rispettosa confidenza.

Ringrazio la professoressa Alessandra Guglielmi per avermi guidato attraverso la nebbia di incertezza e confusione che spesso accompagna la tesi o in senso lato gli ultimi mesi di università. Fin dall'inizio ha infatti condiviso un sincero interesse per il lavoro che avremmo dovuto svolgere e una fiducia nelle mie possibilità di condurlo a termine.

Ringrazio Alessandro Carminati per avermi aiutato in molte delle fasi più critiche della tesi. Il suo intervento sempre preciso e puntuale è stato necessario per risolvere le varie pozzanghere teoriche in cui mi ero impantanato. Inoltre, condividiamo la stessa passione per Julia e, credo, la soddisfazione per aver battuto il non-così-compianto C della vecchia implementazione del modello.

Ringrazio la mia famiglia per avermi aiutato e supportato durante tutti questi anni di università, e i miei amici e compagni di studio, i quali hanno sempre sapientemente fatto emergere le mie migliori potenzialità e risorse. La passione per risolvere problemi, ideare soluzioni creative, perdersi nei calcoli, addentrarsi nel magico mondo della matematica più avanzata, condividere dubbi e ragionamenti: tutto questo ha sempre trovato in voi un'ottima e inaspettata compagnia.

Ringrazio anche tutti i bambini e ragazzi con cui ho avuto modo di lavorare e giocare nei vari campi estivi, per farmi sempre ricordare dello spirito gioioso e leggero con cui si possono approcciare tutte le varie sfide.

Infine, ringrazio tutti i gatti e micini che ho incontrato, anche letteralmente, durante il mio percorso, che con un tenero miagolio o un'affettuosa strusciatina sono sempre riusciti a migliorare le varie giornate.